UNIVERSITÀ DEGLI STUDI DI MILANO

Scuola di Dottorato in Fisica, Astrofisica e Fisica Applicata
Dipartimento di Fisica

Corso di Dottorato in Fisica, Astrofisica e Fisica Applicata
Ciclo XXIX

Stochastic noise approach to non-Markovian decoherence in continuous variable open quantum systems

Settore Scientifico Disciplinare FIS/03

Supervisore: Professor Matteo G.A. PARIS

Coordinatore: Professor Enrico RAGUSA

Tesi di Dottorato di:
Jacopo TRAPANI

Anno Accademico 2015/2016

Commission of the final examination:

Internal Member:
Prof. Alberto Barchielli

External Member:
Prof. Rafael Ferragut
Prof. Giuliano Benenti

Final examination:

Date 19/01/2017

Università degli Studi di Milano, Dipartimento di Fisica, Milano, Italy

Cover illustration:

"number 16", 1961, Mark Rothko

MIUR subjects:

FIS/03

Contents

Introduction iv

List of Publications viii

Acknowledgments ix

1 Preliminaries 1
- 1.1 Introduction to quantum mechanics 1
- 1.2 Quantum optics in phase space 6
- 1.3 Quantum correlations 11
- 1.4 Quantum Discrimination Theory 15
- 1.5 Non-Markovianity 16
- 1.6 Summary 18

2 Stochastic processes 20
- 2.1 General notions 20
- 2.2 Gaussian stochastic processes 22
- 2.3 Summary 25

3 Stochastic modeling of quantum environments 27
- 3.1 Stochastic phase diffusion 27
- 3.2 Stochastic approach to Born-Markov master equation 29
- 3.3 Non-Markovianity of stochastic interactions 35
- 3.4 Summary 36

4 Stochastic approach to non-Markovian decoherence 38
- 4.1 Quantum-to-classical transition with noisy environment 38
- 4.2 Phase communication channels in presence of noise 49
- 4.3 Summary 59

5 Non-Markovianity vs backflow of information 60
- 5.1 Local and global noise: the interaction model 60
- 5.2 Dynamics of Quantum Correlations 65
- 5.3 Non Divisibility vs Information Backflow 68
- 5.4 Summary 70

6 Environment discrimination **72**
6.1 Discrimination protocol for classical environments 72
6.2 Random input Gaussian states 76
6.3 Summary 78

Conclusions **79**

Appendices **81**

Bibliography **84**

Introduction

In the last decades, we have witnessed a massive developement in quantum technologies. Nowadays, we tread the path towards quantum computing, refine quantum communication and cryptography schemes in order to secure reliable transmission of information, manage to implement teleportation protocols over optical fibers. All these achievements and applications rest on quantum information theory, where quantum physics and computer science come together to describe the benefits of using quantum systems in information processing. In fact, storing information within quantum systems allows exploiting features as nonclassicality or quantum correlations to push the efficiency of communication protocols and quantum computing far beyond any achieved classical limit. Quantum information theory thus provides the appropriate mathematical frame, describing quantum resources and setting the rules to manipulate and access information.

The scientific community has put much effort into classifying quantum correlations and scrutinizing their properties, fostered by the fact that correlations often stand as key resource for quantum communication, computation [1], secure communication [2,3] and estimation problems [4]. Historically, quantum correlations were uniquely identified with entanglement. However, this equivalence was progressively questioned and nowadays the existence of more fundamental and profitable correlations as discord or steering is accepted, limiting entanglement to capture aspects of correlations based on non-separability. For instance, quantum discord, an information-deficit between quantum and classical correlations, provides enhancement for computation [5, 6], is a key resource for quantum information protocols [7] and has been proved robust against decoherence [8, 9]. Unfortunately, quantum correlations are fragile: in fact, quantum systems are continuously perturbed by the surrounding environment, which usually softens or even wipes out the quantum properties of a system, nullifying the benefits quantum correlations provide. Indeed, environment-induced decoherence has portrayed for years the role of uninvited (and undesirable) guest in communication schemes, quantum cryptography and quantum information in general, and has been identified as the ultimate obstacle to reliable quantum processing of information. Nevertheless, in the recent years, it has been recognized that the action of an environment on a system may also have some non-detrimental effects, at least for a transient. Indeed, non-trivial spectral structures and memory effects [10–13] may induce recoherence and revivals of quantum features. For this reason, more attention has been paid to studying the effects of noise on the dynamics of the system, so to exploit decoherence or dissipation phenomena to specific goals, within the context of environment engineering [14, 15].

Along with quantum correlations, in the last decade a new figure of merit has emerged as a potential resource for quantum technology: non-Markovianity. Non-markovianity is properly defined in classical theory, but its extension to the quantum world is a challenging task and still is object of discussion. Indeed, many different definitions of quantum non-Markovianity have been provided during the years [16–22], yet neither of these fully recovers the sense of the classical definition. Qualitatively, the term "non-Markovian" is commonly used to address the dynamics of open systems that exhibit memory effects in terms of recoherence or revivals of quantum correlations. Examples of such phenomena occur in biological, solid-state systems [23–30], mechanical oscillators and harmonic lattices [31–39]. For all these systems, the Born-Markov approximation leading to Lindblad form Markovian master equations becomes too sketchy and does not lead to a correct description of the dynamics, as a more detailed characterization of the environment, including the spectral structure and the inherent memory effects, is required. Besides, there is evidence that non-Markovian open quantum systems [40–44] can be useful for quantum technology [45], accomplishing tasks unachievable with Markovian processes [46–49]. However, whether non-Markovianity stands as a general pure resource for enhancing the efficiency of quantum protocols or computation, it is still subject of open debate.

A precise characterization of the vast range of noise-induced phenomena and a full understanding of interaction mechanisms are essential for experimental implementations: on one hand, individuating regimes of recoherence or preservation of quantumness is the first step towards implementation of reliable communication protocols; on the other hand, decoherence may be exploited to specific tasks, such as preparation of arbitrary quantum states [50, 51]. Historically, the problem of noise characterization is tackled down by performing direct measurements on the environment, to the purpose of tracing back to its spectral properties. Alternatively, noise can be characterized indirectly, looking at its effects on the properties of quantum systems. Probing an environment by the use of small quantum systems is convenient for many reasons: firstly, the features of a complex and large environment may be explored by just analyzing a system with a small number of degrees of freedom; secondly, the use of quantum probes allows to assess physical quantities that are not accessible by direct measurements. The proper mathematical tools for indirect noise characterization is provided by quantum estimation [52–55] and quantum discrimination [56] theories. The former allows to infer the value of an unknown parameter with ultimate precision; the latter permits to distinguish two environmental scenarios within a certain tolerance, given a set of measurements performed on the probe.

There are two main paradigms to describe the dynamics of open quantum systems: on the one hand, one may look at system and enviroment as a single global quantum system whose evolution is governed by an overall unitary operator. Upon tracing out the environment' degrees of freedom, one then obtains the dynamics of the system. On the other hand, one may consider the open quantum system under the action of external random forces, i.e. coupled to a stochastic classical field. Here the partial trace is substituted by the average over the different realizations of the stochastic field. While the system-enviroment approach is more fundamental in nature, the approximations employed to achieve manageable dynamical equations often preclude a detailed description of the dynamics. Indeed, systems of interest for quantum technology generally interact with complex environments, with many degrees of freedom, and a fully quantum description may be challenging or even unfeasible. In these situations, classical stochastic modeling of the environment represents a valid and reliable alternative. In fact, it has been shown that for certain system-environment interactions a classical description can be found that

is completely equivalent to the quantum description [57–62]. Besides, there are various experimental evidences that many quantum systems of interest interact with classical forms of noise, typically Gaussian noise [63–65].

This PhD dissertation collects my personal contribution to the analysis and understanding of the role played by classical noise in affecting the dynamics of the correlations of a quantum system, paying serious attention to the overlap between the stochastic approach and the full quantum portrait. I consider a quantum harmonic oscillator coupled to a stochastic classical field, focusing the attention on two distinct decoherence mechanisms acting on the system, phase diffusion and dissipation, looking for regimes in which the stochastic approach successfully overtakes a full quantum description of these physical phenomena. Moreover, I address decoherence and non-Markovianity induced by external noise. As a first, case, I analyze the dynamics of quantumness of a single quantum harmonic oscillator initially prepared in a maximally nonclassical state and interacting with a classical noise. The dynamics of the system is ruled by a stochastic time dependent Hamiltonian describing energy transfer to and from the environment. As a second case, I address the study of the performance of phase communication channels where information is encoded on the quantum state of the system and then properly retrieved after the system has suffered stochastic dephasing. As a third case, I consider two quantum harmonic oscillators interacting with classical noise, addressing the effect of the environment fluctuations on quantum correlations such as entanglement and discord and exploring the connection between non-Markovianity and possible evidence of backflow of information from the environment into the system. Moreover, I describe the effects of both local and common environment scenarios: in the former, each oscillator is coupled to a separate stochastic field, while in the latter both oscillators interact with a common classical source of noise. Finally, I design a proper strategy to distinguish what classical noise a probe quantum system suffers, using the quantum correlations of an entangled state of two harmonic oscillators as a resource for discrimination.

The thesis is organized as follows:

- In chapter 1, I review the basic elements and terminology of quantum mechanics needed for a full comprehension of the content of this thesis. Then I discuss the concept of non-Markovianity and introduce the tools of quantum discrimination theory.
- In chapter 2 I review the basic concepts about stochastic processes, with a focus on Gaussian processes. In particular, I analyze in full detail the physically meaningful Ornstein-Uhlenbeck process.
- In chapter 3 I introduce my contribution to the characterization of stochasic interactions, paying attention to the working regimes where a full quantum description of a system-environment interaction may be substituted by an effective classical (stochastic) one. In particular, I address the case of stochastic phase diffusion and stochastic dissipation.
- In chapter 4 I address the study of both the dynamics of quantumness of highly nonclassical states facing decoherence in a dissipative environment and the channel capacity of a phase-keyed comminication channel in presence of stochastic phase diffusion, making a connection between the appearance of revivals of quantum features and the characteristics of the stochastic field.
- In chapter 5 I address the dynamics of entanglement and discord for two harmonic oscillators interacting with either separate or common stochastic fields and exam-

ine the connection between non-Markovianity and revivals of correlations, usually considered a sign of backflow of information from the environment to the system.

- In chapter 6 I address the problem of designing a proper protocol to successfully discriminate whether a two-mode quantum systems is affected by noise on a local or global scale.

List of Publications

Refereed publications

1. J. Trapani, M. Bina, S. Maniscalco, M.G.A. Paris,
   Collapse and Revivals of Quantum Coherence for a Harmonic Oscillator interacting with a Classical Fluctuating Environment,
   Phys. Rev. A **91**, 022113 (2014).

2. J. Trapani, B. Teklu, S. Olivares, M.G.A. Paris,
   Quantum Phase Communication Channels in the Presence of Static and Dynamical Phase Diffusion,
   Phys. Rev. A **92**, 012317 (2015).

3. B. Teklu, J. Trapani, S. Olivares, M.G.A. Paris,
   Noisy Quantum Phase Communication Channels,
   Phys. Scr. **90**, 074027 (2015).

4. J. Trapani, M.G.A. Paris,
   Nondivisibility versus Backflow of Information in understanding Revivals of Quantum Correlations for continuous-variable Systems interacting with Fluctuating Environments,
   Phys. Rev. A **93**, 042119 (2016).

5. J. Trapani, M.G.A. Paris,
   Entanglement as a Resource for Discrimination of Classical Environments,
   Phys. Lett. A **381**, 245 (2016).

Acknowledgments

These three years went by in the blink of an eye.

I want to thank my supervisor Matteo, for his kindness and infinite patience. A huge thanks goes to the former and present elements of the research group in Milan I have met in these years. It would have been easy to name them three years ago, now they are too many.

A special thanks goes to my roommates, and now friends, Ciccio, Alessandro e Antonio.

I want to thank all my friends over the world: a special mention goes to Gabriele, Domenico, Francesco, Ivan, Tony. Sono *Cose Raffinate*.

Thanks to my parents, Adriana e Camillo, for their unconditional support and love.

Finally, thanks to Elena, no words needed.

CHAPTER 1

Preliminaries

This chapter gathers all the preliminary notions needed to a full understanding of the results of this research project. In the following, the reader finds a rapid and not yet exhaustive review of key concepts of quantum optics and becomes familiar with the notation used through this work.

1.1 Introduction to quantum mechanics

1.1.1 Basic quantum mechanics

In classical mechanics, a system is described by some observable quantities, e.g. energy, position, momentum, whose dynamics is well defined by canonical equations of motion. Indeed, such description entails in its formulation a lot of assumptions that are inherently true in a classical framework but need to be disregarded in a quantum context: for instance, in classical mechanics it holds true that the measurement process does not perturb the system and that all measurable quantities may be simultaneously performed. In the quantum framework, none of these is correct. The measurement process needs to be reconceived and the properties of the system, revealed by typically non-commuting measurements, need to be considered as some information concealed within the system itself. For this reason in quantum mechanics [66] one resorts to the concept of state, a sort of container of all the information required to fully describe a system as an isolated element.

From a mathematical point a view, a state is represented by a normalized vector $|\psi\rangle$ and all the possible states of the system form a complex vector space $\mathcal{M}$ with inner product, that is, a Hilbert space. Since $\mathcal{M}$ is a vector space, a superposition principle holds, that is, any linear combination of states is also a state:

$$|\psi\rangle = \sum_{n=1}^{N} c_n |\psi_n\rangle, \tag{1.1}$$

where the quantities $|c_n|^2$ are interpreted as probabilities of finding the system respectively in state $|\psi_n\rangle$ and therefore obey the constrain

$$\sum_{n_1}^{N} |c_n|^2 = 1. \tag{1.2}$$

The superposition principle not only confers to quantum states a probabilistic representation but enables interference phenomena, that truly represent the authentic source of innovation in quantum mechanics, along with the wave-particle dualism.

In classical mechanics, the system dynamics is related to the evolution of its observable quantities. In the quantum framework, the evolution of a system is described by a time-dependent state $|\psi(t)\rangle$. The dynamics of the quantum state obeys the Schrödinger equation

$$i\hbar\frac{\partial}{\partial t}|\psi(t)\rangle = H(t)|\psi(t)\rangle \tag{1.3}$$

where $H(t)$ is the Hamiltonian operator. The Schrödinger equation is linear and homogeneous, therefore it exists a linear operator $U(t,t_0)$ that turns an initial state $|\psi(t_0)\rangle$ at time t_0 into

$$|\psi(t)\rangle = U(t,t_0)|\psi(t_0)\rangle. \tag{1.4}$$

$U(t,t_0)$ is called time evolution operator, it is unitary and satisfies the following set of properties

$$U(t,t) = \mathbb{I}, \tag{1.5a}$$
$$U(t,t'') = U(t,t')U(t',t''), \tag{1.5b}$$
$$U^\dagger(t,t') = U(t',t). \tag{1.5c}$$

The time evolution operator drives a quantum system from a state to an other and is stricty related to the Hamiltonian operator. It is easy to prove that $U(t)$ obeys a Schrödinger-like equation as well,

$$i\hbar\frac{\partial}{\partial t}U(t,t_0) = H(t)U(t,t_0). \tag{1.6}$$

Taking into account the initial condition $U(t_0,t_0) = \mathbb{I}$, one finds the solution of Eq. 1.6,

$$U(t,t_0) = \mathbb{I} - \frac{i}{\hbar}\int_{t_0}^{t} H(t')U(t',t_0)dt', \tag{1.7}$$

which is only formal, as the evolution operator appears on both sides of the equation.

An explicit solution may be found only in a small number of situations. For instance, when the Hamiltonian operator does not depend on time, the time evolution operator is $U(t) = \exp(-iH(t-t_0)/\hbar)$. In all the other situations, ths solution can be recast in the so-called Dyson series

$$\begin{aligned} U(t) &= \mathbb{I} - i\int_0^t H(t_1)dt_1 + \left(-\frac{i}{\hbar}\right)^2\int_{t_0}^t dt_1\int_{t_0}^t dt_2 H(t_1)H(t_2) + \ldots = \\ &= \mathbb{I} + \sum_{n=1}^{\infty}\frac{1}{n!}\left(-\frac{i}{\hbar}\right)^n\int_{t_0}^t dt_1\cdots\int_{t_0}^t dt_n\mathcal{T}[H(t_1)\cdots H(t_n)], \end{aligned} \tag{1.8}$$

where $\mathcal{T}$ denotes the time ordering operator. The Dyson series is obtained by iterating Eq. 1.7 and can be recast in a more compact way:

$$U(t,t_0) = \mathcal{T}\left\{\exp\left(-i\int_0^t H(t')dt'\right)\right\}. \tag{1.9}$$

Time ordering is essential as long as the Hamiltonian is time-dependent, the only exception being when the Hamiltonian operator function is self-commuting at different times,

that is, $[H(t_1), H(t_2)] = 0$. In that case, the evolution operator assumes a simpler form as most of the terms of the Dyson series vanish.

An explicit form of the time evolution operator may be obtained under specific conditions by means of the Magnus expansion [67, 68]. Magnus' theorem implies that the time evolution operator for linear dynamics can be recast in the form $U(t) = \exp[\Omega(t)]$ where $\Omega(t)$ satisfies the differential equation

$$\frac{d\Omega(t)}{dt} = \sum_{n=0}^{\infty} \frac{B_n}{n!} \mathrm{ad}_{\Omega}^{n} A \tag{1.10}$$

where B_n are the Bernoulli numbers, $A = -iH/\hbar$ and the adjoint is defined recursively by

$$\mathrm{ad}_{\Omega}^{k+1} A = [\Omega, \mathrm{ad}_{\Omega}^{k} A] \quad \text{with} \quad \mathrm{ad}_{\Omega}^{0} A = A. \tag{1.11}$$

Expanding in series the operator function $\Omega(t)$ and using the notation $H(t_k) = H_k$, the first terms of the series read

$$\Omega(t) = \sum_{k=1}^{\infty} \Omega_k(t), \tag{1.12a}$$

$$\Omega_1(t) = -\frac{i}{\hbar} \int_{t_0}^{t} dt_1 H_1, \tag{1.12b}$$

$$\Omega_2(t) = -\frac{1}{2\hbar^2} \int_{t_0}^{t} dt_1 \int_{t_0}^{t_1} dt_2 [H_1, H_2], \tag{1.12c}$$

$$\Omega_3(t) = \frac{i}{6\hbar^3} \int_{t_0}^{t} dt_1 \int_{t_0}^{t_1} dt_2 \int_{t_0}^{t_2} dt_3 \{[H_1, [H_2, H_3]] + [[H_1, H_2], H_3]\}. \tag{1.12d}$$

If the two-time commutator $[H(t_1), H(t_2)]$ is proportional to the identity, as it will happen in one of the models presented afterwards, then only the first two terms of the series survive, simplifying the final form of the evolution operator.

1.1.2 The measurement process

The measurement process assumes a deeper meaning in the quantum framework than it used to do in the classical one. If in classical mechanics measuring a system allows to reveal its properties without perturbing it, in a quantum scenario the state of the system is irremediably affected by the measurement, which acts as an irreversible operation on the state.

The mathematical representation of a quantum measurement is a set of measurement operators $\{M_i\}$, acting on the state space of the measured system. Each M_i refers to an outcome m_i of the measurement that occurs with probability

$$p_i = \langle \psi | M_i^{\dagger} M_i | \psi \rangle \tag{1.13}$$

where the measurement is supposed to act istantaneously on the initial state $|\psi\rangle$. The conservation of probability requires a completeness relation

$$\sum_i M_i^{\dagger} M_i = \mathbb{I}. \tag{1.14}$$

The post-measurement state when M_i acts on the system is

$$|\psi\rangle \to \frac{M_i|\psi\rangle}{\sqrt{\langle\psi|M_i^\dagger M_i|\psi\rangle}}. \tag{1.15}$$

A particular class of measurements is known as *projective measurements*. A projective measurement is described by an Hermitian operator acting on the state space of the measured system. The Hermitian operator admits a spectral decomposition

$$M = \sum_i m_i |i\rangle\langle i| = \sum_i m_i P_i, \tag{1.16}$$

where $|i\rangle$ is the eigenvector corresponding to eigenvalue $m_i = \langle\psi|M_i|\psi\rangle$ and P_i is the projector that leads the input state to the subspace associated to that very eigenvalue.

Projector operators P_i satisfy the orthogonality condition $P_iP_j = \delta_{ij}P_I$ and the completeness relation $\sum_i P_i = \mathbb{I}$. The expected value of each projector P_i measures the probability p_i defined in 1.13 and the average value of the observable M then reads

$$\langle M\rangle = \sum_i m_i p_i = \sum_i m_i \langle\psi|P_i|\psi\rangle. \tag{1.17}$$

When a projective measurement is performed onto the system, the output state will always be an eigenstate of the measurement M, which implies there is no superposition between two different output states. This holds true for projective measurements, but it is not true in general.

In the most general case, the measurement process is represented by a set of positive-semidefinite operators $\{\Pi_d\}$

$$\langle\psi|\Pi_d|\psi\rangle \geq 0, \quad \text{for all } |\psi\rangle, \tag{1.18}$$

that forms a resolution of the identity

$$\sum_d \Pi_d = \mathbb{I}. \tag{1.19}$$

The measurement process is therefore called *positive operator valued measure* or POVM. Unlike projective measurements, there is no limitation on the number of elements a POVM can be made of. Moreover, there is no requirement the elements E_d be mutually orthogonal, which implies that the outputs of the measurement are not orthogonal either.

1.1.3 Density operator

As long as the state of a system is described as a vector, the state is fully determined. However, in practice, the state of a quantum system is often not perfectly known and such lack of information prevents from defining a state in terms of vector. In these situations, the system is said to be in a statistical mixture of states $|\psi_i\rangle$ with probabilities p_i. The mathematical proper tool to describe statistical mixtures is the density operator ρ

$$\rho = \sum_i p_i |\psi_i\rangle\langle\psi_i|, \tag{1.20}$$

where the states $|\psi_i\rangle$ not necessarily orthogonal.

Any complex matrix ρ_{ij} that satisfies the following properties is an eligible representation of a density operator ρ:

1. ρ is Hermitian, that is, $\rho_{ij} = \rho^*_{ji}$;

2. the density matrix has unit trace, Tr[ρ] = 1;

3. ρ is a non-negative operator, that is, its expectation value over any vector $|\psi\rangle$ satisfies $\langle\psi|\rho|\psi\rangle \geq 0$. Of course, the eigenvalues of the density matrix are non-negative.

If one of the p_i is unity, the density operator reduces to a single projector, $\rho = |\psi\rangle\langle\psi|$ and the state of the system is perfectly known. In this case, the state is said to be *pure* and satisfies the condition $\rho^2 = \rho$, which implies $\text{Tr}[\rho^2] = 1$.

Indeed, the condition Tr[ρ^2] = 1 is not satisfied by any statistical mixture of states, so a quantum system is said to be in a *mixed* state if $\text{Tr}[\rho^2] < 1$. It is straightworward to define the purity of a system as $\mu(\rho) = \text{Tr}[\rho^2]$, such that a system is pure only if $\mu(\rho) = 1$.

In the density operator formalism, the dynamics of a quantum system and the measurement process slightly change: the dynamics of the system is now described by a time-dependent density operator, its evolution still being conveyed by the time evolution operator, through the relation

$$\rho(t) = U(t, t_0)\rho(t_0)U^\dagger(t, t_0). \tag{1.21}$$

Besides, the probabilities defined in Eq. 1.13 read

$$p_i = \text{Tr}[M_i \rho M_i^\dagger], \tag{1.22}$$

while the measurement maps the initial density operator ρ into a statistical ensemble of states $\{p_i, \rho'_i\}$ given by

$$\rho'_i = \frac{M_i \rho M_i^\dagger}{\text{Tr}[M_i \rho M_i^\dagger]}. \tag{1.23}$$

Finally, the average value of the operator M reads

$$\langle M \rangle = \text{Tr}[\rho M]. \tag{1.24}$$

1.1.4 Bipartite systems

The density operator of a composite system is defined in a Hilbert space which is the tensor product of the vector spaces of each subsystem. In the case of a bipartite system, the Hilbert space then is $\mathcal{H} = \mathcal{H}_\text{A} \otimes \mathcal{H}_\text{B}$ and the density operator describes the state of the joint subparts (usually referred as Alice and Bob). However, in many situations it is interesting to describe the state of the subsystems and the mathematical tool needed is called *reduced density operator*, which is defined as

$$\rho_\text{A} = \text{Tr}_\text{B}[\rho] \tag{1.25a}$$
$$\rho_\text{B} = \text{Tr}_\text{A}[\rho] \tag{1.25b}$$

where $\text{Tr}_j[\cdot]$ indicates the partial trace over the j-th subsystem.

1.1.5 Open quantum systems

A realistic quantum system can hardly be pictured as isolated: indeed, the interaction with the surrounding environment alters its dynamics and creates system-environment correlations that prevent from describing the system as *closed*. The system is inextricably correlated to the environment and can be then regarded as an *open* subpart of the system-environment complex, but its dynamics fails to be described by means of unitary evolutions.

The theory of open quantum systems provides the necessary tools to describe the dynamics of an open system. In this framework, a system S and the environment B form a composite system, whose Hilbert space is $\mathcal{H} = \mathcal{H}_S \otimes \mathcal{H}_B$. As a whole, the composite system is described as a density operator, whose dynamics is ruled by a unitary evolution. Conversely, the evolution of the reduced density operator representing the quantum system may be retrieved from the evolution of the global state as

$$\rho' = \mathcal{E}(\rho) = \mathrm{Tr}_B[U(\rho \otimes \rho_B)U^\dagger]. \tag{1.26}$$

where $\rho \otimes \rho_B$ is the factorized initial state of the global system.

$\mathcal{E}$ is called *quantum dynamical map* and describes the dynamics of the reduced system alone. A dynamical map is linear and it is chosen to be trace-preserving. In order to keep the positivity of density matrices in presence of entanglement with another extra-system, a dynamical map $\mathcal{E}$ is also required to be completely positive, that is, its extension $\mathcal{E} \otimes \mathbb{I}_k$ to any larger k-dimension space is a positive quantum map as well.

Complete positive maps admit the so-called Kraus representation [69]

$$\mathcal{E}(\rho) = \sum_i K_i \rho K_i^\dagger \tag{1.27}$$

where K_i, called Kraus operators, act on the state space $\mathcal{H}_S$. These operators satisfy the completeness condition $\sum K_i^\dagger K_i = \mathbb{I}$ and each K_i is a quantum operation, so the quantum map may be regarded as a sum of quantum operations acting on the input state.

A dynamical map represents the solution of a differential equation, named *quantum master equation*. Quantum master equations rule the evolution of reduced density operators and are directly derived from a microscopic quantum model of interaction between the system and the environment. An important class of master equations contains those that can be recast in the following form [70]:

$$\frac{d}{dt}\rho(t) = -i[H(t), \rho(t)] + \sum_k \gamma_k(t)\left[L_k(t)\rho(t)L_k^\dagger(t) - \frac{1}{2}\{L_k^\dagger(t)L_k(t), \rho(t)\}\right] \tag{1.28}$$

where $\{O_1, O_2\} = O_1O_2 + O_2O_1$ and L_k are operators acting on the system Hilbert space and depend on the specific model of interaction. Within this class, it is possible to find both Markovian and non-Markovian master equations, depending on the behaviour of the time-dependent coupling functions $\gamma_k(t)$: the strong connection between the behaviour of the coupling functions and the concept of non-Markovianity will be explored later in this chapter.

1.2 Quantum optics in phase space

The harmonic oscillator represents, along with the qubit, the most important concept in quantum mechanics and quantum optics, as it may represent many physical systems,

e.g. phonons, photons, bosonic systems in general. All along this dissertation, I present models where the quantum system interacting with the environment is either a single harmonic oscillator or a couple of bosonic modes. In the following, a short review [71] of the basic notation about bosonic systems and phase space representation.

1.2.1 Basic notation

Each bosonic mode $k = 1, \dots, n$ of a n-partite system is described by annihilation and creation operators $\hat{a}_k$ and $\hat{a}_k^\dagger$, satisfying the commutation relations $[\hat{a}_j, \hat{a}_k^\dagger] = \delta_{kl}$. The free Hamiltonian of n bosonic modes in natural units is given by

$$H = \sum_{k=1}^{n} \left(\hat{a}_k^\dagger \hat{a}_k + \frac{1}{2} \right). \tag{1.29}$$

It is convenient to define the position- and momentum-like operators as

$$\hat{q}_k = \frac{1}{\sqrt{2}}(\hat{a}_k + \hat{a}_k^\dagger) \quad \text{and} \quad \hat{p}_k = \frac{1}{i\sqrt{2}}(\hat{a}_k - \hat{a}_k^\dagger), \tag{1.30}$$

where the commutation relations $[\hat{q}_j, \hat{p}_k] = i\delta_{jk}$ can be rewritten in the compact form

$$[\hat{R}_j, \hat{R}_k] = i\Omega_{jk} \tag{1.31}$$

where the quadrature vector $\hat{\boldsymbol{R}} = (\hat{q}_1, \hat{p}_1, \dots, \hat{q}_n, \hat{p}_n)$ was introduced along with the symplectic matrix

$$\boldsymbol{\Omega} = \bigoplus_{k=1}^{n} \boldsymbol{\omega} \qquad \boldsymbol{\omega} = \begin{pmatrix} 0 & 1 \\ -1 & 0 \end{pmatrix}. \tag{1.32}$$

1.2.2 Characteristic function and quasi-probability functions

The density operator ρ uniquely defines the characteristic function

$$\chi[\rho](\boldsymbol{\Lambda}) = \mathrm{Tr}[\rho \exp\{-i\boldsymbol{\Lambda}^T \boldsymbol{\Omega} \hat{\boldsymbol{R}}\}] \tag{1.33}$$

The characteristic function describes the state of the system by means of its full statistics, i.e. the moments of any order. Within the characteristic function it is possible to distinguish the displacement operator $D(\boldsymbol{\Lambda})$ with $\boldsymbol{\Lambda} = \left(\lambda_x^{(1)}, \lambda_y^{(1)}, \dots, \lambda_x^{(n)}, \lambda_y^{(n)}\right)$:

$$D(\boldsymbol{\Lambda}) = \exp\{-i\boldsymbol{\Lambda}^T \boldsymbol{\Omega} \hat{\boldsymbol{R}}\} = \bigotimes_{k=1}^{n} D_k(\lambda_k) \tag{1.34}$$

where $D_k(\lambda_k) = \exp\{\lambda_k \hat{a}_k^\dagger - \lambda_k \hat{a}_k\}$ with $\lambda_k = \lambda_x^{(k)} + i\lambda_y^{(k)}$.

The characteristic function can be Fourier-transformed, obtaining the so called Wigner function

$$W[\rho](\boldsymbol{X}) = \frac{1}{(2\pi^2)^n} \int d^{2n}\boldsymbol{\Lambda} \exp\{i\boldsymbol{\Lambda}^T \boldsymbol{\Omega} \boldsymbol{X}\} \chi[\rho](\boldsymbol{\Lambda}) \tag{1.35}$$

where $\boldsymbol{X} = (x_1, y_1, \dots, x_n, y_n)^T$.

The Wigner function is a phase space distribution of the quantum state ρ. It is not the only possible one: indeed, it is possible to define a whole class of phase space distributions using a more general definition

$$W_s[\rho](\boldsymbol{X}) = \frac{1}{(2\pi^2)^n}\int d^{2n}\boldsymbol{\Lambda}\exp\left\{\frac{1}{2}s|\boldsymbol{\Lambda}|^2 + i\boldsymbol{\Lambda}^T\boldsymbol{\Omega}\boldsymbol{X}\right\}\chi[\rho](\boldsymbol{\Lambda}) \tag{1.36}$$

where s addresses the order of the Wigner function. In particular, $s = 0$ returns the Wigner function of Eq. 1.35, while $s = 1, -1$ define respectively the Husimi-Q and the Glauber-P function. All these distributions are called quasi-probability functions: they are Fourier-transforms of characteristic functions, as probability distributions in classical theory, but are not positive in general. In particular, the Glauber-P function $P(\alpha)$ is the distribution of a state ρ over the basis of coherent states:

$$\rho = \int d^2\alpha P(\alpha)|\alpha\rangle\langle\alpha| \tag{1.37}$$

where $d^2\alpha = d\Re e(\alpha)d\Im m(\alpha)$.

$P(\alpha)$ resembles a probability distribution but fails to be interpreted as a classical one, as it may assume negative values or even be singular. The Glauber-P function is used to address in a mathematical way the quantum-to-classical transition, as it will be shown in Chapter 4.

1.2.3 Gaussian states

Gaussian states play a fundamental role in quantum information and quantum optics for two reasons: on one hand, many states used in modern laboratories, e.g. the vacuum state, coherent states, single- and two-mode squeezed states, belong to the class of gaussian states; on the other hand, the evolutions achievable with quantum technology are described by linear or quadratic Hamiltonians which preserve gaussianity. In the following, a short review of the basic properties and useful notation about gaussian states.

The formalism of the characteristic and Wigner functions becomes extremely fruitful when dealing with gaussian states. By definition, the state of n bosonic mode system is said to be gaussian if its characteristic function is gaussian, that is,

$$\chi[\rho](\boldsymbol{\Lambda}) = \exp\{-\frac{1}{2}\boldsymbol{\Lambda}^T\boldsymbol{\Omega}\boldsymbol{\sigma}\boldsymbol{\Omega}^T\boldsymbol{\Lambda} - i\boldsymbol{\Lambda}^T\boldsymbol{\Omega}\langle\hat{\boldsymbol{R}}\rangle\} \tag{1.38}$$

where the elements of the covariance matrix $\boldsymbol{\sigma}$ are defined as

$$\sigma_{jk} = \frac{1}{2}\langle\hat{R}_j\hat{R}_k + \hat{R}_k\hat{R}_j\rangle - \langle\hat{R}_j\rangle\langle\hat{R}_k\rangle. \tag{1.39}$$

The positivity of the density matrix ρ imposes a constraint on the the covariance matrix $\boldsymbol{\sigma}$

$$\boldsymbol{\sigma} + \frac{i}{2}\boldsymbol{\Omega} \geq 0, \tag{1.40}$$

where $\boldsymbol{\Omega}$ is defined in Eq.1.32. Of course, gaussian states have a Wigner function which is gaussian as well and reads

$$W[\rho](\boldsymbol{X}) = \frac{\exp\{-\frac{1}{2}(\boldsymbol{X} - \langle\hat{\boldsymbol{R}}\rangle)^T\boldsymbol{\sigma}^{-1}(\boldsymbol{X} - \langle\hat{\boldsymbol{R}}\rangle)\}}{\pi^n\sqrt{\det[\boldsymbol{\sigma}]}}. \tag{1.41}$$

Gaussian states are described by their first and second order-moments, i.e. first-moments vector and covariance matrix. However, what really has put gaussian states on the crest of a wave is that gaussianity is preserved in many quantum optical, optomechanical and micromechanical systems, where Hamiltonians are linear and bilinear in the modes, that is

$$H = \sum_{k=1}^{n} g_k^{(1)} \hat{a}_k^\dagger + \sum_{k \geq l=1}^{n} g_{kl}^{(2)} \hat{a}_k^\dagger \hat{a}_l + \sum_{k,l=1}^{n} g_{kl}^{(3)} \hat{a}_k^\dagger \hat{a}_l + h.c., \tag{1.42}$$

where the three building blocks are the generators of unitary symplectic operations corresponding to displacement $(g_k^{(1)})$, phase shifts or two-mode mixing $(g_{kl}^{(2)})$ and single or two-mode squeezing $(g_{kl}^{(3)})$.

An important theorem due to Williamson states that every covariance matrix can be diagonalized through a symplectic transformation or, equivalently, every gaussian state can be transformed into a thermal state by a symplectic trasnformation. Mathematically, a $2n \times 2n$ covariance matrix $\boldsymbol{\sigma}$ can always be written as

$$\boldsymbol{\sigma} = \boldsymbol{S}\boldsymbol{W}\boldsymbol{S}^T, \tag{1.43a}$$

$$\rho = U_S \nu_{th} U_S^\dagger \tag{1.43b}$$

where ν_{th} is a thermal state, U_S is a symplectic operator with corresponding matrix $\boldsymbol{S}$ and $\boldsymbol{W} = \bigoplus_{k=1}^{n} d_k \mathbb{I}_2$ is a diagonal matrix. The set $\{d_k\}$ contains the moduli of the eigenvalues of $i\boldsymbol{\Omega}\boldsymbol{\sigma}$, namely, the symplectic eigenvalues of $\boldsymbol{\sigma}$. The Williamson theorem is very meaningful: $\boldsymbol{W}$ is the covariance matrix of a n-mode thermal state, provided that $N_k = d_k - \frac{1}{2}$ is the average number of photons in the k-th mode. Once again, the positivity of the density operator ρ imposes that $\boldsymbol{W}$ has to be a physical matrix, that is

$$N_k \geq 0, \quad d_k \geq \frac{1}{2}, \quad \forall k. \tag{1.44}$$

However, there is no general recipe to retrieve the explicit form of the symplectic matrix $\boldsymbol{S}$, except in a few cases. For instance, in the case of a single-mode gaussian state, the density operator ρ can be always broken down into the following form,

$$\rho = D(\lambda) S(\xi) \nu_{th}(N) S^\dagger(\xi) D^\dagger(\lambda) \tag{1.45}$$

where $S(\xi) = \exp\{\xi(\hat{a}^\dagger)^2 - \xi^* \hat{a}^2\}$ is the squeezing operator and $\nu_{th}(N)$ is the thermal state

$$\nu_{th}(N) = \frac{1}{N} \sum_m \left(\frac{N}{N+1} \right)^m |m\rangle\langle m|. \tag{1.46}$$

Two-mode gaussian states will be largely used in Chapter 5, since the states include the simplest entangled state that may be realized in modern quantum laboratories. To introduce the subject, it is useful to first describe the class of gaussian state with the same amount of entanglement. Such states are mutually connected by local symplectic transformations. The most general two-mode gaussian state is:

$$\boldsymbol{\sigma} = \begin{pmatrix} \boldsymbol{A} & \boldsymbol{C} \\ \boldsymbol{C}^T & \boldsymbol{B} \end{pmatrix} \tag{1.47}$$

where $\boldsymbol{A}$, $\boldsymbol{B}$ and $\boldsymbol{C}$ are 2×2 matrices that define four local symplectic invariant

$$I_1 = \det[\boldsymbol{A}] \quad I_2 = \det[\boldsymbol{B}] \quad I_3 = \det[\boldsymbol{C}] \quad I_4 = \det[\boldsymbol{\sigma}]. \tag{1.48}$$

Every covariance matrix can be reduced to the following standard or normal form:

$$\boldsymbol{\sigma} = \begin{pmatrix} a & 0 & c_1 & 0 \\ 0 & a & 0 & c_2 \\ c_1 & 0 & b & 0 \\ 0 & c_2 & 0 & b \end{pmatrix}, \tag{1.49}$$

where the values of a, b, c_1 and c_2 satisfy the conditions $a^2 = I_1, b^2 = I_2, c_1 c_2 = I_3$ and $(ab - c_1^2)(ab - c_2^2) = I_4$. The symplectic eigenvalues of a generic two-mode covariance matrix of a gaussian state only depends on the symplectic invariants by

$$d_{\pm} = \sqrt{\frac{\Delta(\boldsymbol{\sigma}) \pm \sqrt{\Delta(\boldsymbol{\sigma})^2 - 4I_4}}{2}} \tag{1.50}$$

with $\Delta(\boldsymbol{\sigma}) = I_1 + I_2 + 2I_3$.

A relevant class of gaussian states is composed by the two-mode squeezed thermal states, generated by applying the two-mode squeezing operator to a tensor product of thermal states:

$$\rho_{\text{STS}} = S_2(r)\nu_{th}(\bar{n}_1) \otimes \nu_{th}(\bar{n}_2)S_2^{\dagger}(r). \tag{1.51}$$

$$\boldsymbol{\sigma}_{\text{STS}} = \frac{1}{2}\begin{pmatrix} A\,\mathbb{I}_2 & C\sigma_z \\ C\sigma_z & B\,\mathbb{I}_2 \end{pmatrix}, \tag{1.52}$$

where $\sigma_z = \text{diag}(1, -1)$ is the z Pauli matrix and the parameters A, B, C are given by

$$\begin{aligned} A &= \cosh(2r) + 2\bar{n}_1 \cosh^2 r + 2\bar{n}_2 \sinh^2 r \\ B &= \cosh(2r) + 2\bar{n}_1 \sinh^2 r + 2\bar{n}_2 \cosh^2 r \\ C &= (1 + \bar{n}_1 + \bar{n}_2)\sinh(2r). \end{aligned} \tag{1.53}$$

In particular, the case $\bar{n}_1 = \bar{n}_2 = 0$ defines the twin-beam state (TWB).

Of course, the symplectic $\boldsymbol{S}$ of Eq. 1.43a is at hand in the case of a squeezed thermal state, as it coincides with the two-mode squeezing operator $S_2(r) = \exp\{r\hat{a}^{\dagger}\hat{b} + r\hat{a}\hat{b}^{\dagger}\}$. Moreover, it is possible to find the symplectic operator $\boldsymbol{S}$ for any two-mode gaussian state with covariance matrix $\boldsymbol{\sigma}$, which can be written down as [72]

$$\sigma = A^T \boldsymbol{\nu}(\bar{N}_1, \bar{N}_2)A, \tag{1.54}$$

where $\boldsymbol{\nu}(\bar{N}_1, \bar{N}_2)$ is the covariance matrix of a tensor product of single-mode thermal states with average photon number $\bar{N}_j = N_j - \frac{1}{2}$, while

$$A = S_{loc}(r_1, r_2)R(\xi)S_{tm}R(\eta)S_l \tag{1.55}$$

where S_l is the symplectic that drives the covariance matrix in standard form, $S_{tm}(r) = \text{diag}(e^r, e^{-r}, e^{-r}, e^r)$, $S_{loc}(r_1, r_2) = S(r_1) \oplus S(r_2)$.

1.2.4 Uhlmann Fidelity function

The Uhlmann Fidelity [73] is a very common tool in quantum optics to address how similar two quantum states are and its formal definition is given by

$$\mathcal{F}(\rho_{\text{A}}, \rho_{\text{B}}) = \left[\text{Tr}\sqrt{\sqrt{\rho_{\text{A}}}\rho_{\text{B}}\sqrt{\rho_{\text{A}}}}\right]^2. \tag{1.56}$$

The Uhlmann Fidelity is symmetric, ranges from 0 to 1 and reaches its maximum value if and only if $\rho_{\rm A} = \rho_{\rm B}$. Moreover, it can be used to define the Bures distance $D_B(\rho_{\rm A}, \rho_{\rm B})$ as

$$D_B(\rho_{\rm A}, \rho_{\rm B}) = \sqrt{2\Big[1 - \sqrt{\mathcal{F}(\rho_{\rm A}, \rho_{\rm B})}\Big]}, \tag{1.57}$$

which is a metric on the Hilbert space of the system.

The Uhlmann fidelity in Eq. 1.56 simplifies if one of the state, say, $\rho_{\rm A}$ is pure, $\rho_{\rm A} = |\psi\rangle\langle\psi|$:

$$\mathcal{F}(\rho_{\rm A}, \rho_{\rm B}) = \langle\psi|\rho_{\rm B}|\psi\rangle. \tag{1.58}$$

In addition, an explicit form of the Uhlmann Fidelity for gaussian states may be written in terms of first momenta $\hat{\boldsymbol{R}}$ and covariance matrices $\boldsymbol{\sigma}$. For single mode gaussian states, the Fidelity reads

$$\mathcal{F}(\rho_{\rm A}, \rho_{\rm B}) = \frac{\exp\{-\frac{1}{2}(\hat{\boldsymbol{R}}_{\boldsymbol{1}} - \hat{\boldsymbol{R}}_{\boldsymbol{2}})^T(\boldsymbol{\sigma}_1 + \boldsymbol{\sigma}_2)^{-1}(\hat{\boldsymbol{R}}_{\boldsymbol{1}} - \hat{\boldsymbol{R}}_{\boldsymbol{2}})\}}{\sqrt{\Delta + \delta} - \sqrt{\delta}}, \tag{1.59}$$

with $\Delta = \det[\boldsymbol{\sigma}_1 + \boldsymbol{\sigma}_2]$ and $\delta = 4\,\Pi_{k=1}^2(\det[\boldsymbol{\sigma}_k] - \frac{1}{4})$.

For two-mode gaussian states, the Fidelity reads

$$\mathcal{F}(\rho_{\rm A}, \rho_{\rm B}) = {\rm Tr}[\rho_1\rho_2](\sqrt{\mathcal{X}}\sqrt{\mathcal{X} - 1})^2 \tag{1.60}$$

where $\mathcal{X} = 2\sqrt{\mathcal{A}} + 2\sqrt{\mathcal{B}} + \frac{1}{2}$ and

$$\mathcal{A} = \frac{\det[\boldsymbol{\Omega}\boldsymbol{\sigma}_1\boldsymbol{\Omega}\boldsymbol{\sigma}_2 - \frac{1}{4}\mathbb{I}_4]}{\det\boldsymbol{\sigma}_1 + \boldsymbol{\sigma}_2}, \quad \mathcal{B} = \frac{\det[\boldsymbol{\sigma}_1 + \frac{i}{2}\boldsymbol{\Omega}]\det[\boldsymbol{\sigma}_2 + \frac{i}{2}\boldsymbol{\Omega}]}{\det[\boldsymbol{\sigma}_1 + \boldsymbol{\sigma}_2]}. \tag{1.61}$$

1.3 Quantum correlations

Quantum systems may feature non-classicality in many guises. On one hand, quantumness may lie in the state of the system, as there exist states with no classical counterpart, e.g., Fock states or Schrödinger cat states; on the other hand, quantum systems may feature nonclassical correlations: entanglement and quantum discord fall in this category.

Entanglement addresses the correlations of interacting systems in terms of separability and has stood for many years as the sole acknowledged form of nonclassical correlation. However, disentangled states may exhibit nonclassical behaviour based on other concepts apart from separability. For instance, the quantum discord measures correlations that are not reproducible by local operations or classical communication and may be non-zero even for separable states. In the following, I introduce the three types of correlations involved in this dissertation: mutual information, entanglement and quantum discord.

1.3.1 Mutual information

The mutual information is a form of classical correlation, extremely useful in communication protocols: in fact, the mutual information was first introduced in the context of information theory in order to quantify the amount of knowledge shared by two partners, the sender Alice and the receiver Bob, when sending information over a channel.

Alice holds information in terms of a random variable X and its probability distribution $p(x)$. The measure of uncertainty about the random variable X is naturally described by the Shannon entropy

$$S(X) = -\sum_x p(x) \log_2 p(x) \tag{1.62}$$

which is additive, always positive and equals to zero when the probability distribution is singular. The Shannon entropy can easily be extended to the case of two random variables X, Y and reads

$$S(X,Y) = -\sum_{x,y} p(x,y) \log_2 p(x,y), \tag{1.63}$$

where $p(x,y)$ is the joint probability distribution of the two random variables. If X ad Y are independent, $S(X,Y) = S(X) + S(Y)$ as an immediate consequence of the additive property of the Shannon entropy. If X and Y are not independent, gaining information upon X removes uncertainty from Y and viceversa. The remaining uncertainty is given by the conditional entropy

$$S(X|Y) = -\sum_{x,y} p(x,y) \log_2 [p(x|y)] \tag{1.64}$$

where $p(x|y) = \frac{p(x,y)}{p(y)}$ is the conditional probability. Of course, joint and conditional entropies are related: the amount of uncertainty about the couple of random variables X and Y can always be seen as the uncertainty of X plus the unceartainty of Y once X is known, that is

$$S(X,Y) = S(X) + S(Y|X). \tag{1.65}$$

Furthermore, the sum of the uncertainties of two random variables always exceeds their joint entropy. The difference between these quantities is called mutual information

$$I(X:Y) = S(X) + S(Y) - S(X,Y) \tag{1.66}$$

and assesses the amount of correlation between two random variables. If X and Y are independent, the mutual information is zero, that is, measuring X does not reveal any information about Y and viceversa.

All the expressions above have a quantum analog. In the quantum theory, the information is stored in the density operator ρ, which takes over the probability distribution. The quantum version of the Shannon entropy is called von Neumann entropy and is given by

$$S(\rho) = -\mathrm{Tr}[\rho \log_2 \rho]. \tag{1.67}$$

The von Neumann and Shannon entropy share the same properties.

In a similar way, the quantum conditional entropy measures the information gained from ρ_{AB} when ρ_{B} is known:

$$S(\rho_{\mathrm{A}}|\rho_{\mathrm{B}}) = S(\rho_{\mathrm{AB}}) - S(\rho_{\mathrm{B}}) \tag{1.68}$$

Finally, the quantum mutual information can be written as

$$I(\rho_{\mathrm{A}} : \rho_{\mathrm{B}}) = S(\rho_{\mathrm{A}}) + S(\rho_{\mathrm{B}}) - S(\rho_{\mathrm{A}}, \rho_{\mathrm{B}}). \tag{1.69}$$

In the context of communication channels, the mutual information is used to assess the efficiency of a communication protocol, that is, the strategies chosen by the two parties to encode some information on a quantum state and decode it by a proper measurement. The maximum amount of information achievable is called *channel capacity*, which measures the maximum rate of information that can be reliably transmitted over a communication channel.

1.3.2 Entanglement

Quantum systems may exhibit correlations that have no classical counterpart. Classical correlations are generated by local operations and classical communication (LOCC), quantum correlations arise from peculiar features of quantum states. Differently to classical multipartite systems, a quantum system can live in a non-separable state, that is, a state that cannot be written as a convex combination of tensor product states [74]

$$\rho_{\mathrm{AB}}^{(sep)} = \sum_k p_k \rho_k^{(\mathrm{A})} \otimes \rho_k^{(\mathrm{B})}. \tag{1.70}$$

Non-separable states are called entangled states and the entanglement measures the degree on non-separability of a quantum system. Entangled states cannot be reproduced by any LOCC-schemes, which only generate classical separable states. Indeed, entanglement cannot increase under local operations and is even invariant if such operations are unitary. As a result of the interaction with a noisy environment, a system may lose quantum correlations and eventually turn from an entangled to a separable state. This situation is referred as entanglement sudden death and an eventual increase is called revival.

For bipartite systems, the most common measure of entanglement relies on the PPT criterion (positivity under partial transposition): ρ_{AB} is separable if and only if the partially transposed density $\rho_{\mathrm{AB}}^{T_{\mathrm{A}}}$ is a positive operator, where

$$\rho_{\mathrm{AB}}^{T_{\mathrm{A}}} = \sum_k p_k (\rho_k^{(\mathrm{A})})^T \otimes \rho_k^{(\mathrm{B})}. \tag{1.71}$$

The PPT criterion was introduced as a necessary condition by A. Peres [75] and proved to be a sufficient condition for bypartite systems by R. Simon [76]. This criterion allows to easily determine whether a state is entangled or not by only checking the sign of the eigenvalues of $\rho_{\mathrm{AB}}^{T_{\mathrm{A}}}$. If all the eigenvalues are positive the state is separable, othewise the state is entangled.

The PPT criterion assumes an even easier look for gaussian states, benefiting from the covariance matrix formalism. The covariance matrix associated to the partially transposed density operator $\rho_{\mathrm{AB}}^{T_{\mathrm{B}}}$ has to satisfy

$$\tilde{\boldsymbol{\sigma}} + \frac{i}{2}\boldsymbol{\Omega} \geq 0 \tag{1.72}$$

where $\tilde{\boldsymbol{\sigma}} = \boldsymbol{\Delta}_{\mathrm{A}} \boldsymbol{\sigma} \boldsymbol{\Delta}_{\mathrm{A}}$ and the partial transposition operator $\boldsymbol{\Delta}_{\mathrm{A}} = \mathrm{Diag}(1, -1) \oplus \mathbb{I}_2$. The four symplectic invariants of $\tilde{\boldsymbol{\sigma}}$ are given by

$$\tilde{I}_1 = I_1, \quad \tilde{I}_2 = I_2, \quad \tilde{I}_3 = -I_3, \quad \tilde{I}_4 = I_4. \tag{1.73}$$

The symplectic eigenvalues are then given by

$$\tilde{d}_{\pm} = \sqrt{\frac{\tilde{\Delta}(\boldsymbol{\sigma}) \pm \sqrt{\tilde{\Delta}(\boldsymbol{\sigma})^2 - 4I_4}}{2}} \tag{1.74}$$

where $\tilde{\Delta}(\boldsymbol{\sigma}) = I_1 + I_2 - 2I_3$. The PPT criterion requires positivity of the partially transposed density operator. In the covariance matrix formalism, such requirement implies that all the symplectic eigenvalues of $\boldsymbol{\sigma}$ need to exceed the threshold value $\frac{1}{2}$. A gaussian state is then separable if the smallest symplectic eigenvalue $\tilde{d}_-$ satisfies

$$\tilde{d}_- \geq \frac{1}{2}. \tag{1.75}$$

In order to transform this criterion into a suitable measure of entanglement, the logarithmic negativity $\mathcal{N}$ [77] is introduced

$$\mathcal{N} = \max\{0, \log_2 2\tilde{d}_-\}. \tag{1.76}$$

The logarithmic negativity is an increasing monotone function of $\tilde{d}_-$ and is zero when condition 1.75 is satisfied.

1.3.3 Quantum Discord

The total amount of the correlations possessed by a bipartite quantum state ρ_{AB} is called mutual information and is given by

$$\mathcal{I}(\rho_{\mathrm{AB}}) = S(\rho_{\mathrm{A}}) + S(\rho_{\mathrm{B}}) - S(\rho_{\mathrm{AB}}), \tag{1.77}$$

where $S(\rho_j)$ is the Von Neumann entropy of the j-th subsystem. Usually, the mutual information can be divided into two parts: a classical part $\mathcal{C}(\rho_{\mathrm{AB}})$ and a quantum part $\mathcal{D}(\rho_{\mathrm{AB}})$, which takes name of quantum discord. The classical correlations, defined as the maximum amount of information extractable from one subsytem by performing local operations on the other, are given by

$$\mathcal{C}(\rho_{\mathrm{AB}}) = \max_{\Pi_i}\left\{S(\rho_{\mathrm{A}}) - \sum_i p_i S(\rho_{\mathrm{A|B}}^{\Pi_i})\right\} \tag{1.78}$$

where $\rho_{\mathrm{A|B}}^{\Pi_i} = \mathrm{Tr}_{\mathrm{B}}(\rho \mathbb{I} \otimes \Pi_i)$ is the state after the measurement on system B with probability $p_i = \mathrm{Tr}_{\mathrm{A,B}}(\rho_{\mathrm{AB}} \mathbb{I} \otimes \Pi_i)$. The quantum discord is defined as the difference between the total correlations and the classical correlations:

$$\mathcal{D}(\rho_{\mathrm{AB}}) = \mathcal{I}(\rho_{\mathrm{AB}}) - \mathcal{C}(\rho_{\mathrm{AB}}). \tag{1.79}$$

The quantum discord then measures the amount of correlations whose origin cannot be addressed to the action of local operations or classical communication. However, computing the quantum discord may be challenging as it usually implies finding the POVM that maximizes the classical correlations. In the case of Gaussian states, the form of the POVM maximizing the classical correlations is known [78, 79] and the quantum discord depends only on the covariance matrix by the relation

$$\mathcal{D}(\rho) = h(\sqrt{I_2}) - h(d_-) - h(d_+) + h\left(\sqrt{E_{min}}\right), \tag{1.80}$$

where d_- and d_+ are the symplectic eigenvalues of the covariance matrix, I_1, I_2, I_3, I_4 are the so-called symplectic invariants, $h(x) = (x+\frac{1}{2})\log(x+\frac{1}{2}) - (x-\frac{1}{2})\log(x-\frac{1}{2})$ and

$$E_{min} = \begin{cases} \left[\frac{2|I_3| + \sqrt{4I_3^2 + (4I_2-1)(4I_4-1)}}{4I_2-1}\right]^2 & \text{if } R_\sigma \leq 1 \\ \frac{I_1 I_2 + I_4 - I_3^2 - \sqrt{(I_1 I_2 + I_4 - I_3^2)^2 - 4I_1 I_2 I_4}}{2I_2} & \text{if } R_\sigma > 1 \end{cases} \tag{1.81}$$

where

$$R_\sigma = \frac{4(I_1 I_2 - I_4)^2}{(I_1 + 4I_4)(1+4I_2)I_3^2}\,.$$

For Gaussian states satisfying the second condition, the maximum amount of extractable information is achieved by measuring a canonical variable (e.g. by homodyne detection in optical systems [80]). On the other hand, for states falling in the first set, the optimal measurement is more general, and coincides with the projection over coherent states for STSs. For a generic Gaussian state, with covariance matrix σ written in a block form

$$\sigma = \begin{pmatrix} \mathbb{A} & \mathbb{C} \\ \mathbb{C}^T & \mathbb{B} \end{pmatrix} \tag{1.82}$$

the symplectic invariants are $I_1 = \det \mathbb{A}$, $I_2 = \det \mathbb{B}$, $I_3 = \det \mathbb{C}$, $I_4 = \det \sigma$.

1.4 Quantum Discrimination Theory

In this section, I briefly summarize the basic concepts of quantum state discrimination [81–84] and introduce the tools required to implement a discrimination strategy. The purpose of state discrimination is to distinguish, by looking at the outcome of a measurement performed on the system, between two possible hypothesis on the preparation of the system itself. Optimal discrimination schemes are those minimizing the probability of error upon a suitable choice of both the input state and the output measurement. The minimum achievable probability of error, given a pair of output states, may evaluated from the density operators of the two states and it is usually referred to as the Helstrom Bound. Suppose to have a quantum system that may be prepared in two possibile states, corresponding to the two hypotheses $H_{\rm A}$ and $H_{\rm B}$,

$$H_{\rm A} : \rho \to \rho_{\rm A} \quad H_{\rm B} : \rho \to \rho_{\rm B}. \tag{1.83}$$

In order to determine which density matrix describes the true state of the quantum system, one chooses a two-value positive-operator-valued measure (POVM) $\{E_{\rm A}, E_{\rm B}\}$ with $E_{\rm A} + E_{\rm B} = \mathbb{I}$ and $E_{\rm A}, E_{\rm B} \geq 0$. Once the measurement is performed, the observer infers the state of the system with an error probability P_e given by

$$P_e = \frac{1}{2}{\rm Tr}[\rho_{\rm A} E_{\rm B}] + \frac{1}{2}{\rm Tr}[\rho_{\rm B} E_{\rm A}]. \tag{1.84}$$

It is possible to show that the minimum error probability is related to the trace distance between the two states to discriminate, where the trace distance is

$$T(\rho_{\rm A}, \rho_{\rm B}) = \frac{1}{2}||\rho_{\rm A} - \rho_{\rm B}||_1, \tag{1.85}$$

with $||O||_1 = {\rm Tr}\sqrt{O^\dagger O}$. Finally, the minimum error probability, also called *Helstrom bound*, reads

$$P_e = \frac{1}{2}[1 - T(\rho_{\rm A}, \rho_{\rm B})]. \tag{1.86}$$

The trace distance provides a metric on the Hilbert space and is equal to zero if and only if $\rho_{\mathrm{A}} = \rho_{\mathrm{B}}$ while it reaches its maximum value 1 for orthogonal states. Therefore, the error probability ranges from 0, when the two states are orthogonal, to 1, when the two states are identical.

It is worth emphasizing that the performance of any POVM can not outdo the Helstrom Bound, which stands as the ultimate precision in discrimination protocols. Unfortunately, evaluating the Helstrom Bound for continuous variable systems is a challenging task, as it requires performing a trace operation on infinite matrices. Nevertheless, some lower and upper bounds can be found by means of the Uhlmann fidelity function. In fact, defining the lower bound $\mathcal{F}_m$ and the upper bound $\mathcal{F}_M$

$$\mathcal{F}_m \equiv \frac{1-\sqrt{1-\mathcal{F}(\rho_{\mathrm{A}},\rho_{\mathrm{B}})}}{2}, \qquad \mathcal{F}_M \equiv \frac{\sqrt{\mathcal{F}(\rho_{\mathrm{A}},\rho_{\mathrm{B}})}}{2}, \tag{1.87}$$

the error probability ranges within the interval defined by the two bounds [85]

$$\mathcal{F}_m \leq P_e \leq \mathcal{F}_M. \tag{1.88}$$

Another tighter upper-bound for the Helstrom Bound is given by the quantum Chernoff bound (QCB) Q,

$$Q = \inf_{0\leq s\leq 1} \mathrm{Tr}[\rho_{\mathrm{A}}^{s}\rho_{\mathrm{B}}^{1-s}]. \tag{1.89}$$

Even though the QCB does not possess any natural operational meaning, i.e. it cannot be directly related to a measurement process, it becomes a powerful tool in discrimination protocols featuring multicopy states and it is generally pretty easy to evaluate for continuous variable systems. The QCB can be related to the Uhlmann fidelity function and, by means of the QCB, Eq. 1.87 can be upgraded to

$$\mathcal{F}_m \leq P_e \leq \frac{Q}{2} \leq \mathcal{F}_M. \tag{1.90}$$

The explicit formula for the QCB is cumbersome and won't be reported here [86].

1.5 Non-Markovianity

The presence of the environment unavoidably affects the dynamics of a quantum system. Because of the interaction, the quantum system correlates with the environment, resulting in an irreversible dynamics of its state. In this case, the evolution of the state ceases to be pictured by unitary evolutions and dynamical maps are needed to its description instead.

Within the irreversible dynamics, the quantum features of the system may disappear once and for all or revive partially in time, the second option arousing suspicion about the presence of memory effects. Dynamical maps whose evolution is characterized by such memory effects are usually named non-Markovian maps, in opposition to Markovian maps, which describe memoryless dynamics. Such terminology characterizing dynamical maps is heritage of classical theory of stochastic processes, where Markov processes identify discrete chains of time-labeled events whose probability distribution at any time strictly depend exclusively on the output of the previous event. Formulating a similar definition in a quantum scenario is a challenging task: knowing the output of an event implies measuring and measuring affects posterior statistics, therefore the classical definition does not suit a quantum theory. Nowadays, a proper distinction between

quantum Markovian and non-Markovian processes relies on the property of divisibility of the dynamical map describing the evolution. A dynamical map $\mathcal{E}(t, t_0)$ is said to be *divisible* if it follows a decomposition rule such as

$$\mathcal{E}(t, t_0) = \mathcal{E}(t, t_1)\mathcal{E}(t_1, t_0) \quad \forall t_1 : t \geq t_1 \geq t_0. \tag{1.91}$$

where both $\mathcal{E}(t, t_1)$ and $\mathcal{E}(t_1, t_0)$ are CPTP maps. A completely positive map is then said to be non-Markovian if it violates the decomposition rule for some set of times.

Unfortunately, directly proving [87–89] the non-Markovian character of a dynamics is not always possible, as in many situations the full analytic form of the time dependent quantum dynamical map is missing. When the direct verification is not possible, one may exploit witnesses of non-Markovianity, i.e. quantities that vanish in case of a Markovian dynamics. Even though the witnesses may successfully capture the memory feature of a non-Markovian process in many situations, they possess different physical meaning and may be ineffective in some specific situation. In the following, I briefly review two of the most common measures of non-Markovianity, the BLP and the Fidelity measures.

1.5.1 BLP and Fidelity measures of non-Markovianity

The BLP measure was first proposed by Breuer, Laine and Piilo in Ref. [90]. The basic idea behind the BLP measure lies on the fact that Markovian quantum maps are responsible for an irreversible loss of distinguishability between two input states, differently to non-Markovian maps, which may exhibit a partial regrowth of distinguishability in time. The loss of distinguishability is usually given an interpretation in terms of flow of information, travelling from the system into the environment, while a partial increase is interpreted a sign of a reversed flow. The distinguishability between any two states ρ_{A} and ρ_{B} is quantified by the trace distance defined in Eq. 1.85. From a mathematical point of view, the BLP measure is based on the contractive properties of CPTP maps: in fact, a CPTP map Φ is a contraction for the Trace distance,

$$T(\Phi\rho_{\mathrm{A}}, \Phi\rho_{\mathrm{B}}) \leq T(\rho_{\mathrm{A}}, \rho_{\mathrm{B}}). \tag{1.92}$$

This implies that no quantum operation can increase the distinguishability of two quantum states. If a quantum evolution $\mathcal{E}(t, t_0)$ is Markovian, the divisibility property in Eq. 1.91 implies that, at any intermediate time between t and t_0, the quantum evolution splits into two CPTP quantum evolutions that are contractions for the Trace distance. Therefore, any non-monotonic behaviour of the trace distance necessarily means that the divisibility property is not satisfied. BLP introduce the rate of change of the trace distance as

$$\sigma(\rho_{\mathrm{A}}, \rho_{\mathrm{B}}, t) = \frac{d}{dt} T(\rho_{\mathrm{A}}(t), \rho_{\mathrm{B}}(t)). \tag{1.93}$$

While Markovian quantum evolutions always feature a negative rate σ, non-Markovian evolutions may be characterized by a temporary positive derivative of the trace distance, which implies an increase of distinguishability, i.e. a flux of information travelling back to the system. The maximum total amount of information backflow is quantified by the BLP measure:

$$N_{BLP} = \max_{\rho_A, \rho_B} \int_{\sigma>0} dt\, \sigma(t, \rho_{\mathrm{A}}, \rho_{\mathrm{B}}). \tag{1.94}$$

The quantity N_{BLP} collects all the information backflow and defines a sort of degree of non-Markovianity. Of course, if $N_{BLP} > 0$ the dynamics is non-Markovian, but the

converse is not true in general. For this reason, the BLP measure can only be used to witness non-Markovianity and does not hold as a definition of non-Markovianity by itself.

An analogue measure of non-Markovianity can be defined on the Uhlmann Fidelity function, as any CPTP map Φ is a contraction for the Bures distance as well:

$$D_B(\Phi\rho_{\mathrm{A}}, \Phi\rho_{\mathrm{B}}) \leq D_B(\rho_{\mathrm{A}}, \rho_{\mathrm{B}}). \tag{1.95}$$

In a very similar way, it is possible to define the rate of change of the Bures distance as

$$\sigma_B(\rho_{\mathrm{A}}, \rho_{\mathrm{B}}, t) = \frac{d}{dt} D_B(\rho_{\mathrm{A}}(t), \rho_{\mathrm{B}}(t)). \tag{1.96}$$

and associate a quantifier of non-Markovianity N_B

$$N_B = \max_{\rho_A, \rho_B} \int_{\sigma_B > 0} dt\, \sigma_B(t, \rho_{\mathrm{A}}, \rho_{\mathrm{B}}). \tag{1.97}$$

The two measures of non-Markovianity indeed rely on the same mathematical concept, albeit the BLP measure entails more physical sense as it is strictly related to the error probability in discrimination protocols.

As previously anticipated, there is a strong connection between the non-Markovian properties of a dynamical map and the form of master equation the map obeys. Indeed, an operator $\mathcal{L}_t$ is the generator of a Markovian dynamics if and only if it can be written in the so-called *Lindblad form*:

$$\frac{d}{dt}\rho(t) = \mathcal{L}_t[\rho(t)] = -i[H(t), \rho(t)] + \sum_k \gamma_k(t)\left[L_k(t)\rho(t)L_k^\dagger(t) - \frac{1}{2}\{L_k^\dagger(t)L_k(t), \rho(t)\}\right] \tag{1.98}$$

with $\gamma_k(t) \geq 0$ for every k and time t. Therefore, if the coupling becomes negative at any time t, the dynamics is non-Markovian.

1.6 Summary

- The density operator formalism allows to easily describe the state of a system, its evolution and the effect of quantum measurements. The evolution of open quantum systems is represented by means of CPTP maps.
- Quantum correlations are one of the best signature of nonclassicality and have no classical counterpart. Entangled states are defined as non-separable states and cannot be generated by any LOCC scheme. The quantum discord measures the amount of correlations not originating from local or classical operations and may be non-zero even in absence of entanglement.
- Quantum discrimination theory allows to guess with some error probability which among two hypotheses is true by performing a set of measurements on the system. The ultimate error probability is known as Helstrom bound, but other bounds as the Fidelity and the Quantum Chernoff bound are used for continuous variable systems.

- The definition of non-Markovianity relies on the violation of the divisibiility properties of quantum maps. When the explicit form of the quantum map is not known, non-Markovianity may be witnessed by means of the BLP or Fidelity measures, both related to contractive properties of CPTP maps. According to the BLP measure, a non-Markovian dynamics may exhibit a partial increase of distinguishability between quantum states and this regrowth is commonly interpreted as a backflow of information from the environment to the system.

CHAPTER 2

Stochastic processes

In this chapter, I shortly review the basic concepts about stochastic processes [91–94] and introduce some relevant properties of the Ornstein-Uhlenbeck process.

2.1 General notions

Roughly speaking, a stochastic process describes the dynamics of some physical property of a system that evolves with some indeterminacy, instead that obeying a deterministic law. Stochastic processes occur in many branches of knowledge, i.e. economics and medicine. In physics, the most known example of stochastic process is the motion of a particle in Brownion motion.

The property of the system that evolves randomly is addressed by a random variable X that, in a given experiment, takes a particular value x_i, which is called *realization*. Each realization is assigned a probability $p_i = p(x_i)$ in a discrete case. If the set of possible realization is continuous, a probability distribution $p(x)$ is needed. Of course, $p(x)$ is non-negative and normalized.

Random variables are meant to describe non-deterministic features of a physical processes through probabilistic laws. However, in many practical situations, the probability density $p(x)$ is not known and information about the random variable is accessible only through its statistics, i.e. expectation value, variance or higher order statistics.

A random variable X with a probability $p(x)$ over the set of realizations $\{x, x \in \mathbb{R}\}$ can be described by means of the characteristic function

$$\chi(\xi) = \mathbb{E}\Big[e^{i\xi X}\Big], \tag{2.1}$$

which is related to the probability distribution $p(x)$ through a Fourier transform:

$$\chi(\xi) = \int e^{i\lambda x} p(x) dx. \tag{2.2}$$

The characteristic function includes any information about the statistics of the random variable, momenta and cumulants. The *j-th order momentum* m_k is defined as $m_k = \mathbb{E}[X^k]$ and can be generated by the characteristic function through

$$m_j = \frac{1}{i^j} \frac{d^j \chi(\xi)}{d\xi^j}\Big|_{\xi=0}. \tag{2.3}$$

From the knowledge of the moments, the characteristic function can be written in terms of the *cumulants* k_j

$$\chi(\xi) = 1 + \sum_{n=1}^{\infty} \frac{(i\xi)^n}{n!} m_n = \exp\Big\{ \sum_{n=1}^{\infty} \frac{(i\xi)^n}{n!} k_n \Big\} \tag{2.4}$$

where the cumulants and the momenta are related through the following formulas:

$$\begin{aligned} k_1 &= m_1; \\ k_2 &= m_2 - m_1^2 \\ k_3 &= m_3 - 3m_1m_2 + 2m_1^3 \\ &\cdots\cdots\cdots \end{aligned} \tag{2.5}$$

The first and second order cumulants are respectively known as *expectation value* μ and *variance* σ^2: the expectation value μ of a random variable X with set of realizations $\{x, x \in \mathbb{R}\}$ is the

$$\mu = \mathbb{E}[X] = \int xp(x)dx, \tag{2.6a}$$

$$\sigma^2 = \mathbb{E}\Big[(X - \mathbb{E}[X])^2\Big] = \mathbb{E}[X^2] - \mathbb{E}[X]^2. \tag{2.6b}$$

In general, the characteristic function needs the evaluation of any order moments. Nevertheless, there is a whole class of random variables where the evaluation of only first and second momenta is sufficient to a full characterization: gaussian random variables.

A gaussian random variable is described by a gaussian probability distribution $p(x) = \frac{1}{\sqrt{2\pi\sigma^2}} \exp\big[-\frac{(x-\mu)^2}{2\sigma^2}\big]$, where μ is the expectation value and σ^2 is the variance of the random variable. The characteristic function is then given by

$$\chi(\xi) = \exp\left[i\xi\mu - \frac{1}{2}\sigma^2\xi^2\right] \tag{2.7}$$

and is related to the probability distribution $p(x)$ by Fourier-transforming.

In order to address a stochastic process, i.e. the dynamical evolution of a non deterministic physical property of a system, a collection $\{X(t), t \in T\}$ of random variables is needed. Each variable is defined on the same probability space and is indexed by a time parameter t. Of course, random variables at different times may exhibit correlations. In this context, it is useful to define the autocorrelation function $K(t_1, t_2)$,

$$K(t_1, t_2) = \mathbb{E}[X(t_1), X(t_2)] \tag{2.8}$$

where t_1 and t_2 are two different instants of time. In particular, the stochastic processes all over this dissertation are stationary, that is, they are not affected by a shift of time

$$\mathbb{E}[X(t_1 + \tau)X(t_2 + \tau)\dots X(t_n + \tau)] = \mathbb{E}[X(t_1)X(t_2)\dots X(t_n)]. \tag{2.9}$$

In the particular case of the autocorrelation function, a stationary process implies that $K(t_1, t_2)$ only depends The autocorrelation function may even be defined through its Fourier-transform, i.e. through the power spectral density

$$S(\omega) = \int_{-\infty}^{\infty} K(\tau)e^{-i\omega\tau}d\tau. \tag{2.10}$$

Stochastic processes may feature memory effects. Intuitively, memory is associated to physical processes in which a physical property at some time t depends on its value at previous times. When the conditional probabilities satisfy

$$p(x_{n+1}, t_{n+1}|x_1, t_1; \dots; x_n, t_n) = p(x_{n+1}, t_{n+1}|x_{n-k}, t_{n-k}), \tag{2.11}$$

the stochastic process is said to be non-Markovian of order k. When $k = 0$, the process is said to be Markovian, that is, predictions upon the state at any time only depend on the present state of the system or, equivalently, on the conditional transition probability and the initial distribution.

In quantum optics, stochastic processes are often used to represent noisy classical environments that interact with quantum systems. In particular, stochastic processes well suit the case of fluctuating environments, which dynamics show no deterministic behaviour but can be described by means of an autocorrelation function or a power spectrum. In the particular case of gaussian processes, correlations or power spectra are the only needed ingredients to define the process itself, so when addressing noisy environments in terms of gaussian stochastic processes, the noise structure is chosen heuristically.

The models presented in the following chapters will address decoherence phenomena of quantum systems interacting exclusively with gaussian stochastic environments, which will be investigated in a deeper way in the following section.

2.2 Gaussian stochastic processes

A stochastic process $\{X(t), t \in T\}$ is said to be gaussian if, for any integer n and any subset $\{t_1, t_2, \ldots, t_n\}$, the joint characteristic function of n random variables is given by

$$\begin{aligned}&\chi_{[X(t_1),X(t_2),\ldots,X(t_n)]}(\xi_1, \xi_2, \ldots, \xi_n) = \\ &\mathbb{E}\left[\exp\left(i\sum_{k=1}^{n}\xi_k X(t_k)\right)\right] = \exp\left[i\sum_k \xi_k\mu_k - \frac{1}{2}\sum_{j,k}^{n}\xi_j\xi_k K(t_j,t_k)\right]\end{aligned} \tag{2.12}$$

where the average value $\mu_k = \mathbb{E}X(t_k)$ and the covariance kernel is

$$K(t_j, t_k) = \mathbb{E}[X(t_j)X(t_k)] - \mathbb{E}[X(t_j)]\mathbb{E}[X(t_k)]. \tag{2.13}$$

Of course, the previous definition may be easily extended to a continuous case, by letting the time interval $[t_0, t]$ take over the discrete set of values $\{t_k\}$. Then, the continuous gaussian stochastic process is such that

$$\begin{aligned}&\mathbb{E}\left[\exp\left(i\int_{t_0}^{t}\xi(s)X(s)ds\right)\right] = \\ &\exp\left[i\int_{t_0}^{t}\xi(s)\mu(s)ds - \frac{1}{2}\int_{t_0}^{t}\int_{t_0}^{t}\xi(s)\xi(s')K(s,s')ds\,ds'\right],\end{aligned} \tag{2.14}$$

where the last term of Eq. 2.14 is singled out can be written as a β-function:

$$\beta(t, t_0) = \int_{t_0}^{t}\int_{t_0}^{t}\xi(s)\xi(s')K(s,s')ds\,ds', \tag{2.15}$$

which plays the role of variance of the gaussian stochastic process.

2.2.1 Examples of Gaussian processes

In this subsection, I present a small review of the main properties and notions about the gaussian stochastic processes used further in this dissertation is presented, namely, the Orstein-Uhlenbeck (OU) process and the Power-Law (PL).

Ornstein-Uhlenbeck Process

The Ornstein-Uhlenbeck process is a very important example of stationary gaussian process. The OU is used in the Brownian motion model to describe the stochastic behaviour of the velocity of a particle and can be used to address noisy environments with Lorentzian spectra, as will be shown afterwards. A stochastic process is said to be a *Ornstein-Uhlenbeck process* with zero mean if it satisfies:

$$\mu_{OU}(t) = 0; \tag{2.16a}$$

$$K_{OU}(t, t_0) = \frac{\lambda}{2t_{_E}} \exp\left\{ - \frac{|t - t_0|}{t_{_E}} \right\} \tag{2.16b}$$

where λ is a coupling parameter playing the role of the damping rate and $t_{_E}$ is the characteristic time of the environment. Intuitively, the parameter $t_{_E}$ measures the time after which the environment correlations cease to be significative and therefore can be interpreted as the amount of time the environment can store information for. If the correlation time is short, the environment fails to save memory of what has happened before. From a mathematical point of view, as $t_{_E} \to 0$, the autocorrelation function approaches a Dirac-delta distribution, that is, it represents a gaussian white noise. When the correlation time is finite, the power spectrum is

$$S_{OU}(\omega) = \frac{\lambda}{\sqrt{2\pi}(1 + \omega^2 t_{_E}^2)}, \tag{2.17}$$

which is a Lorentzian spectrum.

From Eq. 2.15, considering $\xi(s)$ a constant function $\xi(s) = \xi = 1$, one obtains the variance associated to the Ornstein-Uhlenbeck process:

$$\beta_{OU}(t, t_0) = \lambda\, t_{_E} \left(\frac{t - t_0}{t_{_E}} + e^{-(t-t_0)/t_{_E}} - 1 \right). \tag{2.18}$$

In sake of simplicity, I anticipate that in the next chapters the parameter $t_{_E}$ will occasionally be substituted by its inverse $\gamma = 1/t_{_E}$. The parameter γ intuitively addresses the memory features of the environment and also plays the role of a cut-off frequency in the Lorentzian spectrum.

Power-Law Process

The power-law process is characterized by the autocorrelation function

$$K_{PL}(t, t_0) = \frac{a - 1}{2} \frac{\gamma\lambda}{(1 + \gamma|t - t_0|)^a} \tag{2.19}$$

where $a > 2$. This kernel of correlation generates a variance given by

$$\beta_{PL}(t) = \frac{\lambda}{\gamma} \left[\frac{(1 + \gamma t)^{2-a} + \gamma t(a - 2) - 1}{a - 2} \right]. \tag{2.20}$$

2.2.2 Detuned gaussian processes

In the examples provided in the next chapters, quantum systems interact with classical environments portrayed by stochastic processes. More explicitly, the quantum systems interact with an external zero-mean stochastic field having a time-fluctuating complex amplitude $B(t)e^{i\delta t}$, where δ plays the role of the sytem-CSF detuning and the stochastic field is $B(t) = B_x(t)+iB_y(t)$, whose real and imaginary parts are independent processes.

In this case, it is useful to define the random variable $\phi(t) = B(t)e^{i\delta t}$, such that its real ϕ_x and imaginary ϕ_y parts are given by

$$\phi_x(t) = B_x(t)\cos\delta t - B_y(t)\sin\delta t \tag{2.21a}$$
$$\phi_y(t) = B_x(t)\sin\delta t + B_y(t)\cos\delta t \tag{2.21b}$$

From the mathematical point of view, in Chapter 3 the study of the dynamics requires the evaluation of the joint characteristic function 2.14 of $\phi_x(t)$ and $\phi_y(t)$:

$$\begin{aligned}
&\mathbb{E}\left[\exp\left(i\int_{t_0}^{t}\big(\xi_x\phi_x(s)+\xi_y\phi_y(s)\big)ds\right)\right] = \\
&\exp\left(-\frac{1}{2}\int_{t_0}^{t}\int_{t_0}^{t}\mathbb{E}\big[\xi_x^2\,\phi_x(s)\phi_x(s')+2\xi_x\xi_y\phi_x(s)\phi_y(s')+\xi_y^2\phi_y(s)\phi_y(s')\big]dsds'\right) = \\
&\exp\left(-\frac{1}{2}(\xi_x^2+\xi_y^2)\int_{t_0}^{t}\int_{t_0}^{t}\cos[\delta(s-s')]K(s,s')dsds'\right),
\end{aligned} \tag{2.22}$$

where, the condition $\mathbb{E}[B_x(s)B_x(s')] = \mathbb{E}[B_y(s)B_y(s')] = K(s,s')$ was assumed. Finally, the explicit form of $\beta(t)$, assuming $\xi_x = \xi_y = 1$, is

$$\beta(t,t_0) = \int_{t_0}^{t}\int_{t_0}^{t}\cos[\delta(s-s')]K(s,s')\,ds\,ds'. \tag{2.23}$$

In the following, I report the explicit form of $\beta(t)$ with $t_0 = 0$ for the Ornstein-Uhlenbeck process.

$$\begin{aligned}
\beta_{OU}(t) = \frac{\lambda}{[1+(\delta\,t_{\scriptscriptstyle E})^2]^2}\Big\{&t - t_{\scriptscriptstyle E} + (\delta\,t_{\scriptscriptstyle E})^2(t+t_{\scriptscriptstyle E}) \\
&+ t_{\scriptscriptstyle E}\,e^{-t/t_{\scriptscriptstyle E}}\left[(1-(\delta\,t_{\scriptscriptstyle E})^2)\cos\delta\,t - 2\delta\,t_{\scriptscriptstyle E}\sin\delta\,t\right]\Big\}.
\end{aligned} \tag{2.24}$$

Let's now focus on the explicit form of $\beta(t)$ for the Ornstein-Uhlenbeck process, in order to understand which parameters are relevant for the analysis of the dynamics of the system. As a matter of fact, the function $\beta(t)$ in (2.24) depends only on two parameters (besides the time t), as it can be rescaled in units of $t_{\scriptscriptstyle E}$ by assuming $\tilde{\delta} = \delta t_{\scriptscriptstyle E}$, $\tilde{\lambda} = \lambda\,t_{\scriptscriptstyle E}$, $\tilde{t} = t/t_{\scriptscriptstyle E}$, leading to the expression (in which tildes have already been dropped)

$$\beta_{OU}(t) = \frac{\lambda}{[1+\delta^2]^2}\Big\{t - 1 + \delta^2(t+1) + e^{-t}\left[(1-\delta^2)\cos\delta\,t - 2\delta\,\sin\delta\,t\right]\Big\}. \tag{2.25}$$

As shown in the right panel of Fig. 2.1, the function $\beta_{OU}(t)$ presents oscillations in time depending on the value of the parameter δ. In order to find the regimes of oscillation, one formally imposes the condition $d\beta(t)/dt = 0$, which leads to the following equation

$$\lambda\,\frac{1-e^{-t}(\cos\delta t - \delta\sin\delta t)}{1+\delta^2} = 0 \tag{2.26}$$

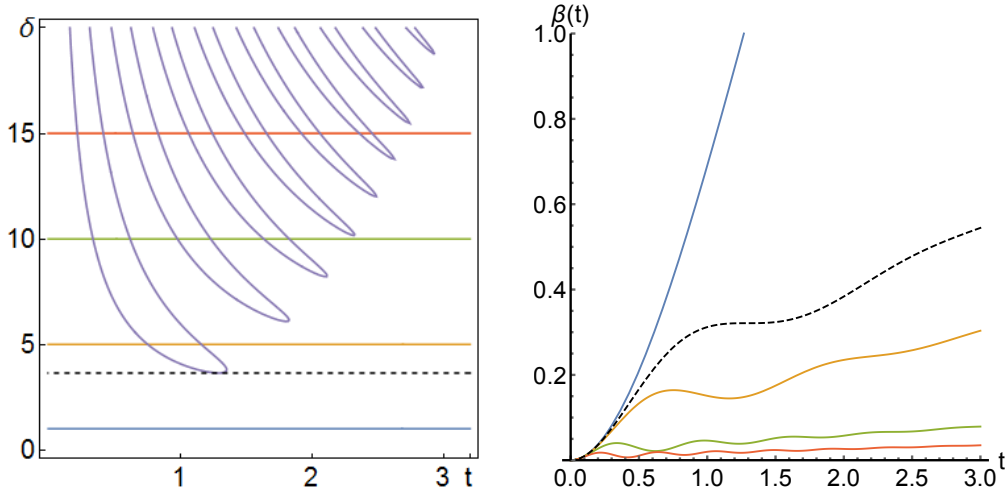

Figure 2.1: Left panel: Contourplot of $d\beta(t)/dt = 0$ as a function of t and δ. The purple curve represents the solution of $d\beta(t)/dt = 0$. The black dashed line represents the maximum value of $\delta = \delta_0$ for which $\beta(t)$ does not oscillate. Right panel: $\beta(t)$ for different values of δ. From bottom to top, the other lines are for $\delta = 1$ (blue), $\delta = 5$ (yellow), $\delta = 10$ (green), $\delta = 15$ (red). An oscillating behavior is present only if $\delta > \delta_0$.

which can not be analitically solved. The left panel of Fig. 2.1 contains a numerical plot of the solutions of (2.26) and shows the existence of a lower bound on the rescaled detuning δ for the oscillations of $\beta_{OU}(t)$. The lower bound is represented by the black dashed line, corresponding to

$$\tilde{\delta}_0 = \frac{3\pi}{2}\left[\text{ProductLog}\left(\frac{3\pi}{2}\right)\right]^{-1} \simeq 3.644\,,$$

which is a value independent of λ (the tilde has been momentarily reinstated).

The existence of a threshold value for the presence of oscillations will be thoroughly discussed in the following chapters in relation to the revivals of quantumness (Chapter 4) and correlations (Chapter 5). At this stage, let's just notice that the existence of a threshold binds the values of the correlation time of the environment $t_{_E}$ and the true detuning δ, as their product has to exceed $\tilde{\delta}_0$ in order to produce oscillations.

Finally, it is worth noting that a large value of $\tilde{\delta}$ induces oscillations, but the corresponding $\beta(t)$ is really small compared to the values assumed in other regimes of detuning. This fact becomes relevant in the context of stochastic interactions: in the next chapters, $\beta(t)$ plays the role of the noise added to the system after the interaction with a classical environment. Therefore, a high value of detuning δ shields the evolution of the system from the detrimental action of the environment.

2.3 Summary

- A collection of random variables $\{X(t), t \in T\}$ parametrized by a discrete or continuous index t describes a stochastic process. Stochastic processes that are fully characterized by their mean and variance are named Gaussian processes.

- The Ornstein-Uhlenbeck process is a stationary Gaussian process, function of two physical parameters: the coupling λ, the correlation time $t_{_E}$ (or its inverse γ).
- The variance $\beta(t)$ of a δ-detuned Ornstein-Uhlenbeck process presents oscillations if and only if the rescaled detuning $\tilde{\delta} = \delta t_{_E}$ exceeds the threshold value $\tilde{\delta}_0 \simeq 3.644$.

CHAPTER 3

Stochastic modeling of quantum environments

In this chapter, I present two different models of interaction between a continuous variable system and a noisy classical environment. I prove that modeling the environment by means of classical stochastic fields allows a proper description of the dynamics in presence of memory effects, without resorting to approximated quantum master equations. Furthermore, the use of classical stochastic fields enables the study of a larger class of processes standard quantum equations are not able to represent. The models under consideration reproduce two of the most common forms of noise a quantum system may suffer, phase diffusion and dissipation.

3.1 Stochastic phase diffusion

The evolution of a quantum system facing phase diffusion noise is described by the quantum master equation [95, 96]

$$\frac{d}{dt}\rho = \frac{\Gamma}{2}\mathcal{L}[\hat{a}^\dagger \hat{a}]\rho\,, \tag{3.1}$$

where $\mathcal{L}[O]\rho = 2O\rho O^\dagger - O^\dagger O\rho - \rho O^\dagger O$ and Γ is the phase damping rate. Following the definition given in Chapter 1, the latter equation is in Lindblad form and therefore is Markovian. The solution of the master equation is formally a gaussian channel $\mathcal{G}_{DP}[\rho]$

$$\mathcal{G}_{DP}[\rho] = \rho(t) = \int_{-\infty}^{\infty} d\psi \frac{1}{\sqrt{\sigma(t)}} \exp\left\{-\frac{\psi^2}{\sigma(t)}\right\} \mathcal{R}(\psi)\rho(0)\mathcal{R}^\dagger(\psi), \tag{3.2}$$

where $\mathcal{R}(\psi)$ is the phase-shift operator $\mathcal{R}(\psi) = \exp\{-i\psi a^\dagger a\}$. Analogously, using the decomposition over the Fock states and integrating over ψ, a generic gaussian channel may be written as

$$\mathcal{G}_{DP}[\rho] = \sum_{m,n} \rho_{nm} e^{-\frac{1}{2}(n-m)^2\sigma(t)} |n\rangle\langle m|, \tag{3.3}$$

where ρ_{nm} is the matrix element of the initial state of the system. The explicit solution of the master equation 3.1 is obtained when $\sigma(t) = \Gamma t$, i.e. when the variance of the gaussian channel shows a linear behaviour in time.

The gaussian channel 3.2 describes the evolution of the system alone, once the degrees of freedom of the environment have already been traced out. However, the phase diffusion master equation is obtained from a microscopic full quantum description of the system-environment interaction. In the following, I will prove that the very same dynamics can be reproduced by means of a stochastic action on the system.

Let's consider a quantum harmonic oscillator interacting with a classical external field. The Hamiltonian of the system may be written as $H = H_0 + H_{DP}$ where the free and interaction Hamiltonians are given by

$$H_0 = \hbar\omega_0 \hat{a}^\dagger \hat{a} \tag{3.4a}$$

$$H_{DP} = \hbar \hat{a}^\dagger \hat{a} \left[\bar{B}(t)e^{i\omega t} + B(t)e^{-i\omega t}\right] , \tag{3.4b}$$

with ω_0 the natural frequency of the oscillator and $B(t)$ a time-dependent fluctuating field with central frequency ω described by a stochastic process whose complex conjugate is $\bar{B}(t)$. From now on, the Hamiltonian H is rescaled in units of $\hbar\omega_0$. As a straightforward consequence, the stochastic classical field $B(t)$, its central frequency ω and the time t become dimensionless quantities (in units of ω_0 and ω_0^{-1} respectively).

Despite the interaction Hamiltionan is time-dependent, the evolution operator assumes a very simple form, as the two-time commutator $[H(t_1), H(t_2)] = 0$. In this case, the evolution operator trivially reads:

$$U(t) = \mathcal{R}(\phi(t)) \tag{3.5a}$$

$$\phi(t) = \int_0^t ds \left[\bar{B}(s)e^{i\omega s} + B(s)e^{-i\omega s}\right] . \tag{3.5b}$$

The system is then subject to a phase shift, where the phase depends on the stochastic field $B(t)$. The evolved state, using the decomposition over the Fock states, then reads:

$$\rho(t) = \left[\mathcal{R}(t)\rho(0)\mathcal{R}^\dagger(t)\right]_B = \sum_{m,n} \rho_{nm} \left[e^{-i\phi(t)(n-m)}\right]_B |n\rangle\langle m|, \tag{3.6}$$

where the stochastic average $[\ldots]_B$ depends on the specific stochastic field chosen and still has to be evaluated.

In this model, the CSF $B(t) = B_x(t) + iB_y(t)$ is described by a Gaussian stochastic process with zero mean $[B_x(t)]_B = [B_y(t)]_B = 0$ and diagonal structure of the autocorrelation matrix

$$[B_x(t_1)B_x(t_2)]_B = [B_y(t_1)B_y(t_2)]_B = K(t_1, t_2) \tag{3.7a}$$

$$[B_x(t_1)B_y(t_2)]_B = [B_y(t_1)B_x(t_2)]_B = 0. \tag{3.7b}$$

The stochastic average in Eq.3.7a can then be easily performed, as the phase $\phi(t)$ is a gaussian variable as well:

$$\left[e^{-i\phi(t)(n-m)}\right]_B = \exp\left\{-\frac{1}{2}(n-m)^2\beta(t)\right\}, \tag{3.8}$$

where $\beta(t)$ can be expressed as

$$\beta(t) = \int_0^t \int_0^t ds_1 ds_2 \, \cos\left[\delta(s_1 - s_2)\right] \, K(s_1, s_2) \, . \tag{3.9}$$

The evolution of the state of the system is then given by a Gaussian channel

$$\rho(t) = \sum_{m,n} \rho_{nm} e^{-\frac{1}{2}(n-m)^2\beta(t)} |n\rangle\langle m| \tag{3.10}$$

provided $\sigma(t) = \beta(t)$. It is now possible to find a meeting point between the stochastic interaction and the full quantum description of the phase diffusion noise: in fact, both dynamics are described by gaussian channels, so the equivalence between the two interactions holds as long as the variances of the channels are identical. As previously shown, the full quantum dynamics features a variance linear in time. Therefore, the stochastic interaction perfectly represents its quantum analogue only in a regime in which $\beta(t)$ is linear in time as well. In the following, I once again report the explicit form of the $\beta_{OU}(t)$ function for the Ornstein-Uhlenbeck kernel and explore some particular regimes:

$$\beta_{OU}(t) = \frac{\lambda}{[1+(\delta\, t_{_E})^2]^2}\Big\{t - t_{_E} + (\delta\, t_{_E})^2(t + t_{_E}) + t_{_E}\, e^{-t/t_{_E}}\left[(1-(\delta\, t_{_E})^2)\cos\delta\, t - 2\delta\, t_{_E}\sin\delta\, t\right]\Big\}. \tag{3.11}$$

which leads to the following approximated expressions:

$$\beta_{OU}(t) \simeq \lambda t + \lambda t_{_E}\, e^{-t/t_{_E}}\cos\delta t \qquad t_{_E} \ll 0 \tag{3.12a}$$

$$\beta_{OU}(t) \simeq \frac{\lambda}{\delta^2 t_{_E}}(1-\cos\delta t) \qquad t_{_E} \gg 0, \delta \gg 1 \tag{3.12b}$$

$$\beta_{OU}(t) \simeq \frac{\lambda t^2}{2t_{_E}}(1-\delta^2 t^2) \qquad t_{_E} \gg 0, \delta \ll 1 \tag{3.12c}$$

As it is apparent from eq. 3.12a, it is possible to recover a linear regime of $\beta_{OU}(t)$ when the correlation time of the environment approaches zero, i.e. when the classical noise has a delta-correlated spectrum. Therefore, the stochastic model is a faithful representation of quantum phase diffusion in the regime $t_{_E} \ll 0$, provided the coupling λ satisfies $\lambda = \Gamma$.

3.2 Stochastic approach to Born-Markov master equation

3.2.1 From Brownian motion to Born-Markov master equation

The propagation of a mode of radiation in a noisy channel is usually described as the interaction of the mode of the system with an extensive environment, a *bath* composed of a large number of external modes, which may represent the free field or the phonon modes of a solid. In a full quantum model [97, 98], the mode of the system a is coupled to the bath modes c_k with frequency ω_k and the interaction Hamiltonian is given by

$$H_I = \hat{a}\sum_k g_k c_k^\dagger e^{-i(\omega_a-\omega_k)t} + \hat{a}^\dagger \sum_k g_k c_k e^{i(\omega_a-\omega_k)t} \tag{3.13}$$

where g_k are the coupling constants of each mode, while ω_a denotes the system transition frequency. Indeed, the interaction hamiltonian presented in Eq. 3.13 is the result of the secular approximation on the more general quantum Brownian motion Hamiltonian:

$$H_I^{(BM)} = \sum_k g_k (a\, e^{-i\omega_a t} + a^\dagger e^{i\omega_a t})(c\, e^{-i\omega_k t} + c_k^\dagger e^{i\omega_k t}) \tag{3.14}$$

where the two terms oscillating faster are neglected in the secular approximation.

The evolution of a quantum brownian particle is described by the master equation given by

$$\frac{d}{dt}\rho = -i[H_0,\rho]+ \\ -\Delta(t)[X,[X,\rho]] + \Pi(t)[X,\{P,\rho\}] - \frac{i}{2}r(t)[X^2,\rho] + i\gamma(t)[X,[P,\rho]], \tag{3.15}$$

where $\Delta(t)$ and $\Pi(t)$ are dissipative terms, whereas $r(t)$ modifies the frequency of the oscillator and $\gamma(t)$ is a damping term.

The latter master equation can be solved, but a closed form for the time-dependent parameters $\Delta(t), \Pi(t), r(t), \gamma(t)$ is achievable only in the weak coupling limit:

$$\Delta(t) = \int_0^t \kappa(s)\cos(\omega_a s)\,ds \tag{3.16a}$$

$$\Pi(t) = \int_0^t \kappa(s)\sin(\omega_a s)\,ds \tag{3.16b}$$

$$\gamma(t) = \int_0^t \mu(s)\sin(\omega_a s)\,ds \tag{3.16c}$$

$$r(t) = \int_0^t \mu(s)\cos(\omega_a s)\,ds \tag{3.16d}$$

where $\kappa(s)$ and $\mu(s)$ are the noise and dissipation kernels, related to the correlation function (and the spectral density $J(\omega)$) of the environment:

$$\kappa(s) \quad = \langle\{F(s),F(0)\}\rangle \quad = 2\int_0^\infty d\omega J(\omega)\coth(\omega/2K_BT)\cos(\omega s), \tag{3.17a}$$

$$\mu(s) \quad = \langle[F(s),F(0)]\rangle \quad = -\int_0^\infty d\omega J(\omega)\sin(\omega s), \tag{3.17b}$$

where $F(t) = \sum_k \left(c_k e^{-i\omega_k t} + c_k^\dagger e^{i\omega_k t}\right)$ is the overall external field.

Performing the secular approximation, the master equation 3.15 reduces to

$$\frac{d}{dt}\rho(t) = \frac{\Delta(t)+\gamma(t)}{2}\mathcal{L}[a]\rho + \frac{\Delta(t)-\gamma(t)}{2}\mathcal{L}[a^\dagger]\rho. \tag{3.18}$$

where the explicit expressions for $\Delta(t)$ and $\gamma(t)$ depend on the spectral density $J(\omega)$. The latter equation is a *time-dependent quantum optical master equation*. The solution of this approximated master equation is represented by the characteristic function

$$\chi_s[\rho(t)](\boldsymbol{\mu}) = \exp\left\{\frac{\boldsymbol{\mu}^T\boldsymbol{\mu}}{2}\left(s - 2\Delta_\Gamma(t)\right)\right\}\chi[\rho(0)]\left(e^{-\Gamma(t)}\boldsymbol{\mu}\right) \tag{3.19}$$

where the quantities $\Delta_\Gamma(t)$ and $\Gamma(t)$ are given by

$$\Gamma(t) = 2\int_0^t \gamma(s)\,ds, \tag{3.20a}$$

$$\Delta_\Gamma(t) = e^{-\Gamma(t)}\int_0^t e^{\Gamma(s)}\Delta(s)\,ds. \tag{3.20b}$$

The coefficients $\Delta(t)$ and $\gamma(t)$ play a fundamental role in determining whether the quantum map is Markovian or not. In fact, the master equation 3.18 is in Lindblad form when the coefficients $\Delta(t) \pm \gamma(t) \geq 0$ for any time t.

Assuming the environment is represented as a reservoir with Ohmic spectral density, with Lorentz-Drude cut-off ω_c,

$$J_O(\omega) = \frac{2\omega}{\pi} \frac{\omega_c^2}{\omega_c^2 + \omega^2}, \tag{3.21}$$

it is possible to evaluate the explicit expressions for $\gamma(t)$ and $\Delta(t)$, which are reported in Appendix A. Let's now discuss some relevant regimes.

Long time limit

In the asymptotic limit $t \to \infty$, the coefficients $\gamma(t)$ and $\Delta(t)$ tend to some constant values Δ_M, γ_M given by

$$\Delta_M = \omega_a \frac{\omega_c^2}{\omega_a^2 + \omega_c^2} \coth(\omega_a / 2KT) \tag{3.22a}$$

$$\gamma_M = \omega_a \frac{\omega_c^2}{\omega_a^2 + \omega_c^2} \tag{3.22b}$$

In the asymptotic limit, the dynamics of the system is then ruled by the Born-Markov quantum optical master equation

$$\frac{d}{dt}\rho(t) = \frac{\Gamma}{2}\big\{(N+1)\mathcal{L}[a]\rho + N\mathcal{L}[a^\dagger]\big\}\rho, \tag{3.23}$$

where N is the number of thermal photons in the environment, which is related to the temperature T via $N = (e^{\omega_0/KT-1})^{-1}$, and $\Gamma = \gamma_M$ is the dissipation rate.

The formal solution of the master equation 3.23 is easily expressed in terms of the Wigner function of the output state

$$W[\rho(t)](\boldsymbol{X}) = \int_{\mathbb{R}^2} d^2\,\boldsymbol{Z} G_t(\boldsymbol{X}|\boldsymbol{Z}) W_0(\boldsymbol{Z}) \tag{3.24}$$

where $W_0(\boldsymbol{X}) = W[\rho(0)](\boldsymbol{X})$ is the Wigner function of the input state and the propagator $G_t(\boldsymbol{X}|\boldsymbol{Z})$ is given by

$$G_t(\boldsymbol{X}|\boldsymbol{Z}) = \frac{\exp\big\{-\frac{1}{2}(\boldsymbol{X} - e^{-\frac{1}{2}\Gamma t}\boldsymbol{Z})^T \boldsymbol{\Sigma}_t^{-1} (\boldsymbol{X} - e^{-\frac{1}{2}\Gamma t}\boldsymbol{Z})\big\}}{2\pi\sqrt{\det[\boldsymbol{\Sigma}_t]}}. \tag{3.25}$$

In the latter definition, $\boldsymbol{\Sigma}_t = (1 - e^{-\Gamma t})\boldsymbol{\sigma}_\infty$, with $\boldsymbol{\sigma}_\infty$ is a 2×2 asymptotic diffusion matrix $\boldsymbol{\sigma}_\infty = \mathrm{Diag}\{N + \frac{1}{2}, N + \frac{1}{2}\}$.

Let's spend a few words about the general solution 3.24: the Wigner function of the output state is a convolution between the wigner function of the input state and the gaussian propagator. Therefore, the output Wigner function is not trivial, unless the input state is gaussian. In that case, the gaussianity is preserved during the interaction and the output state is gaussian as well. Assuming a gaussian input state, the evolution of the covariance matrix follows:

$$\boldsymbol{\sigma}(t) = e^{-\Gamma t}\boldsymbol{\sigma}_0 + (1 - e^{-\Gamma t})\boldsymbol{\sigma}_\infty. \tag{3.26}$$

where $\boldsymbol{\sigma}_0$ is the input covariance matrix. Eq. 3.26 perfectly displays the Markovian properties of the dynamics: the presence of the environment asymptotically erases the contribution of the input state and the dynamics actually describes an irreversible thermalization process. Moreover, it's worth noting that, for small times ($\Gamma t \ll 1$) and high temperature ($N \gg 1$), the output covariance matrix reduces to

$$\boldsymbol{\sigma}(t) \simeq \boldsymbol{\sigma}_0 + \Gamma t\, \boldsymbol{\sigma}_\infty \simeq \boldsymbol{\sigma}_0 + N\Gamma t\, \mathbb{I}_2 \tag{3.27}$$

which describes the detrimental action of the environment, adding thermal noise linearly in time to the system in the early stage of the evolution.

Indeed, this kind of detrimental is a feature of gaussian channels [99–101]:

$$\mathcal{G}_N[\rho](\boldsymbol{\Delta}) = \int_{\mathbb{C}} d^2\boldsymbol{\mu} \frac{\exp\{-\boldsymbol{\mu}^T \boldsymbol{\Delta}^{-1} \boldsymbol{\mu}\}}{\pi\sqrt{\det[\boldsymbol{\Delta}]}} D(\boldsymbol{\mu}) \rho D^\dagger(\boldsymbol{\mu}), \tag{3.28}$$

equivalently described by the s-ordered characteristic function:

$$\chi_s[\mathcal{G}_N[\rho](\boldsymbol{\Delta})](\boldsymbol{\mu}) = \exp\left\{ -\frac{1}{2}\Big(s\boldsymbol{\mu}^T\boldsymbol{\mu} - 2\boldsymbol{\mu}^T\boldsymbol{\Delta}\boldsymbol{\mu} \Big) \right\} \chi_0[\rho](\boldsymbol{\mu}). \tag{3.29}$$

In fact, the covariance matrix of a gaussian state along this channel evolves as

$$\boldsymbol{\sigma}_N = \boldsymbol{\sigma}_0 + \frac{1}{2}\boldsymbol{\Delta}. \tag{3.30}$$

By comparing 3.27 and 3.30, one obtains that, for small times $\Gamma t \ll 1$ and high number of photons $N \gg 1$, the gaussian channel is a solution of the Born-Markov quantum optical master equation, provided the condition

$$\boldsymbol{\Delta} = 2N\Gamma t\, \mathbb{I}_2. \tag{3.31}$$

High temperature regime

In the high temperature regime $T \gg 1$, the explicit form of $\Delta(t)$ reads

$$\Delta(t) \underset{T\gg 1}{\simeq} 2K_B T \frac{\omega_c^2}{\omega_c^2 + \omega_0^2} \left\{ 1 - e^{-\omega_c t} \left[\cos(\omega_0 t) - \frac{\omega_0}{\omega_c} \sin(\omega_0 t) \right] \right\}, \tag{3.32}$$

while $\gamma(t)$ does not change as it is not temperature-dependent. Consequently, for large temperature the master equation coefficients $\Delta(t) \pm \gamma(t) \simeq \Delta(t)$ and Eq. 3.18 becomes

$$\frac{d}{dt}\rho(t) \underset{T\gg 1}{\simeq} \frac{\Delta(t)}{2}\mathcal{L}[a]\rho + \frac{\Delta(t)}{2}\mathcal{L}[a^\dagger]\rho, \tag{3.33}$$

which is a high temperature version ($N \gg 1$) of the Born-Markov master equation with time-dependent coefficients. In this case, the non-Markovian features of the map only depend on $\Delta(t)$, such that if $\Delta(t)$ is negative for some time t, the evolution is non-Markovian.

Moreover, it is interesting to evaluate $\Delta_\Gamma(t)$, as it plays a fundamental role in the dynamics in the phase space: in fact, observing Eq. 3.19, it is possible to see that when $\Gamma(t) \ll 1$, that is, $\Gamma t \ll 1$ for the Born-Markov master equation, the characteristic function becomes gaussian, which means that the solution of the time-dependent Born-Markov

master equation turns into a Gaussian channel, provided $\mathbf{\Delta} = \Delta_\Gamma(t)\mathbb{I}_2$. The explicit expression of $\Delta_\Gamma(t)$ for high temperature reads:

$$\Delta_\Gamma(t) = \frac{\omega_c K_B T}{(\omega_c^2+\omega_0^2)^2}\Big\{\omega_0^2(1+\omega_c t) - \omega_c^2(1-\omega_c t) + \\ + e^{-\omega_c t}\Big[(\omega_c^2-\omega_0^2)\cos(\omega_0 t) - 2\omega_c\omega_0\sin(\omega_0 t)\Big]\Big\} \tag{3.34}$$

3.2.2 Stochastic approach to Born-Markov master equation

Now, let's consider a quantum harmonic oscillator interacting with a classical external field. The Hamiltonian of the system may be written as $H = H_0 + H_{SC}$ where the free and interaction Hamiltonians are given by

$$H_0 = \hbar\omega_0 a^\dagger a \tag{3.35a}$$

$$H_{SC} = \hbar\left[a\bar{B}(t)e^{i\omega t} + a^\dagger B(t)e^{-i\omega t}\right], \tag{3.35b}$$

with ω_0 the natural frequency of the oscillator and $B(t)$ a time-dependent fluctuating field with central frequency ω described by a stochastic process with zero mean, whose complex conjugate is $\bar{B}(t)$. Once again, the Hamiltonian H is rescaled in units of $\hbar\omega_0$. As a straightforward consequence, the stochastic classical field $B(t)$, its central frequency ω and the time t become dimensionless quantities (in units of ω_0 and ω_0^{-1} respectively).

The Hamiltonian in the interaction picture reduces to:

$$H_I(t) = ae^{-i\delta t}\bar{B}(t) + a^\dagger e^{i\delta t}B(t), \tag{3.36}$$

where $\delta = 1-\omega$ is the detuning between the natural frequency of the oscillator and the central frequency of the CSF (in units of ω_0). The corresponding evolution operator is given by

$$U(t) = \mathcal{T}\exp\left\{-i\int_0^t ds\, H_I(s)\right\}, \tag{3.37}$$

where $\mathcal{T}$ denotes time ordering.

Notice, however, that as far as $B(t_1)\bar{B}(t_2) = [B(t_1)\bar{B}(t_2)]^*$, the two-time commutator $[H_I(t_1), H_I(t_2)]$ is proportional to the identity

$$[H_I(t_1), H_I(t_2)] = 2\,i\sin\left[\delta(t_2-t_1)\right]\, B(t_1)\bar{B}(t_2)\,\mathbb{I}, \tag{3.38}$$

and this form allows to evaluate time ordering using the Magnus expansion, which results to be exact at the second order already. According to the Magnus expansion, the evolution operator may be written as

$$U(t) = \exp(\Omega_1 + \Omega_2) \tag{3.39}$$

where:

$$\Omega_1 = -i\int_0^t ds_1\, H_I(s_1) = a^\dagger\phi_t - a\phi_t^* \tag{3.40a}$$

$$\phi_t = -i\int_0^t ds_1\, e^{i\delta s_1}B(s_1) \tag{3.40b}$$

and

$$\Omega_2 = \frac{1}{2}\int_0^t ds_1 \int_0^{s_1} ds_2 \; [H_I(s_1), H_I(s_2)] \propto \mathbb{I}. \tag{3.41}$$

Since Ω_2 is proportional to the identity the evolution of an initial density operator $\rho(0)$ reads

$$\rho(t) = \left[e^{\Omega_1}\rho(0)\, e^{\Omega_1^*}\right]_B = \left[D(\phi_t)\rho(0)D^\dagger(\phi_t)\right]_B \tag{3.42}$$

where $D(\lambda)$ is the displacement operator and $[\dots]_B$ denotes the average over the different realization of the stochastic process. Eq. (3.42) shows that the interaction Hamiltonian with a classical field results in a time-dependent displacement of argument ϕ_t, related to the classical field $B(t)$ and, then, strongly affected by its stochasticity.

Using the Glauber decomposition [102] for the initial state

$$\rho(0) = \int \frac{d^2\mu}{\pi}\, \chi_0[\rho(0)](\mu)\, D^\dagger(\mu)\,, \tag{3.43}$$

where $\chi_0[\rho](\mu)$ denotes the symmetrically ordered characteristic function, the state evolves as

$$\rho(t) = \int \frac{d^2\mu}{\pi}\, \left[e^{\mu\phi^*(t)-\mu^*\phi(t)}\right]_B \chi_0[\rho(0)](\mu) D^\dagger(\mu)\,, \tag{3.44}$$

where, for any Gaussian stationary process, it is possible to write

$$\left[e^{\mu\phi^*(t)-\mu^*\phi(t)}\right]_B = e^{-|\mu|^2\sigma(t)} \tag{3.45}$$

and $\beta(t)$ can be expressed as

$$\beta(t) = \int_0^t\int_0^t ds_1 ds_2 \; \cos\left[\delta(s_1-s_2)\right]\; K(s_1,s_2)\,. \tag{3.46}$$

The s-ordered characteristic function $\chi_s[\rho(t)](\mu)$ of the evolved state is given by

$$\chi_s[\rho(t)](\mu) = \chi_0[\rho(0)](\mu)\; \exp\left\{\frac{1}{2}|\mu|^2\,(s-2\beta(t))\right\}\,, \tag{3.47}$$

which corresponds to a Gaussian noise channel:

$$\rho(t) = \mathcal{G}_N[\beta(t)\mathbb{I}_2] = \int \frac{d^2\mu}{\pi\beta(t)} e^{-\frac{|\mu|^2}{\beta(t)}}\; D(\mu)\rho(0)\, D^\dagger(\mu), \tag{3.48}$$

As a result, while Eq.3.42 suggests that a single realization of the stochastic field drives the input state over the phase space via a displacement operation, the stochastic average of all these possible evolutions of the state results in a diffusive evolution, where $\beta(t)$, namely the variance of the Gaussian channel, plays the role of the diffusive coefficient. The variance $\beta(t)$ is only determined by the explicit stochastic process chosen.

Nevertheless, it is straightforward that the stochastic field approach allows to simulate the dynamics ruled by the time dependent Born-Markov master equation as long as $\Gamma(t) \ll 1$ and in regime of high temperature. In fact, under these assumptions, the full quantum model and the stochastic approach lead to dynamics described by a gaussian channel and share the same characteristic function, as long as $\beta(t)$ is chosen identical to $\Delta_\Gamma(t)$.

Along the line of what was done with stochastic dephasing, in order to have a perfect equivalence between the stochastic approach and the full quantum model, one needs to find a regime in which the variances of the channels are identical. Assuming the stochastic field $B(t)$ obeys a Ornstein-Uhlenbeck process, one finds that $\beta(t)$ and $\Delta_\Gamma(t)$ for a Ohmic reservoir at large temperatures coincide by defining $\lambda = \Gamma K_B T$ and assuming $\omega_0 = \delta$, that is, the original Ohmic spectrum is detuned from the system frequency ω_0.

This latter result is meaningful but not surprising: indeed, the correlation function $\kappa(s)$ in Eq. 3.17a for a Lorentz-Drude spectrum at high temperature reduces to

$$\begin{aligned}\kappa(s) &\underset{T\gg 1}{\simeq} 2\int_0^\infty d\omega\, J_{LD}(\omega)\frac{K_B T}{\omega}\cos(\omega s)\\ &= 2K_B T\int_0^\infty d\omega\, J_{OU}(\omega)\cos(\omega s) = K_B T\, K_{OU}(s).\end{aligned} \tag{3.49}$$

For this reason, a classical stochastic field described by an Ornstein-Uhlenbeck process faithfully represents the full quantum dynamics in the specified regimes and yields the very same variance $\beta(t) = \Delta_\Gamma(t)$.

Finally, it is important to stress that whatever specific gaussian process is chosen, the stochastic approach is not able to reproduce all aspects of the quantum dynamics: the stochastic description stands as an equivalent model only when the approximations $\Gamma t \ll 1$ and $N \gg 1$ are both valid.

3.3 Non-Markovianity of stochastic interactions

In this section, I address the study of the non-Markovianity of the stochastic interactions presented before. Let's start by reminding the conditions by which a quantum map $\mathcal{E}$ is Markovian: on one hand, the dynamical map must be completely positive and trace preserving (CPTP); on the other hand, a Markovian map has to be divisible, i.e. satisfy a composition rule

$$\mathcal{E}(t,t_0) = \mathcal{E}(t,t_1)\mathcal{E}(t_1,t_0) \quad \forall t_1 : t \geq t_1 \geq t_0. \tag{3.50}$$

In both models, the composition of the maps corresponds to a convolution, leading to $\mathcal{E}(\Delta t_2)\mathcal{E}(\Delta t_1) = \mathcal{E}(\Delta t_1 + \Delta t_2)$. However, this condition holds if and only if

$$\beta(\Delta t_1 + \Delta t_2) = \beta(\Delta t_1) + \beta(\Delta t_2), \tag{3.51}$$

which depends on the properties of the kernel of correlations that determines the stochastic process. In the case of Ornstein-Uhlenbeck and Power-Law processes, the divisibility condition is not satisfied, as neither of the two processes features an additive variance $\beta(t)$, for any choice of finite and strictly positive parameters. Therefore, stochastic phase diffusion and stochastic dissipation are both represented by non-Markovian dynamical maps.

Nevertheless, in the regime of small correlation time of the environment, the variance $\beta(t)$ becomes a linear function of time and additivity is restored, which implies that the map turns Markovian only when $t_{_E} \to 0$, i.e. the very same regime in which the solutions of the stochastic models satisfy the Markovian master equations.

As shown in the previous section, the stochastic approach allows to properly simulate the dynamics ruled by the time-dependent Born-Markov master equation in the high temperature regime, which is Markovian if and only if $\Delta(t) \geq 0$, as a negative coupling rate would lead to a violation of the complete positivity of the map.

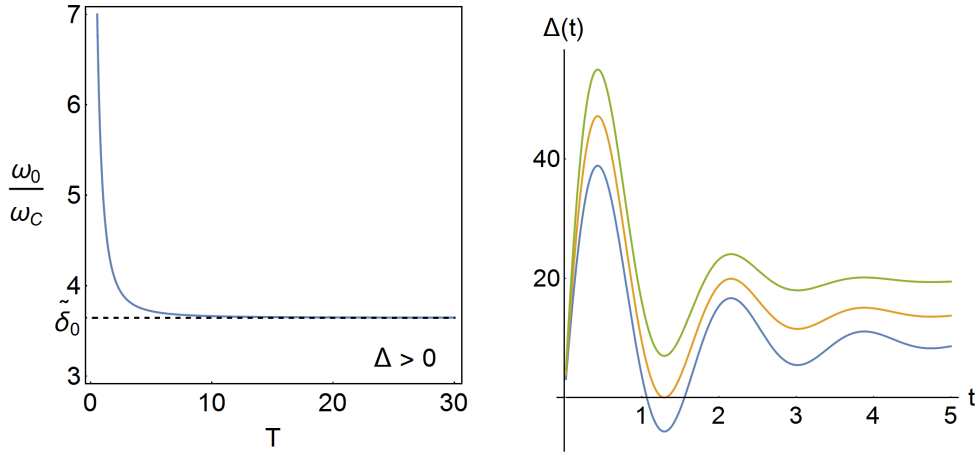

Figure 3.1: Left panel: contourplot showing the condition $\Delta(t) = 0$ as a function of temperature T and ratio ω_0/ω_c. The ratio ω_0/ω_c tends to a asymptotic value $\tilde{\delta}_0$ retrieved classically. Right panel: dynamics of the rate $\Delta(t)$ at high temperature $T = 100$ for many values of ratio $\tilde{\delta} = \omega_0/\omega_c$, $\tilde{\delta} = 1.25\,\tilde{\delta}_0$ (blue), $\tilde{\delta} = \tilde{\delta}_0$ (orange), $\tilde{\delta} = 0.8333\,\tilde{\delta}_0$ (green). When $\tilde{\delta} > \tilde{\delta}_0$, the rate $\Delta(t)$ assumes negative values.

The explicit mapping is given by $\beta(t) = \Delta_\Gamma(t)$, where $\Delta_\Gamma(t)$ is given by Eq. 3.20b. An oscillating behaviour of $\beta(t)$ actually addresses a temporary negative rate $\Delta(t)$, displaying the non-Markovian features of the dynamics. As shown in Chapter 2, the oscillations of $\beta(t)$ depend on a dimensionless parameter $\tilde{\delta}_0$, such that any value larger than this threshold induces oscillations. The very same threshold actually exists even in the full quantum model at high temperatures: the left panel of Fig. 3.1 shows a contourplot of the values of temperature and ratio ω_0/ω_c such that $\Delta(t) = 0$. The value of the threshold changes with the temperature, approaching the asymptotic value $\tilde{\delta}_0$, obtained with the stochastic approach. The right panel shows the time-dependence of the rate $\Delta(t)$ at high temperature. The figure shows that, when the ratio ω_0/ω_c is larger than the threshold value $\tilde{\delta}_0$ (blue line), the rate assumes negative values, i.e. the dynamics is non-Markovian.

As a result, the stochastic approach successfully manages to address and reveal the non-Markovian features of the full quantum models it describes the dynamics of. Therefore, classical stochastic fields may be used to properly introduce non-Markovian effects without resorting to solve quantum master equations.

3.4 Summary

- The evolution of a quantum system affected by Markovian phase diffusion can always be portrayed by stochastic fields, the explicit mapping being given by setting the coupling parameter $\lambda = \Gamma$.
- Stochastic fields may reproduce the dynamics of a quantum system ruled by a time-dependent quantum optical master equation only in its early stage ($\Gamma t \ll 1$) and in the regime of high temperatures $T \gg 1$. The explicit mapping is obtained setting $\lambda = \Gamma N$.

- Stochastic phase diffusion and stochastic dissipation lead to non-Markovian dynamics. Moreover, the stochastic modelization fully captures the non-Markovianity of the time-dependent quantum optical master equation: the very same threshold $\tilde{\delta}_0$ triggering oscillations of $\beta(t)$ actually distinguishes markovian and non-markovian regimes of the full quantum dynamics.

CHAPTER 4

Stochastic approach to non-Markovian decoherence

This chapter is devoted to the analysis of the evolution of quantum features of systems perturbated by stochastic noise. As shown in the previous chapter, under precise conditions the stochastic noise may reproduce quantum environments in terms of faithful mapping. Now, it is time to see how the forms of stochastic noise introduced affect the dynamics of the quantum features. In particular, this chapter is divided in two: in the first part, I analyze the evolution of quantumness of states facing stochastic dissipation, comparing the results to those obtained with a full quantum Markovian environment; in the second part, I study the performance of phase communication channels, focusing on the benefits the stochastic approach confers.

4.1 Quantum-to-classical transition with noisy environment

Let's consider a quantum harmonic oscillator interacting with a classical stochastic field. The interaction Hamiltonian is

$$H_I(t) = ae^{-i\delta t}\bar{B}(t) + a^\dagger e^{i\delta t}B(t). \tag{4.1}$$

In the previous chapter, the dynamics of a system subject to this kind of stochastic interaction was proven to be represented by a Gaussian channel

$$\rho(t) = \int \frac{d^2\mu}{\pi\beta(t)} e^{-\frac{|\mu|^2}{\beta(t)}}\, D(\mu)\rho(0)\, D^\dagger(\mu), \tag{4.2}$$

where the variance $\beta(t)$ depends on the specific stochastic process chosen. Also, as previously shown, the Gaussian channel faithfully describes the early stage of the thermalization process of the system, and so does the stochastic mapping. Therefore, one expects a system interacting with a classical noise to suffer decoherence, eventually lose its quantum features and cross the border to the classical realm, i.e. relax to a statistical mixture of classical-like states. Of course, this quantum-to-classical transition occurs in a finite time, which will be addressed as *survival time of nonclassicality*.

As previously anticipated in Chapter I, the notion of nonclassicality relies on the Glauber P-function. In fact, a state featuring a positive P-function is a statistical mixture of coherent states, which are considered classical-like states because of their statistics. Therefore, if the P-function of a state is positive, the state is said to be *classical*, otherwise the state is *nonclassical*. This very definition may be expressed in a quantitative way by means of the *nonclassical depth*.

The nonclassical depth η of a quantum state [103] is defined as the minimum number of photons to be added to a state in order to erase all of its quantum features. In terms of the s-ordered Wigner functions, the nonclassical depth is given by

$$\eta = \frac{1}{2}(1 - \bar{s}) \,,$$

where $\bar{s}$ is the largest value of s for which the corresponding s-ordered Wigner function $W_s[\rho](\alpha)$ is positive and may be seen as a classical probability distribution. In turn, η definitely has to satisfy $0 \leq \eta \leq 1$: on one hand, if $\eta = 0$, no photons need to be added, which means that any s-ordered Wigner function is positive; on the other hand, $\eta = 1$ implies that every Wigner function (except the Husimi Q that is always positive) is nonclassical, Glauber P-function included.

The nonclassical depth allows to easily define the survival time of nonclassicality: a nonclassical state turns classical in a finite time t_Q when a noisy environment adds a number of photons equivalent to the nonclassical depth of the initial state. Therefore, at time t_Q, the P-function of the state becomes strictly positive.

In this part of the dissertation, I use the *nonclassical depth criterion* to analyze the relation between the survival time of nonclassicality and the parameters of the classical stochastic field. In particular, I show that the correlation time of the environment and the detuning play a fundamental role in inducing revivals of quantumness and increasing the survival time of nonclassicality beyond the limit of a Markovian interaction, retrieved by performing the limit $t_{_E} \to 0$.

Finally, I consider other three criteria of nonclassicality: the negativity of the Wigner function, the Vogel criterion, based on the characteristic function, and the Klyshko criterion for the photon-number distribution. While the sole nonclassical depth criterion represents a proper (i.e., necessary and sufficient) criterion for nonclassicality, the other quantities have the advantage of being good candidates for an experimental implementation.

Let's start assuming the system is initially prepared in a Fock state $|n\rangle$ or in a superposition of coherent states with opposite phases, the so-called Schrödinger-cat state:

$$|\psi_{cat}\rangle = \frac{1}{\mathcal{N}}\big(|\alpha\rangle + |-\alpha\rangle\big) \tag{4.3}$$

where $|\alpha\rangle$ indicates a coherent state and is $\mathcal{N} = 2\left[1 + \exp(-2|\alpha|^2)\right]$.

Since they have maximal nonclassical depth, Fock and cat states represent the proper preparation to analyze the quantum-to-classical transition in full details. Actually, as will be clearer afterwards, any pure state other than Gaussian pure states would be equally good to address the dynamics of the nonclassical depth. On the other hand, sufficient criteria as the Vogel criterion and the Klyshko criterion do depend on the specific state under investigation, and thus having in mind a specific class of states will be of help to properly address the detection of nonclassicality in realistic conditions.

The s-ordered characteristic and Wigner functions of the Schrödinger-cat state $\rho_{\text{cat}} =$

$|\psi_{\text{cat}}\rangle\langle\psi_{\text{cat}}|$ are respectively given by

$$\chi_s[\rho_{\text{cat}}](\mu) = \frac{2}{\mathcal{N}}\, e^{-\frac{1}{2}(1-s)|\mu|^2} \left[\cos\left(2\,\text{Im}\,\mu\alpha^*\right) + e^{-2|\alpha|^2}\cosh\left(2\,\text{Re}\,\mu\alpha^*\right)\right]. \tag{4.4a}$$

$$W_s[\rho_{\text{cat}}](\xi) = \frac{2\, e^{-\frac{2|\xi|^2}{1-s}}}{\mathcal{N}\pi(1-s)} \times \left[e^{\frac{2s|\alpha|^2}{1-s}}\cos\left(\frac{4}{1-s}\,\text{Re}\,\xi\alpha^*\right) + e^{-\frac{2|\alpha|^2}{1-s}}\cosh\left(\frac{4}{1-s}\,\text{Im}\,\xi\alpha^*\right)\right]. \tag{4.4b}$$

The s-ordered characteristic and Wigner functions of a generic Fock state $\rho_F = |n\rangle\langle n|$ are respectively given by

$$\chi_s[\rho_F](\mu) = \exp\left\{-\frac{(1-s)|\mu|^2}{2} L_n(|\mu|^2)\right\}, \tag{4.5a}$$

$$W_s[\rho_F](\beta) = (-1)^n \frac{2}{\pi(1-s)}\left(\frac{1+s}{1-s}\right)^n \times \exp\left\{-\frac{2|\beta|^2}{1-s}\right\} L_n\left(\frac{4|\beta|^2}{1-s^2}\right). \tag{4.5b}$$

where $L_n(x)$ is the Laguerre polynomial of order n.

As it is apparent from their expressions, the s-ordered Wigner functions of both classes of states are not positive function for any $-1 < s \leq 1$. Correspondingly, the nonclassical depth η of a Fock or cat state is equal to one [104] independently on α or n, i.e. the cat and the number states are maximally nonclassical states independently on their energy, as the first positive Wigner function corresponds to $s = -1$, i.e. the Husimi Q function. More generally, the nonclassical depth is $\eta = 1$ [105] for any pure state other than Gaussian pure states (squeezed coherent state); squeezed states have $0 \leq \eta \leq \frac{1}{2}$ depending on the squeezing parameter, while coherent state have $\eta = 0$, properly capturing the fact that they are the closest analog to classical states for the quantum harmonic oscillator.

4.1.1 Dynamics of quantumness

Nonclassical depth

The interaction with the environment portrayed by the classical stochastic field turns the initial P distribution into a positive function after a finite interaction time t_Q. In addition, depending on the value of coupling, correlation time or detuning revivals of coherence (sudden birth of quantumness) may be observed. In order to determine these thresholds, one should consider the evolved state $\rho(t)$ and evaluate the time-dependent value of the nonclassical depth. Actually, it is sufficient to evaluate the nonclassical depth only for the initial state since the normally-ordered characteristic function $\chi_1[\rho(t)](\mu)$ (which generates the P distribution) corresponds to the $\tilde{s}$-ordered characteristic function of the initial cat state $\chi_{\tilde{s}}[\rho(0)](\mu)$ (see Sec. 3.2.2):

$$\chi_s[\rho(t)](\mu) = \chi_0[\rho(0)](\mu)\, \exp\left\{\frac{1}{2}|\mu|^2\,[s - 2\beta(t)]\right\} = \chi_{\tilde{s}}[\rho(0)](\mu)\,. \tag{4.6}$$

where $\tilde{s} = [s - 2\beta(t)]$.

As the nonclassical depth of the cat or the Fock states is equal to one, the P distribution becomes positive when it turns into a Husimi Q function, which corresponds

to $\tilde{s} = -1$. This happens in a finite (dimensionless) time t_Q that is straightforwardly defined by

$$\beta(t_Q) = 1, \tag{4.7}$$

while for a state with initial nonclassical depth η_0 the decoherence time t_Q is given by the solution of the equation $\beta(t_Q) = \eta_0$.

Let's immediately spend a few words about the condition 4.7: for values of t such that $\beta(t) > 1$, the P distribution is a positive function and the state is classical. It is worth noticing that the nonclassical depth criterion only depends on $\beta(t)$, that is, on the amount of noise added to the system, which is indipendent on the initial state parameter α or n. Moreover, as was shown in Chapter 2, $\beta(t)$ is an oscillating function, so a suitable choice of the parameters could bring to oscillations around the nonclassical depth value η_0, that is, revivals of quantumness.

Let's now assume the stochastic field is generated by an Ornstein-Uhlenbeck process and let's firstly focus on the resonant interaction ($\delta = 0$). In this case the non-rescaled $\beta(t)$ reduces to:

$$\beta(t) = \lambda t + \lambda t_E \left(e^{-\frac{t}{t_E}} - 1 \right), \tag{4.8}$$

and the equation $\beta(t) = 1$ has a single solution for any pairs of values of λ and t_E, which represents sudden death of quantumness without any revival. As anticipated previously, the autocorrelation function of the process approches a Dirac delta in the limit of small t_E. Performing the limit at this state, one obtains $\lim_{t_E \to 0} \beta(t) = \lambda t$. This form of $\beta(t)$ leads to a Markovian regime resembling the Born-Markov optical master equation when $t_E \ll 1$ and $\lambda = \Gamma N$. In the Markovian limit the decoherence time $t_Q^{(M)}$ is given by:

$$t_Q^{(M)} = \frac{1}{\lambda} = \frac{1}{\Gamma N}. \tag{4.9}$$

In the non-Markovian case, one has

$$t_Q = \frac{1}{\lambda} + t_E + t_E\, \xi\left(-e^{-1-(\lambda t_E)^{-1}}\right) = t_Q^{(M)} + t_E \left[1 + \xi\left(-e^{-1-t_Q^{(M)}/t_E}\right)\right] \tag{4.10}$$

where $\xi(x)$ is the product-log function, i.e. the positive real solution y of the equation $x = ye^y$. Using this expression, it is possible to show numerically that $t_Q > t_Q^{(M)}$ for any value of t_E and λ, i.e. the non-Markovian character of the field preserves the initial nonclassicality for longer times compared to the Markovian case. This is illustrated in the left panel of Fig. 4.1 which shows the ratio $t_Q/t_Q^{(M)}$ as a function of $\gamma = 1/t_E$ for different values of λ: the ratio is larger than unity for any value of γ and it increases for increasing λ, i.e. nonclassicality is better preserved for larger coupling. For increasing γ, the decoherence time t_Q reaches the Markovian limit independently on the value of the coupling.

Let's analyze now what happens in presence of detuning between the natural frequency of the system and the central frequency of the field. In this case the equation $\beta(t) = 1$ may have more than one solution (fixing all the parameters δ, t_E and λ) and thus revivals of coherence may appear. The right panel of Fig. 4.1 shows the contour plots $\sigma(t_Q) = 1$ as a function of time and γ for different values of the detuning δ and for a fixed value $\lambda = 1$ of the coupling. The regions lying to the right of the curves correspond to $\beta(t) > 1$, i.e. classicality (CL), whereas regions of nonclassicality (NCL) $\beta(t) < 1$ lie to the left. There are two main effects: i) at fixed γ the decoherence time t_Q

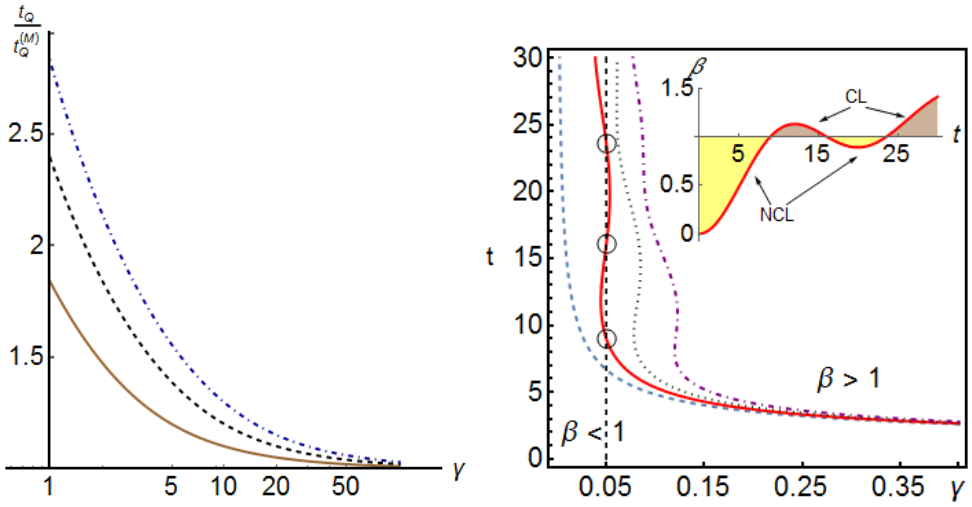

Figure 4.1: Evolution of quantumness according to the nonclassical depth criterion.
Left panel: resonant decoherence time t_Q as a function of the memory parameter γ, for different values of the coupling $\lambda = 1$ (solid brown), $\lambda = 2$ (dashed black) and $\lambda = 3$ (dot-dashed blue). For $\gamma \to \infty$, t_Q approaches the Markovian limit $t_Q^{(M)}$ independently on λ.
Right panel: contour plots of $\beta(t_Q) = 1$, in the off-resonance case, as a function of γ for a fixed value of the coupling $\lambda = 1$ and different values of the detuning $\delta = 0.3$ (solid red), $\delta = 0.4$ (dotted green) and $\delta = 0.5$ (dot-dashed purple). The dashed blue curve is chosen as a reference for the resonant case $\delta = 0$. In the regions lying to the left of the curves we have $\beta(t) < 1$, i.e. nonclassicality. The vertical line (dashed black) denotes points at fixed $\gamma = 0.05$ and the black circles indicate the three solutions of $\beta(t_Q) = 1$ for $\delta = 0.3$. Correspondingly, the regions of nonclassicality (NCL) and classicality (CL) are highlighted in the inset.

increases with the detuning, the effect is more pronounced for smaller γ; ii) revivals of quantumness, i.e. sudden death followed by sudden birth of quantumness, appear at fixed (and not too large) values of γ. This is illustrated in the right panel of Fig. 4.1 and in the corresponding inset, where, for $\delta = 0.3$ (solid red line) and $\gamma = 0.05$, $\beta(t)$ displays re-coherence effects. Notice that all the detuned curves satisfy the necessary condition for an oscillating $\beta(t)$, that is $\tilde{\delta} > \tilde{\delta}_0$. Nevertheless, only the red curve exhibits revivals of quantumness. Notice also that for increasing γ, revivals disappear and t_Q becomes more and more independent on the detuning, thus further confirming that a large value of γ approaches the Markovian limit.

Wigner negativity

A different notion of nonclassicality is based on the negativity of the Wigner function which is never singular, but it can take on negative values for nonclassical states, such as Fock states or superposition of coherent states [106]. The notion of nonclassicality arising from the negativity of the Wigner function is not equivalent to the nonclassical depth and it has been linked to non-local properties [107, 108]. More precisely, it has been shown that posivity of the Wigner function implies that the corresponding quantum state cannot violate any Bell inequality involving only position and momentum measurements. In turn, squeezed vacuum states display a positive Wigner function even though their nonclassical depth ranges from $\eta = 0$ to $\eta = \frac{1}{2}$, increasing with energy.

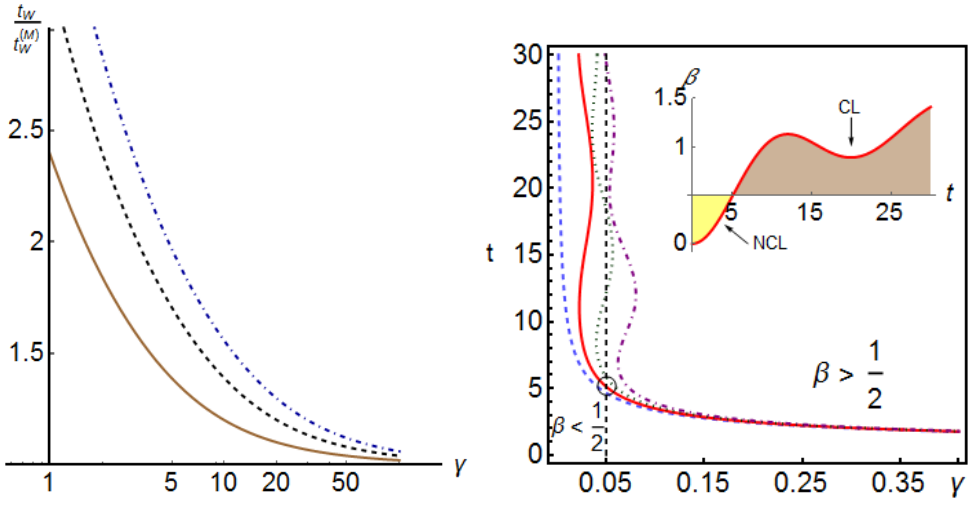

Figure 4.2: Dynamics of quantumness according to the Wigner negativity criterion.
Left panel: Wigner decoherence time t_W for a resonant interaction as a function of the memory parameter γ, for different values of coupling $\lambda = 1$ (solid brown), $\lambda = 2$ (dashed black) and $\lambda = 3$ (dot-dashed blue). For $\gamma \to \infty$, t_W approaches the Markovian limit $t_W^{(M)}$ independently on λ.
Right panel: contour plots of $\beta(t_W) = \frac{1}{2}$ in the off-resonance case as a function of γ for a fixed value of the coupling $\lambda = 1$ and different values of the detuning $\delta = 0.3$ (solid red), $\delta = 0.4$ (dotted green) and $\delta = 0.5$ (dot-dashed purple). The dashed blue curve is chosen as a reference for the resonant case $\delta = 0$. In the regions lying to the left of the curves we have $\beta(t) < \frac{1}{2}$, i.e. nonclassicality. The vertical line (dashed black) denotes points at fixed $\gamma = 0.05$ and the black circle indicates the solutions of $\beta(t_W) = \frac{1}{2}$ for $\delta = 0.3$. Correspondingly, the regions of nonclassicality (NCL) and classicality (CL) are highlighted in the inset.

It's possible to evaluate the time t_W in which the P function turns into a Wigner function in the very same way the nonclassical depth time was evaluated in the previous section. The condition that t_W must satisfy, in order to change from a normally ordered into a symmetrically ordered characteristic function, is

$$\beta(t_W) = \frac{1}{2}. \tag{4.11}$$

Exactly as the nonclassical depth criterion, the Wigner decoherence time depends only on $\beta(t)$ and it is not affected by the initial state parameter α or n. For a state with initial nonclassical depth equal to η_0, the Wigner decoherence time is the solution of $\sigma(t_W) = \eta_0 - 1/2$ if $\eta_0 > \frac{1}{2}$ or $t_W = 0$ otherwise.

In the Markovian limit $\gamma \gg 1$ the decoherence time $t_W^{(M)}$ of the cat or the Fock state is simply half of $t_Q^{(M)}$

$$t_W^{(M)} = \frac{1}{\lambda} = \frac{1}{2\Gamma N} = \frac{1}{2} t_Q^{(M)}. \tag{4.12}$$

The behaviour of the Wigner decoherence time in the non-Markovian case is illustrated in Fig. 4.2. The left panel shows that t_W is significantly increased by the presence of time correlations in the CSF (non-Markovian behavior), whereas the right panel reveals re-coherence effects for certain values of the detuning and memory parameters. In particular, the vertical black line ($\gamma = 0.05$) intercepts the solid red line ($\delta = 0.3$) just once,

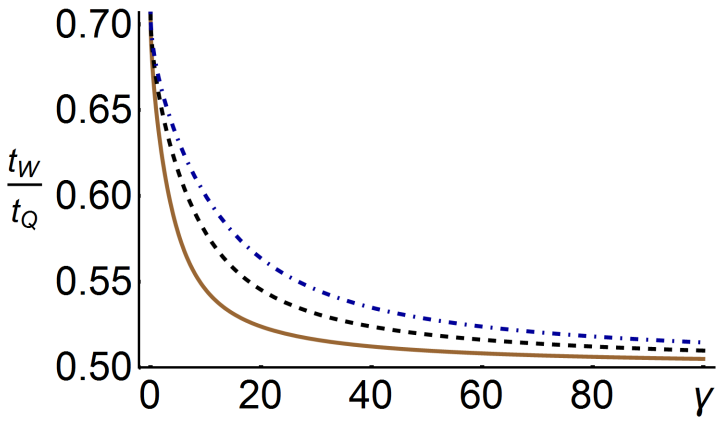

Figure 4.3: The ratio t_W/t_Q as a function of γ for different values of coupling $\lambda = 1$ (solid brown), $\lambda = 2$ (dashed black) and $\lambda = 3$ (dot-dashed blue). For $\gamma \gg 1$ the ratio approaches the Markovian value $\frac{1}{2}$, whereas for $\gamma \ll 1$ it approaches to the $\frac{1}{\sqrt{2}}$, due to the quadratic dependence on time of $\beta(t)$.

which means that revivals of nonclassicality revealed by the nonclassical depth criterion (see Fig.1) are not captured by the Wigner criterion.

Fig. 4.3 displays a comparison between t_Q and t_W by showing their ratio as a function of γ. For large values of the memory parameter γ (i.e. in the Markovian limit) the ratio approaches $\frac{1}{2}$, according to Eq. (4.12). In all the other cases, the ratio increases and approaches the limiting value $\frac{1}{\sqrt{2}}$ for $\gamma \to 0$. This may be understood as a consequence of the behaviour of $\beta(t)$, as reported in Eq. (3.12c). Indeed, $\beta(t)$ is basically linear in time for large γ, whereas it shows a quadratic behaviour for $\gamma \ll 1$.

The study of the Wigner negativity criterion in the off-resonance regime confirms the main conclusions drawn from the analysis of the nonclassical depth: for $\delta \neq 0$ the Schrödinger cat coherence survives longer and sudden death and birth of nonclassicality may appear.

Vogel criterion

The criteria illustrated previously allow to discriminate classical states from nonclassical ones, and to follow the dynamics of decoherence, by inspecting the time evolution of a quasi-probability distribution in the phase-space. Starting from the criterion based on the posivity of the P-function a sufficient criterion, suitable for experimental implementation, has been suggested and developed [109] According to this criterion, a state is nonclassical (i.e. its P-function is singular) if there exists some complex number $\mu = (u, v)$ such that the normally ordered characteristic function satisfies the following inequality

$$|\chi_1[\rho(t_V)](\mu)| > 1, \tag{4.13}$$

where $\chi_1[\rho(t)](\mu) = \chi_0[\rho(t)](\lambda)\mathrm{e}^{e^{\frac{1}{2}|\mu|^2}}$. It should be emphasized that this is only a sufficient condition to characterize nonclassical states. However, it has an advantage stemming from the fact that the symmetric characteristic function can be directly measured via balanced homodyne detection [110]. It is worth noticing, however, that in contrast with the two criteria shown previously, the Vogel criterion do depend on the state under investigation, i.e. the smallest interaction time t_V for which Eq. (4.13) is satisfied,

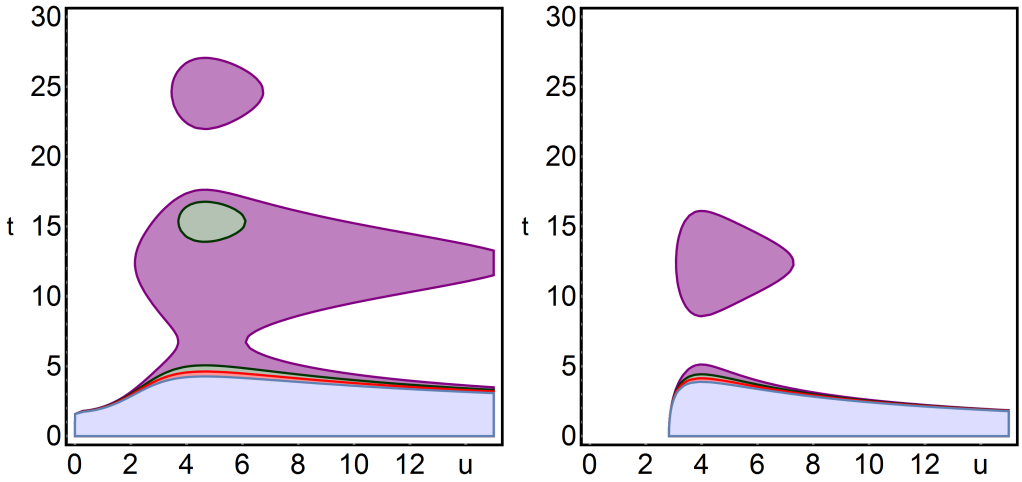

Figure 4.4: (Color Online) Left panel: cat state Vogel time t_V as a function of u, with $|\alpha| = \sqrt{2}$. Right panel: Vogel time t_V as a function of u for Fock state $|2\rangle$. In both panels, $\gamma = 0.05$ and filled regions correspond to $|\chi_1[\rho(t_V)(u,0)| > 1$. From bottom to top: the blue region represents the resonant interaction ($\delta = 0$), whereas the red ($\delta = 0.3$), green ($\delta = 0.4$) and purple ($\delta = 0.5$) regions correspond to the off-resonance case. The spots for the green and the purple regions indicate the presence of revivals of nonclassicality.

depends on the amplitude α for the Schrödinger state or on the specific Fock state $|n\rangle$. Here, I consider cat states with real amplitude $\alpha = \alpha^* = \sqrt{2}$, the reason of this choice being justified later (see next section). The Fock state $|n = 2\rangle$ is chosen such that the number of photons approximates the cat mean number of photons $\langle a^\dagger a\rangle \simeq 2$.

The plots in the left and right panels of Fig. 4.4, for cat and Fock states respectively, show the regions for which $|\chi_1[\rho(t_V)](\mu)| > 1$, as a function of $\mathrm{Re}(\mu) = u$ (with $v = 0$) and varying the detuning parameter δ (different colors). As it is possible to see in both figures, after a certain time t_V nonclassicality disappears, but the sudden birth and sudden death of quatumness is present also according to the Vogel criterion (look, for example, at the green and purple regions) and consistently with the two previous criteria, as far as the off-resonance interaction ($\delta \neq 0$) between the system and the CSF is set.

Klyshko Criterion

Klyshko introduced a criterion for nonclassicality based on the properties of the photon number distribution of the state under investigation [111]. The criterion, which is only sufficient for nonclassicality, may be seen as a generalization of the customary condition on the Fano factor of the distribution, and states that the state ρ is nonclassical if there exists an integer number n such that:

$$B(n) = (n+2)p(n)p(n+2) - (n+1)[p(n+1)]^2 < 0, \tag{4.14}$$

where $p(n) = \langle n|\rho(t)|n\rangle$ is the photon number probability of the state ρ. Analogously to the Vogel criterion, this nonclassicality witness is of interest since it is *experimentally friendly*, being based on the photon distribution, which may be obtained by photon counting or by on-off detectors [112, 113]. The analysis of the Schrödinger cat nonclassicality, according to the Klyshko criterion, discloses that $B(1)$ becomes negative after

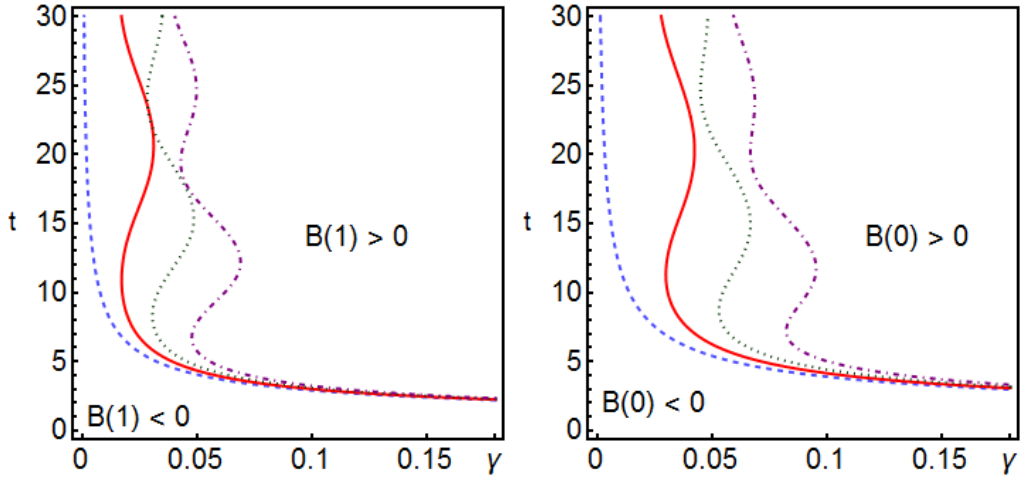

Figure 4.5: (Color Online) Left panel: Dimensionless decoherence time t_K for the Klyshko criterion as a function of γ for the cat state with $\alpha = \sqrt{2}$. Right panel: Decoherence time t_K for the Klyshko criterion as a function of γ for the Fock state $|2\rangle$. In both panels, dashed blue curve represents the resonant interaction ($\delta = 0$), whereas solid red ($\delta = 0.3$), dashed green ($\delta = 0.4$) and dot-dashed purple ($\delta = 0.5$) curves refer to the off-resonance case. In the regions lying to the left of the curves we have $B(1) < 1$, i.e. nonclassicality.

a certain time t_K dependent on the detuning δ and the memory parameter γ. As it is shown in the left panel of Fig. 4.5, the Klyshko criterion confirms that the cat survival time increases for short γ and it is affected by detuning. Also in this case, sudden death and birth of quantumness can be observed, as for fixed γ there exist more than one time t_K that satisfies the Klyshko criterion (4.14). A similar behaviour is shown for the Fock state $|2\rangle$ in the right panel of Fig. 4.5, the only difference being the use of the quantity $B(0)$ instead of $B(1)$ to detect the quantum-to-classical transition. As mentioned earlier, the parameter α of the cat state is set to $|\alpha| = \sqrt{2}$. In turn, this choice maximizes the effectiveness of Klyshko criterion, i.e. is the value corresponding to the longest survival time by Klyshko criterion [114].

4.1.2 Decoherence times comparison

In the previous sections I went through a quantitative analysis of the nonclassicality dynamics of the Schrödinger cat and the Fock state, analyzing four different nonclassicality criteria. The interaction of a quantized harmonic oscillator with a CSF, in terms of an OU process, allows to preserve the nonclassicality of each input state for certain periods of times and this result has been confirmed by the different nonclassicality criteria. In order to emphasize that Vogel and Klyshko criteria are only sufficient and that they do not show any monotony properties, a quantitative analysis for both input states is shown in Table 4.1, which contains the times corresponding to the sudden death of quantumness achieved according to the four considered criteria, for several values of the detuning δ. In particular, they are obtained by fixing the value of the parameter $\gamma = 0.05$, which is responsible of an appreciable memory effect in the considered OU process.

As is apparent from the data, the times estimated with the Vogel criterion (or the Klyshko criterion) are always shorter than the nonclassical depth and the Wigner nega-

Schrödinger-cat state:

δ	0	0.3	0.4	0.5
t_Q	6.676	8.982	47.467	81.091
t_W	4.645	5.118	5.823	29.355
t_V	4.272	4.624	5.067	16.773
t_K	4.054	4.349	4.694	17.700

Fock (number) state:

δ	0	0.3	0.4	0.5
t_Q	6.676	8.982	47.467	81.091
t_W	4.645	5.118	5.823	29.355
t_V	3.886	4.140	4.425	5.128
t_K	5.412	6.253	21.329	49.527

Table 4.1: Dimensionless decoherence times, obtained for $\gamma = 0.05$, $\lambda = 1$ and different values of the detuning δ, corresponding to the sudden death of quantumness of the evolved Schrödinger cat state (Upper Table) and the evolved Fock state (Lower Table), according to the four nonclassicality criteria: nonclassical depth (t_Q), Wigner negativity (t_W), Vogel criterion (t_V) and Klyshko criterion (t_K).

tivity decoherence times. This is consistent with the fact that Vogel and Klyshko criteria provide only sufficient conditions for the loss of quantumness. Indeed, it is possible to still have an amount of nonclassicality in the evolving state which is undetected by these two criteria. Actually, Diosi demonstrated that for some nonclassical states the Vogel criterion is not satisfied [115]. In other words, the evolved cat or Fock state may still show some quantumness, according to other nonclassicality criteria, while the Vogel criterion is no longer violated.

Data contained in Table 4.1 clearly show that it is not possible to establish any order relation between the Vogel and the Klyshko decoherence times, and that the two experimentally achievable criteria may fail to return decoherence times comparable to the nonclassical depth time, which should be considered as the proper quantity to individuate the quantum to classical transition.

Power-law process

As mentioned in the introduction, the main conclusions of the analysis of the decoherence are qualitatively independent on the nature of the CSF used to model the environment. In order to show this explicitly, and to briefly illustrate the quantitative effects of a different modelling, I report here the results obtained for a Gaussian process characterized by a long range power-law autocorrelation function. The attention will be focused on the nonclassical depth criterion, as it is the most relevant one. I report once again the explicit form of $\beta_{PL}(t)$ for the power-law process in the case of the resonant interaction ($\delta = 0$) is the following:

$$\beta(t) = \lambda t + \lambda \frac{(1+\gamma t)^{2-a} - 1}{\gamma(a-2)}. \tag{4.15}$$

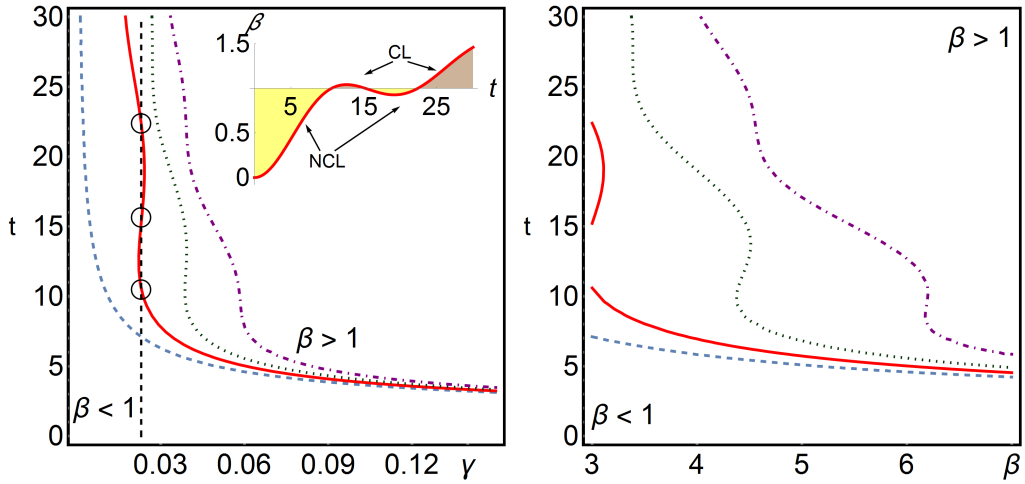

Figure 4.6: (Color online) Dynamics of quantumness according to the nonclassical depth criterion for a cat states evolving in classical environment with power-law autocorrelation function. In both panels, the dashed blue curve represents the resonant case $\delta = 0$, whereas solid red ($\delta = 0.3$), dotted green ($\delta = 0.4$), dot-dashed purple ($\delta = 0.5$) curves refer to the off-resonance case. Left panel: nonclassical depth time t_Q as a function of γ in the case of a Gaussian power-law process, for fixed $a = 3$ and $\lambda = 1$. For $\gamma \gg 1$ the nonclassical depth time t_Q approaches the Markovian limit independently of δ. Sudden death and birth of quantumness are highlighted by the circles along the dashed black line at $\gamma = 0.023$ and, correspondingly, in the inset. Right panel: nonclassical depth time t_Q as a function of β and fixed $\gamma = 0.023$.

This expression can be approximated in some particular regimes to:

$$\beta(t) \simeq \lambda t + \frac{\lambda\gamma t^2}{(a-2)(1+\gamma t)^a} \qquad (\gamma \gg 1) \quad (4.16)$$

$$\beta(t) \simeq \frac{\lambda t^2}{2}(a-1) \qquad (\gamma \ll 1) \quad (4.17)$$

As apparent from (4.16), for $\gamma \to \infty$ the nonclassical depth time approaches the Markovian limit $\beta(t) \propto t$. Also for the power-law process γ plays the role of a memory parameter. In the nonresonant case, the analytic form of $\beta(t)$ is extremely complex and is not reported in this dissertation, whereas the results are explained in the following.

The presence of sudden death and sudden birth of quantumness for the nonresonant interaction is shown, for an initial cat state, in the left panel of Fig. 4.6, where, for fixed γ and different choices of the detuning parameter $\delta \neq 0$, more than one value of time t_Q satisfies nonclassical depth criterion. In the right panel of Fig. 4.6 I show the nonclassical depth time as a function of the parameter a of power-law autocorrelation function. Furthermore, the presence of sudden death and birth of nonclassicality depends not only on the particular combination of parameters (δ, γ), but also on the parameter α itself. Actually, Fig. 4.6 shows that nonclassicality revivals can be also observed for the power-law process just like for the OU process, and that this phenomenon is mostly due to the introduction of the detuning parameter.

4.2 Phase communication channels in presence of noise

The transmission of classical information along an ideal bosonic quantum channel is optimized by encoding information onto Fock number states, according to a thermal distribution, and then retrieving this information by the measurement of the number of photons [116–118]. This strategy allows to achieve the ultimate channel capacity, i.e. to maximize the mutual information between the sender and the receiver, given a constraint on the overall energy sent through the channel, thus outperforming other encoding/decoding scheme involving different degrees of freedom of the radiation field, e.g. the amplitude or the phase.

Taking into account the unavoidable noise that affects the information carriers along the channel, the situation becomes more involved and a question arises on whether different coding/encoding schemes may offer better or comparable performances. Indeed, in the presence of a phase insensitive noise, e.g. amplitude damping, also coherent coding has been shown to achieve the ultimate channel capacity [119, 120].

In this section, I address communication channels based on phase encoding [121–123] and analyze in details their performances in the presence of phase diffusion, which represents the most detrimental kind of noise affecting this kind of channel [124,125]. In particular, we will consider communication schemes where the information is encoded by modulating the phase of a coherent signal, which then travels through a phase-diffusing environment before arriving at the receiver station and being detected.

As shown in Chapter 3, the evolution of a system in presence of phase diffusion is portrayed by a Gaussian channel where phase *static* noise is induced by a stationary environment. Moreover, stochastic interactions may successfully reproduce this kind of evolution and even unlock the possibility of exploring in an easy way non-Markovian *dynamical* noise scenarios. In this chapter, I test the efficiency of phase communication protocols in static and dynamical noisy environments, by evaluating the mutual information for both ideal phase receivers and covariant phase-space-based ones (corresponding to the marginal phase distribution of the Husimi Q-function). I then compare their performances each other and with the capacity of other relevant channels.

4.2.1 Phase-keyed communication channels

A schematic diagram of a quantum phase communication channel is depicted in Fig. 4.7. The sender encodes a finite number N of symbols using N different values of a phase shift ϕ_k, where $\phi_k < \phi_j$ if $k < j$ and $0 \leq k < N$. I assume a choice of equidistant phase values $\phi_k = 2\pi k/N$. The phase ϕ_k is encoded onto a *seed* state ρ_0 of a single-mode radiation field by the unitary phase-shift operation $U(\phi) = \exp(i\phi\, a^\dagger a)$, a being the annihilation operator, $[a, a^\dagger] = 1$, namely:

$$\rho_0 \to \rho_k \equiv U(\phi_k)\rho_0 U^\dagger(\phi_k)\,. \tag{4.18}$$

The signal then propagates along the channel to the receiver station, where it is detected by a suitable measurement scheme in order to retrieve the information it carries. More explicitly: the receiver performs a phase measurement on the output state and, once the phase is measured, he chooses a strategy to associate the measured value to one of the symbols of the sender's alphabet. The inference strategy should match the (continuous) output from the phase measurement to a symbol from a discrete alphabet. The straightforward choice consists in associating each phase value with the closest ϕ_k within a margin of error. To this aim the receiver divides the full phase range $[0, 2\pi)$ into N bins,

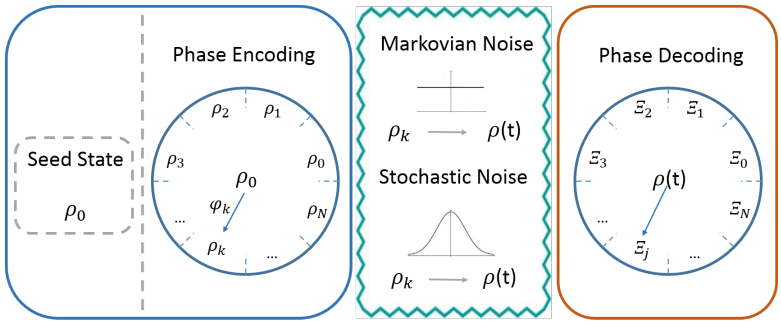

Figure 4.7: (Color online) Schematic representation of a phase communication channel. The sender encodes a finite number N of symbols using N different values of a phase-shift $\phi_k = 2\pi k/N$ imposed to a *seed* coherent state ρ_0. The signal then propagates along the channel, to the receiver station, in the presence of either static or dynamical noise and it is finally detected by a suitable measurement scheme in order to retrieve the carried information.

corresponding to the intervals

$$\Xi_j = [\phi_j - \Delta, \phi_j + \Delta)\,,$$

where $\Delta = \pi/N$ and $\bigcup_{j=1}^{N} \Xi_j = [0, 2\pi)$. More generally, the width of each bin may be different and dependent on j, though a symmetric choice is easily proven optimal. If ϕ denotes the value of the receiver's outcome, the inference rule is expressed as follows:

$$\text{if} \quad \phi \in \Xi_j \Rightarrow \quad \phi \to \phi_j\,. \tag{4.19}$$

The positive operator-valued measure (POVM) $\{\Pi(\phi_j)\} \equiv \{\Pi_j\}$ describing the measurement strategy employed by the receiver can be written as:

$$\Pi_j = \int_{\phi_j - \Delta}^{\phi_j + \Delta} \pi(\theta) d\theta, \tag{4.20}$$

where $\pi(\theta)$ is the actual POVM of the phase measurement performed by the receiver. A POVM for a covariant phase measurement may always written as [126, 128]:

$$\pi(\theta) = \frac{1}{2\pi} \sum_{n,m=0}^{\infty} A_{n,m} e^{-i(n-m)\theta} \left|n\right\rangle \left\langle m\right|, \tag{4.21}$$

where $A_{n,m}$ are the elements of a positive and Hermitian matrix $\boldsymbol{A}$, which is measurement-dependent. Covariance follows easily from Eq. (4.21), since $U(\phi)\pi(\theta)U^{\dagger}(\phi) = \pi(\theta + \phi)$ and thus

$$\Pi_j = U(\phi_j)\Pi_0 U^{\dagger}(\phi_j). \tag{4.22}$$

The combination of Eqs. (4.20) and (4.21) brings to an explicit form of the POVM Π_j, given by

$$\Pi_j = \sum_{n,m=0}^{\infty} A_{n,m} f_{n-m}(j) |n\rangle\langle m| \tag{4.23}$$

where the structure of the POVM is determined by the resolution function

$$f_d(j) = \frac{1}{2\pi}\int_{\phi_j-\Delta}^{\phi_j+\Delta} e^{-id\theta}d\theta = \frac{\sin\Delta\pi}{\pi d}e^{-id\phi_j}, \tag{4.24}$$

with the property $\sum_{j=1}^{N} f_d(j) = \delta_{d,0}$, where δ is the Kronecker delta.

The figure of merit to assess the performances of a communication channel is the mutual information between sender and receiver. This quantity measures the amount of information shared by the two parties and can be written as

$$\begin{aligned} I &= \sum_{k,j=0}^{N-1} p(k,j)\log_2\frac{p(k,j)}{p(k)\,p'(j)} \\ &= \sum_{k,j=0}^{N-1} p(j|k)p(k)\log_2\frac{p(j|k)}{p'(j)}, \end{aligned} \tag{4.25}$$

where $p(j|k)$ is the conditional probability of measuring a phase ϕ_j given the input phase ϕ_k; $p(k)$ is the *a priori* probability distribution of transmitting a ϕ_k-encoded seed state; $p(k,j) = p(j|k)\,p(k)$ is the joint probability to send the symbol ϕ_k and obtaining the outcome ϕ_j and, finally, $p'(j) \equiv p'(\phi_j)$ is the probability of the outcome ϕ_j, given by $p'(j) = \sum_{k=0}^{N-1} p(j|k)p(k)$.

Maximization over the probability $p(\phi_k)$ leads to the so called channel capacity, i.e. the maximum information transmitted through the channel per use. In particular, I analyze the case of uniform encoding probability, $p(k) = N^{-1}$, i.e. the letters have the same probability to be sent through the channel. The conditional probability of an outcome ϕ falling in the bin Ξ_j given the initial state ρ_k is

$$p(\phi\in\Xi_j|\rho_k) \equiv p(j|k) = \mathrm{Tr}[\rho_k\Pi_j]. \tag{4.26}$$

Under these conditions, the mutual information reduces to

$$I = \frac{1}{N}\sum_{k,j=0}^{N-1}\mathrm{Tr}[\varrho_k\Pi_j]\log_2\left\{\frac{\mathrm{Tr}[\varrho_k\Pi_j]}{N^{-1}\sum_{h=0}^{N-1}\mathrm{Tr}[\varrho_h\Pi_j]}\right\}. \tag{4.27}$$

By using the covariance property of the POVM and its explicit form given in Eq. (4.23), the conditional probability can be expressed as

$$\begin{aligned} p(j|k) &= \mathrm{Tr}[\rho_k\Pi_j] = \mathrm{Tr}[\rho_0\Pi_{j-k}] \\ &= \sum_{n,m=0}^{\infty} A_{n,m}f_{n-m}(j-k)\rho_{n,m}. \end{aligned} \tag{4.28}$$

Note that $\sum_k p(j|k) = \sum_k \mathrm{Tr}[\rho_k\Pi_j] = 1$, which follows from the symmetries of the resolution function, $f_{-d}(j) = f_d(j)$, i.e. $f_{-d}(-j) = f_d(j)$. Upon introducing the positive quantity $s = |j-k|$, we obtain a simpler form for the mutual information

$$I \equiv I(N,\bar{n}) = \log_2 N + \sum_{s=0}^{N-1} q(s)\log_2 q(s) \tag{4.29}$$

where $\bar{n}$ is the average number of photons of the seed signal and

$$q(s) = \sum_{n,m=0}^{\infty} A_{n,m} f_{n-m}(s) \rho_{n,m}$$
$$= \frac{1}{N}\Big\{1 + \sum_{n=0}^{\infty}\sum_{d=1}^{\infty} A_{n,n+d}\left[f_d(s)\rho_{n,n+d} + c.c.\right]\Big\}. \tag{4.30}$$

The function $q(s)$ measures the probability of finding a $2\pi s/N$ phase difference between the input and output signal, whatsoever value the encoded phase may assume.

The function $q(s)$ and thus the performances of the communication channel do depend on the measurement performed by the receiver through the matrix $(A_{n,m})$ and on the seed state via the matrix elements $\rho_{n,m} = \langle n|\rho_0|m\rangle$. In the following, I will focus on two particular phase measurements: the canonical phase measurement [126–130] and a phase-space-based one, i.e. the marginal phase distribution obtained from the Husimi Q-function [131–140]. The latter is a feasible phase measurement achievable, e.g., by heterodyne or double-homodyne detection. For the canonical measurement one has $A_{n,m} = 1$, whereas for the Q-measurement $A_{n,m} = \Gamma[1 + \frac{1}{2}(n+m)](n!m!)^{-\frac{1}{2}}$, $\Gamma[x]$ being the Euler Gamma function.

4.2.2 Quantum phase communication channels with static phase diffusion

In this section, I address quantum phase communication channels in the presence of phase diffusion, and start by considering situations where the environmental noise is static. Any phase communication channel is based on the observation that the optical field produced by a laser provides a convenient quantum system for carrying information. In particular, coherence of laser source ensures that a well-defined phase can be attributed to a light mode. Still, the unavoidable presence of noise generates a phase diffusion, which ultimately limits the coherence of the light. The master equation governing the evolution of the light beam in a static phase diffusing environment may be written as [125, 141]:

$$\frac{d}{dt}\rho = \frac{\Gamma}{2}\mathcal{L}[a^\dagger a]\rho\,, \tag{4.31}$$

where Γ plays the role of the static phase noise factor. An initial state $\rho(0)$ evolves with time as

$$\rho(t) = \sum_{n,m=0}^{\infty} e^{-\frac{1}{2}\tau(n-m)^2}\rho_{n,m}|n\rangle\langle m|\,, \tag{4.32}$$

where the rescale time $\tau = \Gamma t$ is introduced. One can easily see that the diagonal elements $\rho_{n,n}$ are unaffected by the phase noise, thus, energy is conserved, whereas the off-diagonal elements decay away exponentially.

Let's assume that the input seed is a coherent state of the radiation field, namely, $\rho_0 = |\alpha\rangle\langle\alpha|$ with:

$$|\alpha\rangle = e^{-|\alpha|^2/2}\sum_{n=0}^{\infty}\frac{\alpha^n}{\sqrt{n!}}|n\rangle\,. \tag{4.33}$$

Without lack of generality, α may be assumed real. The density matrix elements associated with the initial coherent state ρ_0 are

$$\rho_{n,m} = e^{-\bar{n}}\frac{\bar{n}^{(n+m)/2}}{\sqrt{n!m!}}, \tag{4.34}$$

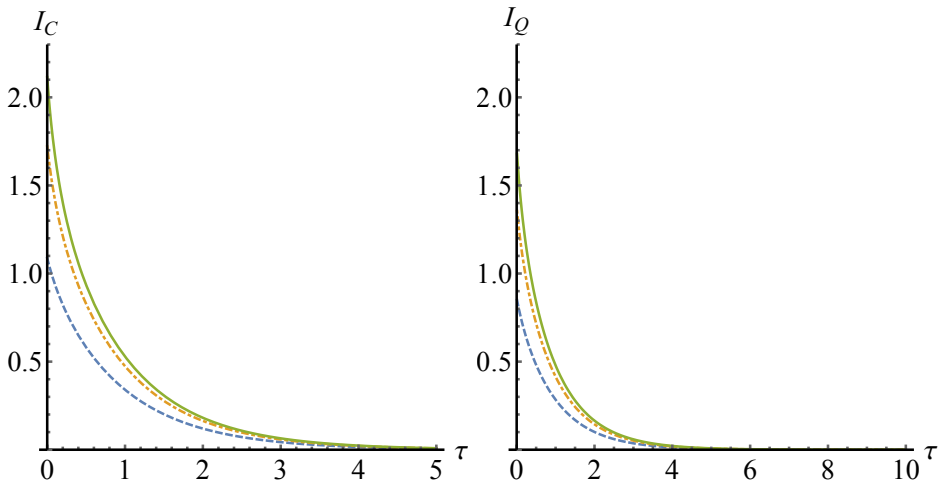

Figure 4.8: (Color online) Phase communication channels in the presence of static phase diffusion. The upper panels show the mutual informations for the ideal receiveir I_C (left) and the Q one I_Q (right) as a function of the noise parameter $\tau = \Gamma t$ for different values of the average number of photons: from bottom to top, $\bar{n} = 1$ (dashed blue), $\bar{n} = 2$ (dotdashed orange), $\bar{n} = 3$ (solid green). We set the alphabet size to $N = 20$.

where $\bar{n} \equiv \alpha^2$ is the average number of photons of the coherent state ρ_0. Exploiting Eq. (4.32), one finds that the state arriving at the receiver after the propagation through the noisy channel has the following density matrix elements:

$$\rho_{n,m} \to \rho_{n,m}(t) = e^{-\frac{1}{2}\tau(n-m)^2}\rho_{n,m}, \tag{4.35}$$

which can be used to evaluate the mutual information as written in Eq. (4.29) once the POVM describing the measurement is given and, thus, the $f_{n-m}(s)$ are assigned.

The POVM describing the ideal (canonical) measurement is obtained from Eq. (4.21) with $A_{n,m} = 1$, $\forall n, m$. In turn, the probability $q(s)$ after the phase diffusion process reads:

$$q_C(s) = \frac{1}{N}\left\{1 + 2e^{-\bar{n}}\sum_{n=0}^{\infty}\sum_{d=1}^{\infty}\mathrm{sinc}\left(\frac{\pi d}{N}\right)e^{-\frac{1}{2}d^2\tau}\cos\left[\frac{\pi d}{N}(2s+1)\right]\frac{\bar{n}^{n+d/2}}{\sqrt{n!(n+d)!}}\right\}, \tag{4.36}$$

where $\mathrm{sinc}(x) = \sin(x)/x$. The mutual information I_C directly follows from Eq. (4.29).

The probability $q_Q(s)$ for the Q-measurement process is obtained using $A_{n,m} = \Gamma[1 + \frac{1}{2}(n+m)](n!m!)^{-\frac{1}{2}}$:

$$q_Q(s) = \frac{1}{N}\left\{1 + 2e^{-\bar{n}}\sum_{n=0}^{\infty}\sum_{d=1}^{\infty}\mathrm{sinc}\left(\frac{\pi d}{N}\right)e^{-\frac{1}{2}d^2}\cos\left[\frac{\pi d}{N}(2s+1)\right]\frac{\Gamma(1+n+\frac{d}{2})\bar{n}^{n+d/2}}{n!(n+d)!}\right\}. \tag{4.37}$$

The corresponding mutual information I_Q is again obtained using Eq. (4.29).

The panels of Fig. 4.8 show the mutual information as a function of the rescaled time variable τ, which plays the role of a noise parameter, for ideal (left panel) and Q (right

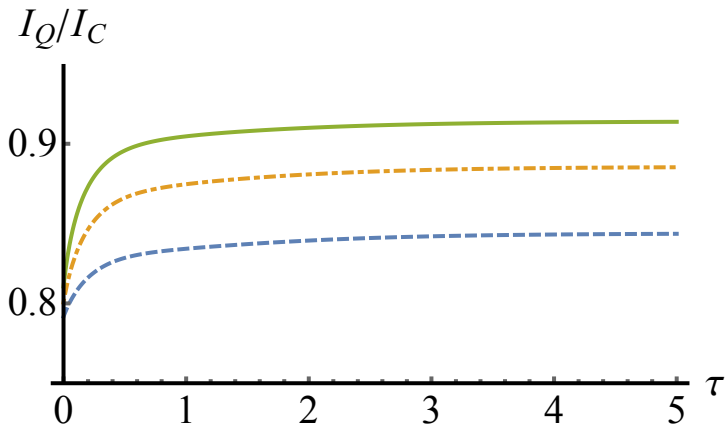

Figure 4.9: The lower panel shows the ratio I_Q/I_C as a function of τ for different values of the average number of photons: from bottom to top, $\bar{n} = 1$ (dashed blue), $\bar{n} = 2$ (dotdashed orange), $\bar{n} = 3$ (solid green).

panel) phase-receivers and for different values $\bar{n}$ of the average number of photons of the seed state. The size of the alphabet is set to $N = 20$. As it is apparent from the plots, phase diffusion leads to an unavoidable loss of information. The mutual information I_Q for Q receivers shows the same vanishing behavior in time as the ideal one I_C, though its value is always slightly smaller. In order to provide a quantitative assessment, I show their ratio I_Q/I_C in Fig. 4.9, as a function of τ for different values of $\bar{n}$. The ratio is always below one, thus confirming that Q receivers are not as efficient as the ideal ones. The ratio slighty increases with time, i.e. for long distance channels, and with the energy of the seed signal.

In order to further assess the performances of phase channels let's now compare the mutual informations I_C and I_Q with the capacity of a (realistic) coherent channel and with the ultimate quantum capacity of a single-mode channel, which is achieved by the photon number channel. In a coherent channel information is encoded onto the amplitude of a coherent signal and then retrieved by heterodyne or double-homodyne detectors, the channel capacity is achieved by Gaussian modulation of the amplitude and is given by

$$C_{COH}(\eta) = \log(1 + \eta\bar{n}), \tag{4.38}$$

where $\bar{n}$ is again the average number of photon per use of the channel, and η is the overall (amplitude) loss along the channel. On the other hand, the ultimate quantum capacity of a single-mode channel, which also saturates the Holevo-Ozawa-Yuen bound [116], is achieved by the photon number channel

$$C_{PHN} = (\bar{n} + 1)\log_2(\bar{n} + 1) - \bar{n}\log_2\bar{n}. \tag{4.39}$$

where information is encoded onto the number of quanta transmitted through the channel according to a thermal distribution, and the decoding stage is performed by photodetection.

At first, let's address noiseless phase channels and consider, for both receivers, the ratio between the corresponding mutual information and the ultimate capacity, i.e. $\gamma_C = I_C/C_{PHN}$ and $\gamma_Q = I_Q/C_{PHN}$. The two quantities are reported in the upper left panel of Fig. 4.10 as a function of the number of symbols in the phase alphabet, and for different

values of the average number of photons $\bar{n}$. The plots reveal that an alphabet of about $N \simeq 50$ symbols is enough to reach the asymptotic value of both ratios, and in turn of I_C and I_Q. Also, the plots show that the ratio with the ultimate capacity is comparable to that of noiseless coherent channels, with ideal phase receivers slightly outperforming the coherent channel and the Q one being slightly outperformed. Using this size of the alphabet, we have evaluated γ_C and γ_Q as a function of the average photon number $\bar{n}$. Results are shown in the upper right panel of Fig. 4.10, confirming that phase channels with ideal receivers performs slightly better than coherent ones, whereas Q receivers lead to slightly worse performances.

Let's now compare phase channel with coherent ones in the presence of noise. In the lower panels of Fig. 4.10 I show the ratios $\beta_k = I_k/C_{COH}$, $k = C, Q$ between the mutual information of our phase channels and the capacity of the coherent channel as a function of the noise parameters, τ and η of the two channels. Results for different values of the average number of photons $\bar{n}$ are shown. In both cases an energy-dependent threshold on the amount of noise appears, above which phase channels become more effective than coherent ones.

Finally, let's discuss the performances of the two receivers in the relevant quantum regime of low number of photons, $\bar{n} \ll 1$, and large number of letters, $N \gg 1$. As it can be argued from the upper right of Fig. 4.10, both I_C and I_Q grow linearly with $\bar{n}$ for $\bar{n} \ll 1$, and this resembles the behaviour of both the coherent capacity and the ultimate quantum capacity. This means that, albeit being suboptimal, phase channels offer good performances when low energy should be transmitted through the channel. This finding can be confirmed by expanding the mutual information up to the first order in the average photon number of the seed signal, arriving at the expressions for the ideal measurement and the Q-receiver one

$$I_{\mathrm{ID}} \overset{\bar{n}\ll 1}{\simeq} \frac{\bar{n}\,\mathrm{sinc}^2\left(\frac{\pi}{N}\right) e^{-\tau}}{\log 2} \overset{N\gg 1}{\simeq} \frac{\bar{n}\, e^{-\tau}}{\log 2} \tag{4.40a}$$

$$I_{\mathrm{Q}} \overset{\bar{n}\ll 1}{\simeq} \frac{\pi}{4}\frac{\bar{n}\,\mathrm{sinc}^2\left(\frac{\pi}{N}\right) e^{-\tau}}{\log 2} \overset{N\gg 1}{\simeq} \frac{\pi}{4}\frac{\bar{n}\, e^{-\tau}}{\log 2}, \tag{4.40b}$$

their ratio approaching the limiting value of $\pi/4$.

4.2.3 Dynamical phase diffusion

In many experimental situations, the exchange of information between sender and receiver takes place in noisy environments which cannot be described in terms of a Markovian master equations. In such cases, a full quantum description of the interaction may be inconvenient, as the approximations needed to obtain solvable dynamical equations could preclude the study of interesting features of the dynamics itself.

In the following, I consider a stochastic phase diffusion model corresponding to the quantum map

$$\rho(\tau) = \int_{-\infty}^{\infty} \frac{d\phi}{\sqrt{2\pi\beta(\tau)}}\, e^{-\frac{\phi^2}{2\beta(\tau)}}\, U(\phi)\rho(0)U^\dagger(\phi), \tag{4.41}$$

where, for convenience, I still use the rescaled time $\tau = \Gamma t$. The static environment of the previous section is recovered for $\beta(\tau) = \tau$. The quantum map (4.41) turns the input state ρ_k into a statistical mixtures of states with a time-dependent Gaussian distribution of the phase around the original phase ϕ_k. In this model, I assume as stochastic process a Ornstein-Uhlenbeck process, whose non-rescaled variance is given in Eq. 2.24.

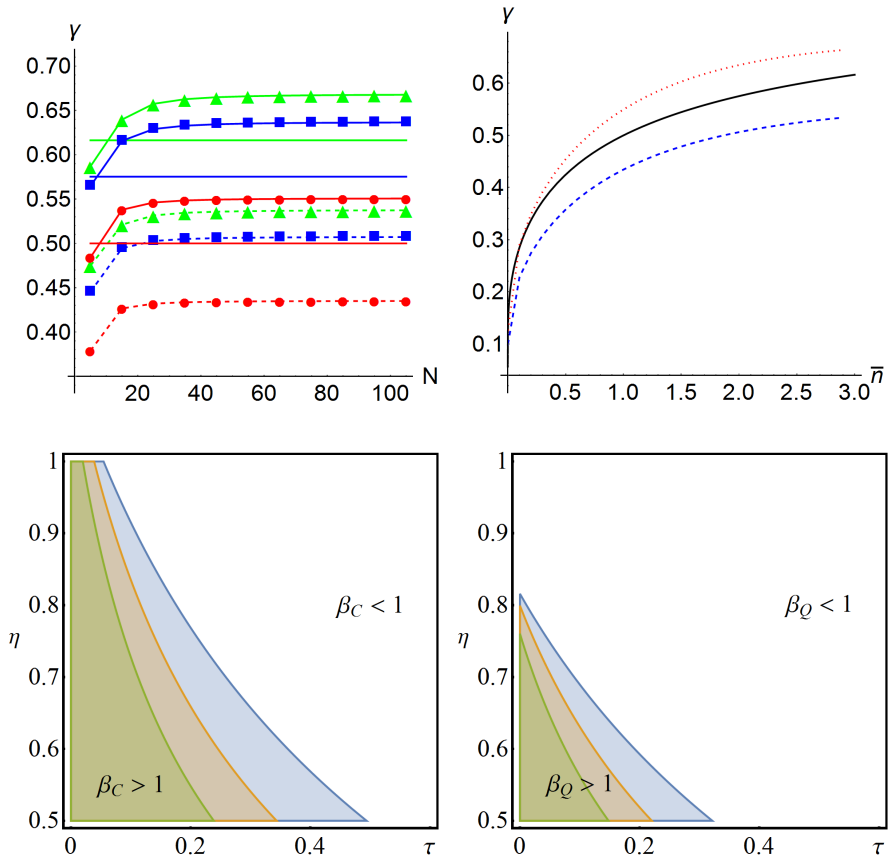

Figure 4.10: (Color online) The upper left panel shows the ratios γ_C (symbols joined by solid lines) and γ_Q (symbols joined by dotted lines) as a function of the number of symbols in the alphabet for noiseless phase channels ($\eta = 1$). Red circles correspond to $\bar{n} = 1$, blue squares to $\bar{n} = 2$ and green triangles to $\bar{n} = 3$. Solid lines are the ratios C_{COH}/C_{PHN} for the same three values of $\bar{n}$ (from bottom to top) with the same color code. The upper right panel shows the ratios γ_C (dotted red), C_{COH}/C_{PHN} (solid black) and γ_Q (dashed blue) for noiseless channels as a function of $\bar{n}$ and for a fixed value of $N = 50$. The lower panels show the regions $\beta_C > 1$ and $\beta_Q > 1$, respectively, as functions of $\tau = \Gamma t$ and η. From left to right we have the regions corresponding to $\bar{n} = 1, 2, 3$ (green, orange and blue, respectively). When $\beta_k > 1$, $k = C, Q$, the phase channels become more effective than coherent ones. The boundary of each region singles out an energy-dependent threshold on the noise parameters.

In the Markovian limit $\tau_E \ll \tau$, the latter may be re-written as

$$\sigma(\tau) \simeq \tau \tag{4.42}$$

whereas, in the presence of highly correlated environments $\tau_E \gg \tau$, it becomes

$$\sigma(\tau) \simeq \frac{1}{2}\tau^2/\tau_E. \tag{4.43}$$

If the environment shows non-zero correlation time the dynamics of mutual information may be dramatically altered, showing either a different decay rate or the appearance of

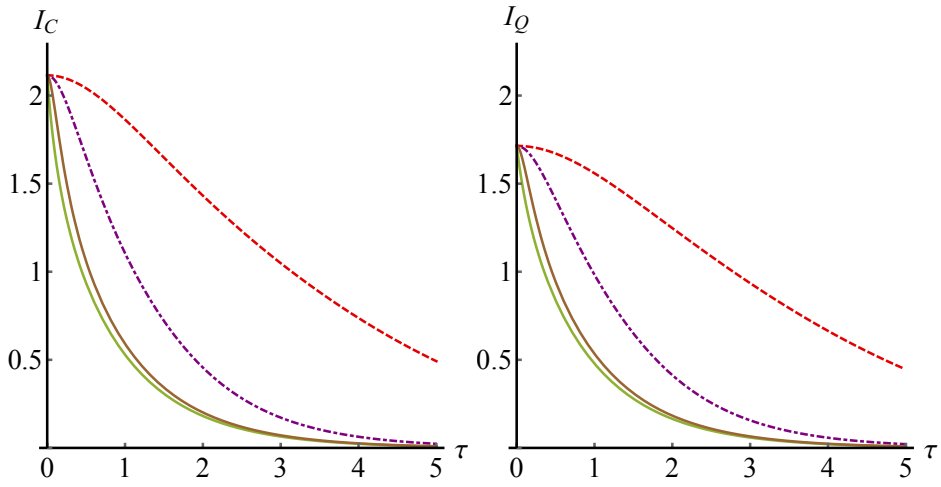

Figure 4.11: (Color Online) Phase communication channels in the presence of dynamical phase diffusion. The upper panels show the mutual informations I_C (left) and I_Q (right) as function of $\tau = \Gamma t$ for different values of the correlation time τ_E of the environment. From bottom to top, $\tau_E = 0.1$ (solid brown), 1 (dotdashed purple) , 10 (dashed red). The lower solid green curve is the mutual information in the static case. The other parameters read as follows: $N = 20$, $\bar{n} = 3$.

oscillations. In the following, I first analyze the case of a *resonant enviroment* with zero detuning $\delta = 0$ and then focus attention to nonresonant situations. In both cases, the probabilities $q_k(s)$, $k = C, Q$ are still given by Eqs. (4.36) and (4.37) with the replacement

$$\exp\left(-\frac{1}{2}d^2\tau\right) \longrightarrow \exp\left[-\frac{1}{2}d^2\sigma(\tau)\right] .$$

Let us start with the case of a resonant environment ($\delta = 0$). Under such condition, $\beta(t)$ reduces to

$$\beta(\tau) = \left[\tau - \tau_E(1 - e^{-\tau/\tau_E})\right] \tag{4.44}$$

and the channel appears to be more robust against the effects of noise, at least for a short time dynamics, compared to the static case. In order to illustrate this feature, Fig. 4.11 shows the mutual informations I_C and I_Q as a function of τ for different values of τ_E. As it is apparent from the plot, the presence of a non-zero correlation time of the environment τ_E better preserves mutual information against phase diffusion for both ideal and Q receiver. As it happens in the static case the mutual information vanishes with time. However, a time-correlated environment allows a "concave dynamics" of the mutual information, which lasts longer, the higher is the correlation time. This behaviour is due to the transition from linear to quadratic behaviour of $\beta(\tau)$ (see Eq. 4.43), which may be observed for increasing τ_E. I also show the mutual information for the static case (solid green line) for comparison. Fig. 4.12 shows the ratio I_Q/I_C as a function of τ. Upon comparing this plot with Fig. 4.9 it is possible to conclude that dynamical noise is more detrimental for Q receivers than for ideal ones.

Let's now analyze the effects of detuning between the frequency of the information carrier and the central frequency of the CSF. As it is possible to see from the panels of Fig. 4.13, the dynamics of the mutual information is strongly affected by the detuning

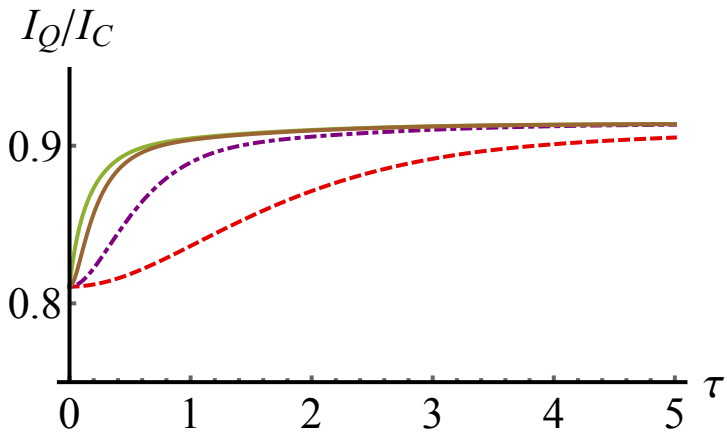

Figure 4.12: The lower panel shows the ratio I_Q/I_C as a function of τ for the same values of τ_E and of the other parameters. From top to bottom, $\tau_E = 0.1$ (solid brown), 1 (dotdashed purple), 10 (dashed red). The lower solid green curve is the mutual information in the static case. The other parameters read as follows: $N = 20$, $\lambda = 1$, $\bar{n} = 3$.

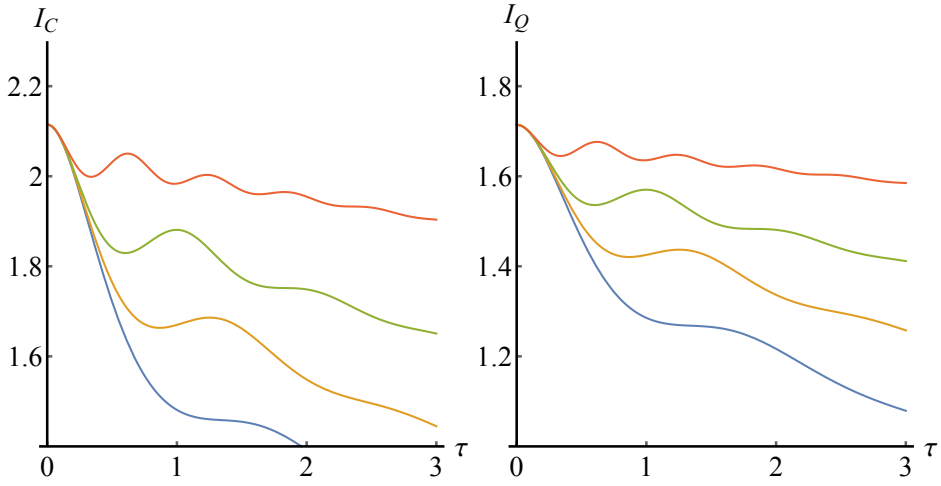

Figure 4.13: (Color online) Phase communication channels in the presence of dynamical phase diffusion. The panels show the mutual information I_C (left) and I_Q (right) as a function of $\tau = \Gamma t$ for different values of detuning. From top to bottom $\delta = 10$ (red), $\delta = 6$ (green), $\delta = 4.5$ (orange), and $\delta = 3.5$ (blue). The other parameters are given by $N = 20$, $\lambda = 1, \bar{n} = 3, \tau_E = 1$.

for both kind of receivers. On the one hand, the detuning contributes to the significative slowdown of the damping of mutual information and, on the other hand, it is responsible for the appearance of revivals of mutual information, present only when $\delta > \delta_0$.

4.3 Summary

- The quantum-to classical transition in a noisy dissipative environment occurs in a finite time that depends exclusively on the nonclassical depth of the input state.
- The presence of classical memory in the environment strongly influences the decoherence time, increasing the survival time of nonclassicality and leading to dynamical sudden death and birth of quantumness.
- Phase commonication channels based on phase modulation of coherent states are robust, especially for large alphabets in the low-energy regime, and their performances are comparable to those of coherent channels in the presence of loss.
- In the presence of stochastic phase diffusion, phase channels become more robust, the channel capacity being preserved by the time correlations of the environment.
- Detuning beyond the threshold value $\tilde{\delta}_0$ induces revivals of mutual information.

CHAPTER 5

Non-Markovianity vs backflow of information

In the previous chapters, I have shown that classical stochastic fields may reproduce phase diffusive and dissipative environments, leading to non-Markovian dynamics of the system. Moreover, I have shown that single-mode continuous variable systems may exhibit recoherence phenomena and revivals of quantum features as quantumness or mutual information in particular regimes of interaction. In this chapter, I address the effects of classical stochastic fields on the evolution of correlations between two-mode systems.

In this framework, the first goal is analyzing in details the dynamics of a bipartite system made of two independent quantum harmonic oscillators interacting with classical fluctuating environments. In particular, I compare the dynamics of correlations in two different environmental situations. On one hand, I consider a local noise model, where each oscillator interacts with its own classical environment. On the other hand, I consider the situation where both the oscillators interact with a common environment, described by a single stochastic field. A similar analysis has been performed for qubit systems [142, 143] revealing the existence of a rich phenomenology.

The second goal consists in better analyzing the connections between the dynamics of quantumness, e.g. revivals of quantum correlations and the quantum-to-classical transition, and the non-Markovian features of the dynamical map. In particular, I investigate the role of non-Markovianity itself (i.e. non-divisibility of the quantum dynamical map) against the role of the backflow of information, which is a sufficient (but not necessary) condition to prove non-Markovianity and, in turn, often used to witness its presence.

5.1 Local and global noise: the interaction model

Let's consider two non-interacting harmonic quantum oscillators with natural frequencies ω_1 and ω_2 and analyze the dynamics of this system in two different regimes: in the first one, each oscillator is coupled to one of two independent non-interacting stochastic fields, this scenario is dubbed as the *local noise* case. In the second regime, the oscillators are coupled to the same classical stochastic field, so this case is referred to as *common noise*. In both case, the Hamiltonian H is composed by a free and an interaction term. The free Hamiltonian H_0 is given by

$$H_0 = \hbar \sum_{j=1}^{2} \omega_j a_j^\dagger a_j. \tag{5.1}$$

Unlike the free Hamiltonian H_0, which is the same in the description of both models, the interaction term H_I differs. In the following subsections, I introduce the local and the common interaction Hamiltonian.

5.1.1 Local interaction scenario

The interaction Hamiltonian H_{L} in the local model reads

$$H_{\text{L}}(t) = \sum_{j=1}^{2} a_j \bar{B}_j(t) e^{i\delta_j t} + a_j^\dagger B_j(t) e^{-i\delta_j t} \tag{5.2}$$

where the annihilation operators a_1, a_2 represent the oscillators, each coupled to a different local stochastic field $B_j(t)$ with $j = 1, 2$, and $\delta_j = \omega_j - \omega$ is the detuning between the carrier frequency of the field and the natural frequency of the j-th oscillator. The Hamiltonian is rescaled in units of a reference level of energy $\hbar\omega_0$. Under this condition, the stochastic fields $B_1(t), B_2(t)$, their central frequency ω, the interaction time t, and the detunings all become dimensionless quantities.

The presence of fluctuating stochastic fields leads to an explicitly time-dependent Hamiltonian, whose corresponding evolution operator is given by

$$U(t) = \mathcal{T} \exp\left\{ -i \int_0^t ds\, H_{\text{L}}(s) \right\}, \tag{5.3}$$

where $\mathcal{T}$ is the time ordering. However, as the interaction Hamiltonian is linear in the annihiliation and creation operators of the two oscillators, the two-time commutator $[H_{\text{L}}(t_1), H_{\text{L}}(t_2)]$ is always proportional to the identity. In particular, when the stochastic fields satisfy the conditions $B_j(t_1)\bar{B}_j(t_2) = B_j(t_2)\bar{B}_j(t_1)$, with $j = 1, 2$, the two-time commutator becomes

$$[H_{\text{L}}(t_1), H_{\text{L}}(t_2)] = \sum_{j=1,2} 2i\, \bar{B}_j(t_1) B_j(t_2) \sin\left[\delta_j (t_1 - t_2)\right] \mathbb{I}_{12} \tag{5.4}$$

This form of the two-time commutator allows to use the Magnus expansion to simplify the expression of the evolution operator (5.3) into

$$U(t) = \exp\left(\Xi_1 + \Xi_2\right) \tag{5.5}$$

where Ξ_1 and Ξ_2 are given by

$$\Xi_1 = -i \int_0^t ds_1\, H_I(s_1), \tag{5.6a}$$

$$\Xi_2 = \frac{1}{2} \int_0^t ds_1 \int_0^{s_1} ds_2\, [H_I(s_1), H_I(s_2)]. \tag{5.6b}$$

The specific form of Ξ_1 for the local (Ξ_1^{L}) scenario is given by

$$\Xi_1^{\text{L}} = \sum_{j=1}^{2} \left(a_j^\dagger \phi_j(t) - a_j \phi_j^*(t) \right) \tag{5.7}$$

where the displacement parameter $\phi_j(t)$ is given by

$$\phi_j(t) = -i \int_0^t ds\, e^{-i\delta_j s} B_j(s) \quad \text{with } j = 1, 2. \tag{5.8}$$

The evolution of the density operator of the system then reads

$$\rho_L(t) = \left[e^{\Xi_1^{\text{L}}}\rho(0)e^{(\Xi_1^{\text{L}})^*}\right]_B = \left[D(\phi_a,\phi_b)\rho_0 D^\dagger(\phi_a,\phi_b)\right]_B \tag{5.9}$$

where $D_j(\alpha) = \exp(\alpha\, a_j^\dagger - \alpha^* a_j)$ is the displacement operator, $D(\alpha_1,\alpha_2) = D(\boldsymbol{\alpha}) = D_1(\alpha_1)D_2(\alpha_2)$ and, once again, $[\ldots]_B$ is the average over the realizations of the stochastic fields.

In the local scenario, each CSF $B_j(t) = B_j^{(x)}(t) + iB_j^{(y)}(t)$, is described as a Gaussian stochastic process with zero mean $[B_j^{(x)}(t)]_F = [B_j^{(y)}(t)]_F = 0$ and autocorrelation matrix given by

$$\left[B_j^{(x)}(t_1)B_k^{(x)}(t_2)\right]_F = \left[B_j^{(y)}(t_1)B_k^{(y)}(t_2)\right]_F = \delta_{jk}K_j(t_1,t_2), \tag{5.10a}$$

$$\left[B_j^{(x)}(t_1)B_k^{(y)}(t_2)\right]_F = \left[B_j^{(y)}(t_1)B_k^{(x)}(t_2)\right]_F = 0. \tag{5.10b}$$

where the kernel autocorrelation function of each process is different in the most general case. By means of the Glauber decomposition of the initial state $\rho(0)$

$$\rho(0) = \int \frac{d^4\boldsymbol{\zeta}}{\pi^2}\chi[\rho(0)](\boldsymbol{\zeta})D^\dagger(\boldsymbol{\zeta}), \tag{5.11}$$

where $\chi[\rho](\boldsymbol{\zeta})$ is the symmetrically ordered characteristic function, the density matrix of the evolved state reads

$$\rho_{\text{L}}(t) = \mathcal{G}_{\text{L}}[\rho(0)] = \int \frac{d^4\boldsymbol{\zeta}}{\pi^2} g_{\text{L}}(\boldsymbol{\zeta})D(\boldsymbol{\zeta})\rho(0)D^\dagger(\boldsymbol{\zeta}) \tag{5.12}$$

where $g_{\text{L}}(\boldsymbol{\zeta})$ is a Gaussian function

$$g_{\text{L}}(\boldsymbol{\zeta}) = \frac{\exp(-\frac{1}{2}\,\boldsymbol{\zeta}\cdot\boldsymbol{\Omega}\cdot\boldsymbol{\sigma}_{\text{L}}^{-1}\cdot\boldsymbol{\Omega}^T\cdot\boldsymbol{\zeta}^T)}{\sqrt{\det[\boldsymbol{\sigma}_{\text{L}}]}} \tag{5.13}$$

where $\boldsymbol{\sigma}_{\text{L}}$ and the symplectic matrix $\boldsymbol{\Omega}$ are given by

$$\boldsymbol{\Omega} = \begin{pmatrix} 0 & 1 \\ -1 & 0 \end{pmatrix} \quad \boldsymbol{\sigma}_{\text{L}} = \begin{pmatrix} \beta_1(t)\,\mathbb{I}_2 & 0 \\ 0 & \beta_2(t)\,\mathbb{I}_2 \end{pmatrix}. \tag{5.14}$$

The matrix $\boldsymbol{\sigma}_{\text{L}}$ is the covariance matrix of the noise function $g_{\text{L}}(\boldsymbol{\zeta})$ and its matrix elements are given by

$$\beta_j(t,t_0) = \int_{t_0}^{t}\int_{t_0}^{t} ds_1 ds_2 \cos[\delta_j(s_1-s_2)]K_j(s_1,s_2). \tag{5.15}$$

The dynamical map in Eq. (5.12) corresponds to a two-mode Gaussian noise channel [144, 145], i.e a random displacement according to a Gaussian probability distribution. In the local scenario, each mode evolves independently: the environment affects each mode separately by adding a different noise $\beta_j(t,t_0)$ to each subsystem.

5.1.2 Common interaction scenario

The Hamiltonian H_{C} in the common interaction model reads

$$H_{\mathrm{C}}(t) = \sum_{j=1}^{2} a_j e^{i\delta_j t}\bar{B}(t) + a_j^{\dagger} e^{-i\delta_j t} B(t) \tag{5.16}$$

where each oscillator, represented by the annihilation operators a_1, a_2, is coupled to a common stochastic field $B(t)$ which is described as a Gaussian stochastic process with zero mean $[B^{(x)}]_B = [B^{(y)}]_B = 0$ and the very same autocorrelation matrix of the local scenario.

Along the same lines of the local interaction model derivation, the Magnus expansion simplifies the evaluation of the evolution operator. By asking the stochastic field to satisfy the relation $B(t_1)\bar{B}(t_2) = B(t_2)\bar{B}(t_1)$, the two-time commutator reads

$$[H_{\mathrm{C}}(t_1), H_{\mathrm{C}}(t_2)] = \bar{B}(t_1)B(t_2) \sum_{j=1,2} 2i \,\sin\left[\delta_j(t_1 - t_2)\right] \mathbb{I}_{12}. \tag{5.17}$$

The evolution operator for the common scenario is the same described in Eq. (5.5), where the specific form of Ξ_1 in the common interaction model is given by

$$\Xi_1^{\mathrm{C}} = \sum_{j=1}^{2} \left(a_j^{\dagger}\psi_j(t) - a_j \psi_j^{*}(t) \right) \tag{5.18}$$

where

$$\psi_j(t) = -i \int_0^t ds\, e^{-i\delta_j s} C(s) \quad \text{with } j = 1, 2. \tag{5.19}$$

The two displacement parameters $\psi_1(t)$ and $\psi_2(t)$ only differ for the detuning parameters, which are different in the most general case.

The evolution of the density operator of the system reads

$$\rho(t) = \left[e^{\Xi_1^{\mathrm{C}}} \rho(0) e^{(\Xi_1^{\mathrm{C}})^*} \right]_B = \left[D(\psi_1, \psi_2)\rho_0 D^{\dagger}(\psi_1, \psi_2) \right]_B \tag{5.20}$$

which, following the same steps of the derivation shown before, leads to

$$\rho_{\mathrm{C}}(t) = \mathcal{G}_{\mathrm{C}}[\rho(0)] = \int \frac{d^4\boldsymbol{\zeta}}{\pi^2} g_{\mathrm{C}}(\boldsymbol{\zeta}) D(\boldsymbol{\zeta}) \rho(0) D^{\dagger}(\boldsymbol{\zeta}) \tag{5.21}$$

where we use the Gaussian function

$$g_{\mathrm{C}}(\boldsymbol{\zeta}) = \frac{\exp(-\frac{1}{2}\,\boldsymbol{\zeta}\cdot\boldsymbol{\Omega}\cdot\boldsymbol{\sigma}_{\mathrm{C}}^{-1}\cdot\boldsymbol{\Omega}^T\cdot\boldsymbol{\zeta}^T)}{\sqrt{\det[\boldsymbol{\sigma}_{\mathrm{C}}]}} \tag{5.22}$$

$\boldsymbol{\sigma}_{\mathrm{C}}$ being its covariance matrix, given by

$$\boldsymbol{\sigma}_{\mathrm{C}} = \begin{pmatrix} \beta_1(t)\,\mathbb{I}_2 & \boldsymbol{R} \\ \boldsymbol{R} & \beta_2(t)\,\mathbb{I}_2 \end{pmatrix} \qquad \boldsymbol{R} = \begin{pmatrix} \beta_{\mathrm{C}}(t) & \gamma_{\mathrm{C}}(t) \\ \gamma_{\mathrm{C}}(t) & \beta_{\mathrm{C}}(t) \end{pmatrix} \tag{5.23}$$

with the matrix elements given by

$$\beta_c(t,t_0) = \int_{t_0}^{t}\int_{t_0}^{t} ds_1 ds_2 \cos[(\delta_1 s_1 - \delta_2 s_2)] K(s_1,s_2), \tag{5.24a}$$

$$\gamma_c(t,t_0) = \int_{t_0}^{t}\int_{t_0}^{t} ds_1 ds_2 \sin[(\delta_1 s_1 - \delta_2 s_2)] K(s_1,s_2). \tag{5.24b}$$

The local interaction adds noise to the two-mode systems affecting each subsystem separately, while in the common scenario the evolution is more involved: correlations between the modes arise from a non-direct interaction, which is vehiculated by the common classical stochastic field through the terms given in 5.24.

5.1.3 Covariance Matrix dynamics in local and common interaction

The dynamical maps described by Eqs. (5.12) and (5.21) belong to the class of Gaussian channels , i.e. the evolution, in both regimes, preserves the Gaussian character of input states. In turn, this is a useful feature, since in this case quantum correlations, entanglement and discord, may be evaluated exactly and only depend on the covariance matrix of the output state.

In order to get quantitative results, the environment fluctuations are described by identical Ornstein-Uhlenbeck processes. Moreover, I assume the case of resonant oscillators ($\omega_1 = \omega_2 = \omega_0$), which implies that the oscillators are identically detuned from the central frequency of the classical stochastic field, i.e.

$$\delta_1 = \delta_2 = \delta = 1 - \frac{\omega}{\omega_0}\,.$$

This assumptions simplifies the expression of the state dynamics: in the local scenario, leading to $\beta_1(t) = \beta_2(t) = \beta(t)$ and, in turn,

$$\rho_{\text{L}}(t) = \mathcal{E}_{\text{L}}[\rho(0)](t) = \int \frac{d^4\boldsymbol{\zeta}}{(\pi\beta(t))^2} \exp\left(-\frac{|\boldsymbol{\zeta}|^2}{\beta(t)}\right) D(\boldsymbol{\zeta})\rho(0)D^\dagger(\boldsymbol{\zeta}) \tag{5.25}$$

where $\beta(t)$ with the Ornstein-Uhlenbeck kernel is given in Eq. 2.24.

In the common noise case, the condition of resonant oscillators implies $\beta_1(t) = \beta_2(t) = \beta_c(t) = \beta(t)$ and $\gamma_c(t) = 0$, leading to simplified matrices $\boldsymbol{R}$ and $\boldsymbol{\sigma}_{\text{C}}$ given by

$$\boldsymbol{R} = \begin{pmatrix} \beta(t) & 0 \\ 0 & \beta(t) \end{pmatrix} \quad \boldsymbol{\sigma}_{\text{C}} = \begin{pmatrix} \beta(t)\mathbb{I}_2 & \boldsymbol{R} \\ \boldsymbol{R} & \beta(t)\mathbb{I}_2 \end{pmatrix} \tag{5.26}$$

corresponding to the Gaussian channel

$$\rho(t) = \mathcal{E}_{\text{C}}[\rho(0)](t) = \int \frac{d^2\zeta}{\pi\beta(t)} \exp\left(-\frac{|\zeta|^2}{\beta(t)}\right) D(\zeta,\zeta)\rho(0)D^\dagger(\zeta,\zeta). \tag{5.27}$$

The initial state $\rho(0)$ of the system is assumed to be a generic squeezed thermal state ρ_{STS}, which is a zero-mean Gaussian state, described by a Gaussian characteristic function $\boldsymbol{\sigma}_{\text{STS}}$ given in Eq. 1.52. As the squeezed thermal state is a Gaussian state and the dynamics in both scenarios is described by a Gaussian channel, the output state at any time is Gaussian as well, so it is determined only by the covariance matrix. By evaluating the

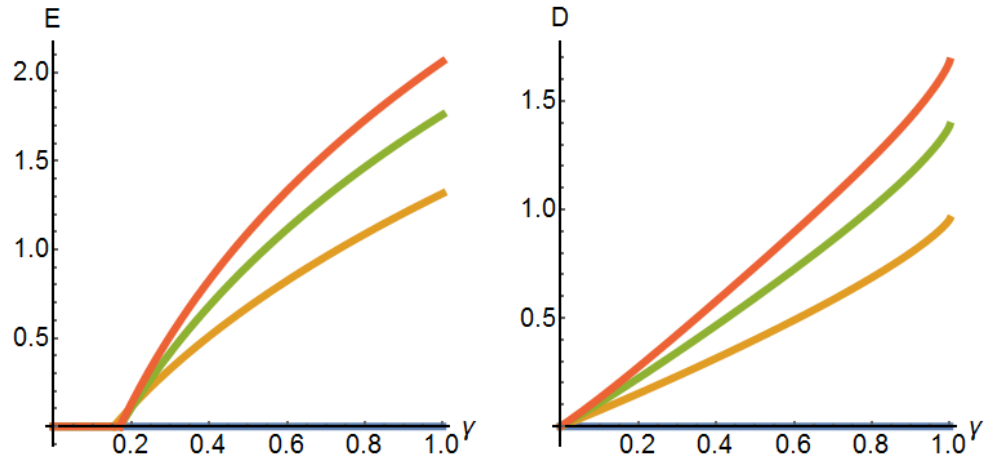

Figure 5.1: Quantum correlations of STS for different values of the energy ϵ. Left panel: Entanglement of a STS as a function of squeezing parameter γ. The STS is entangled as long as γ overtakes a threshold value that depends on the energy ϵ. Right panel: Discord of a STS as a function of squeezing parameter γ. The STS is always a discordant state unless $\gamma = 0$. In both panels, from bottom to top, $\epsilon = 0$ (blue line), $\epsilon = 1$ (yellow line), $\epsilon = 2$ (green line), $\epsilon = 3$ (red line).

characteristic function of the evolved state, one finds that the covariance matrices of the state at time t in the local and common scenarios are

$$\boldsymbol{\beta}_{\text{L}}(t) = \boldsymbol{\sigma}_{\text{STS}} + 2\,\boldsymbol{\sigma}_{\text{L}}(t), \tag{5.28a}$$

$$\boldsymbol{\beta}_{\text{C}}(t) = \boldsymbol{\sigma}_{\text{STS}} + 2\,\boldsymbol{\sigma}_{\text{C}}(t)\,, \tag{5.28b}$$

where $\boldsymbol{\sigma}_{\text{L}}(t)$ and $\boldsymbol{\sigma}_{\text{C}}(t)$ are given in Eqs. (5.14) and (5.26) respectively.

A closing remark about the output states: in the local scenario, the interaction with the stochastic fields adds noise to the system without affecting the off-diagonal terms, so the output state in the local scenario is always a STS, with a larger thermal component. Conversely, the output state in the common scenario ceases to be an STS as soon as the interaction starts.

5.2 Dynamics of Quantum Correlations

In order to assess the dynamics of entanglement and discord in the presence of noise, it is useful to briefly review the static properties of quantum correlations [146] for a squeezed thermal state. Considering the case of identical thermal states ($\bar{n}_1 = \bar{n}_2 = \bar{n}$) it is possible to use a convenient representation of STSs, built upon re-parametrizing the covariance matrix by means of its total energy $\epsilon = 2(\bar{n} + n_s + 2\bar{n}\,n_s)$, with $n_s = \sinh^2 r$, and a normalized squeezing parameter $\gamma \in [0, 1]$, such that

$$n_s = \gamma\epsilon \qquad \bar{n} = \frac{(1-\gamma)\epsilon}{1+2\gamma\epsilon}.$$

Note that, for $\gamma = 0$ the state has only thermal energy ($\epsilon = \bar{n}$) while for $\gamma = 1$ the total amount of energy comes from the two-mode squeezing operation ($\epsilon = \sinh^2 r$).

Fig.5.1 shows the quantum correlations of a STS as a function of the energy ϵ and the squeezing parameter γ. The left panel shows that the STS is entangled as long as γ

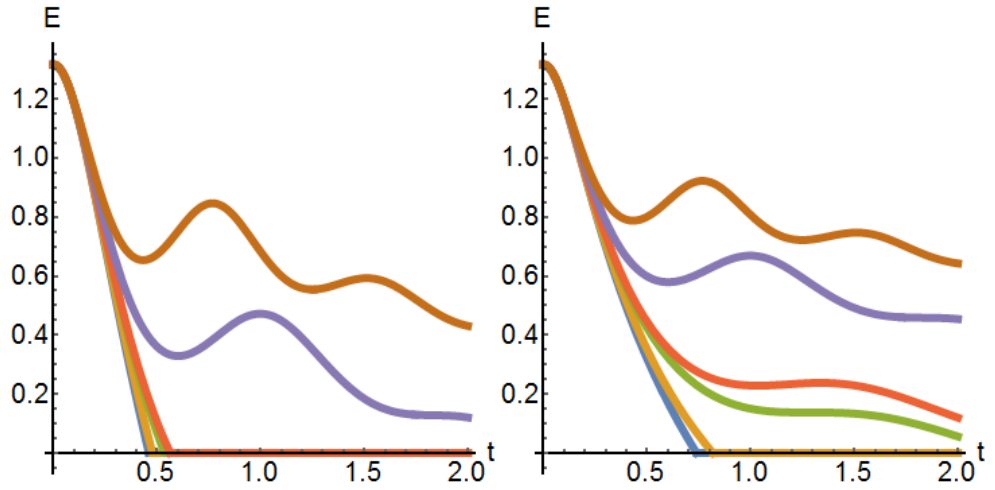

Figure 5.2: (Color Online) Dynamics of entanglement in presence of CSFs for different values of rescaled detuning δ. Left panel: Entanglement dynamics in local scenario as a function of time t. Right panel: Entanglement dynamics in common scenario as a function of time t. In both scenarios, the entanglement possessed by the system may revive. In both panels, $\epsilon = 1, \gamma = 1, \lambda = 1$, and, from bottom to top, $\delta = 0$ (blue), $\delta = 2$ (yellow), $\delta = \delta_0$ (green), $\delta = 4$ (red), $\delta = 6$ (purple), $\delta = 8$ (brown).

overtakes a threshold value which depends on the total amount of energy. Conversely, the quantum discord of a STS is always positive, unless the state is purely thermal, i.e. with zero squeezing ($\gamma = 0$).

Let's analyze the dynamics of quantum correlations of initially maximally entangled squeezed thermal states ($\gamma = 1$) and two-mode thermal states ($\gamma = 0$) in presence of local and common stochastic environments. In order to be able of comparing the results of the different scenarios, the analysis is limited to the case of resonant oscillators and identical the rescaled coupling constant $\lambda^{(c)}$ for the common scenario and $\lambda^{(1)}, \lambda^{(2)}$ for the local scenario, $\lambda^{(c)} = \lambda^{(1)} = \lambda^{(2)} = \lambda$ (all the tildes indicating rescaled parameters have been dropped).

Let's start by addressing the dynamics of correlations of an initially entangled STS: the panels in Fig. 5.2 show how the classical stochastic fields, whether they be local or common, induce loss of correlations in time. However, the decay rate of correlations is not the same in both scenarios: indeed, the presence of a common stochastic field is less detrimental, i.e. the interaction with the same environment leads to a slower loss of correlations. This effect may be seen as the consequence of the fact that the interaction of a two-mode systems with a common environment may be rewritten as the nonsymmetric interaction of two collective modes with separate enviroments. In particular, decoherence strongly affects only one of the collective mode, and this mechanism is physically responsible for a slower loss of correlations.

In both panels, the green line corresponds to $\delta = \delta_0$, the threshold value over which $\beta(t)$ shows an oscillating behavior. As it is possible to see, $\delta = \delta_0$ plays the role of the threshold value also in the case of the correlations. In fact, revivals of entanglement appear only for detunings bigger than δ_0. However, the left panel allows to point out an important issue: $\delta > \delta_0$ is a necessary condition for an oscillating $\beta(t)$, though revivals of entanglement also depend on the rescaled coupling λ. In other words, when $\delta >$

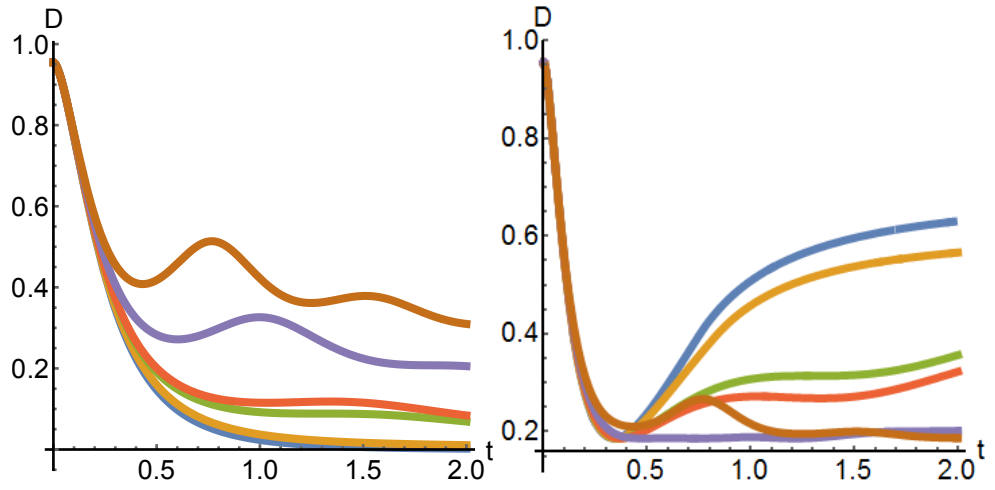

Figure 5.3: Dynamics of discord in presence of CSFs for different values of rescaled detuning δ. Left panel: Discord dynamics in local scenario as a function of time t. The initial discord decreases in time. Right panel: Discord dynamics in common scenario as a function of time t. The initial discord decreases, reaches a minimum and the increases monotonically as a consequence of the interaction. In both panels, $\epsilon = 1, \gamma = 1, \lambda = 1$, and, from bottom to top, $\delta = 0$ (blue line), $\delta = 2$ (yellow line), $\delta = \delta_0$ (green line), $\delta = 4$ (red line), $\delta = 6$ (purple line), $\delta = 8$ (brown line).

δ_0, the symplectic eigenvalue $\tilde{d}_-$ flows in time in unison with $\beta(t)$, without necessarily violating the separability condition $\tilde{d}_- \geq \frac{1}{2}$. This explains the presence of a plateau in the entanglement of the common scenario with $\delta = \delta_0$.

Let's now focus on the discord dynamics shown in Fig. 5.3. While the entanglement shows a vanishing behaviour in both scenarios in any setup of parameters, the same cannot be said for the quantum discord. While in the local scenario the initial discord tends to vanish, the common interaction introduces some correlations which clearly arise after the drop of the initial discord [147]. The effect of the common stochastic field on the dynamics of the quantum discord is even clearer in the case of thermal input states (squeezing parameter $\gamma = 0$). The upper left panel of Fig. 5.4 shows the discord evolution of the state $\rho = \nu_1 \otimes \nu_2$ in the common scenario. The interaction transforms the initial zero-discord state into a discord state without affecting the separability of the input state (the symplectic eigenvalue $\tilde{d}_-$ always satisfies the condition $\tilde{d}_- \geq \frac{1}{2}$, as is apparent from the upper right panel of Fig. 5.4). Furthermore, the quantum discord tends to an asymptotic value which depends on both the energy ϵ and the squeezing parameter γ of the input Gaussian state, but it is not affected by the parameters of the environment λ and δ. Indeed, this can be seen as a consequence of the non-markovianity of the quantum map, as the long-time dynamics is influenced by the input state. A contourplot of the asymptotic value of the Discord as a function of ϵ and γ is shown in the lower right panel of Fig. 5.4. Finally, it is worth mentioning that the POVM (see Eq.1.81) minimizing the quantum discord changes in time preserving the continuity of the discord itself. As an example, the lower left panel of Fig. 5.4 reports one particular scenario where the regions corresponding to the two POVMs are coloured differently.

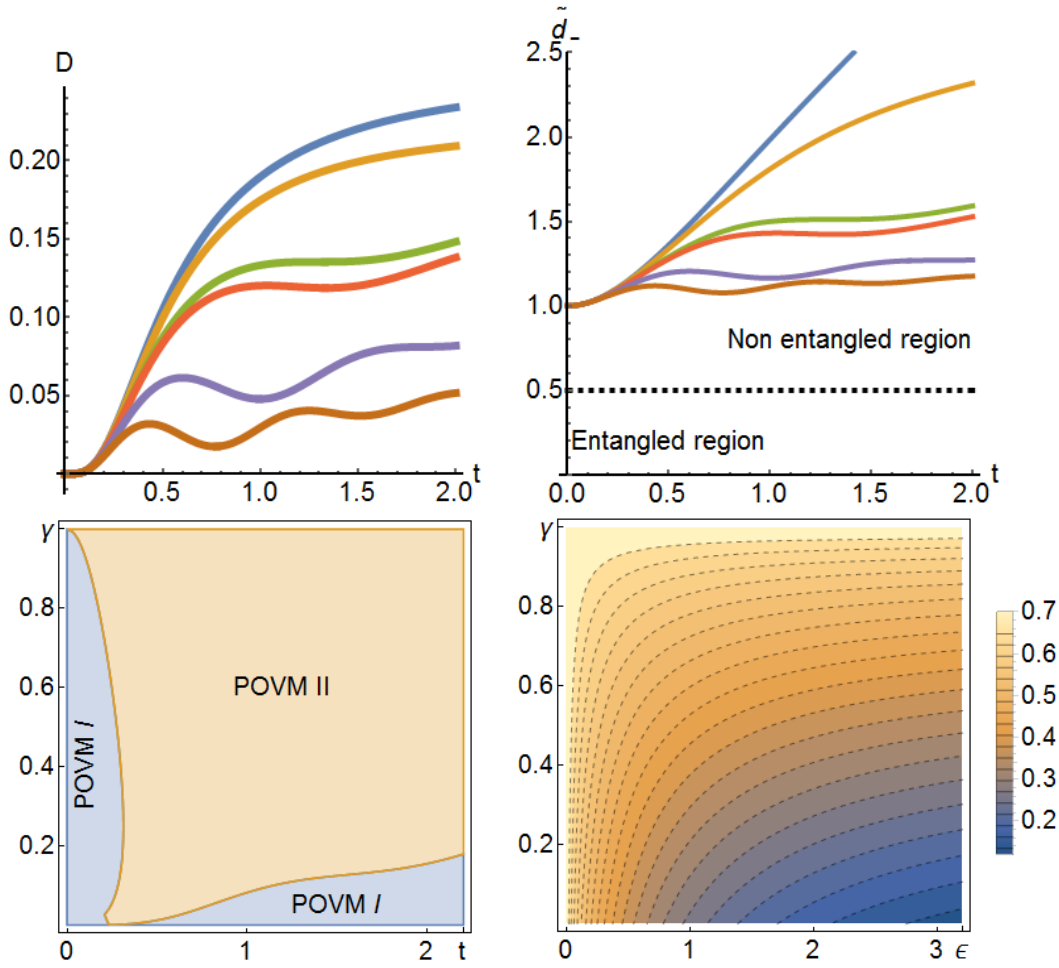

Figure 5.4: Upper panels: Correlations of a two-mode thermal state. Left panel: discord dynamics in time t for different values of δ. The initially zero-discord state becomes a discord state because of the interaction. Right panel: dynamics of symplectic eigenvalue $\tilde{d}_-$ for different values of δ. The state always remains separable, though becoming a discord state. In both panels we have $\epsilon = 1, \gamma = 0, \lambda = 1$ and, from top to bottom, $\delta = 0$ (blue line), $\delta = 2$ (yellow line), $\delta = \delta_0$ (green line), $\delta = 4$ (red line), $\delta = 6$ (purple line), $\delta = 8$ (brown line). Lower left panel: Regionplot of the POVM minimizing the quantum discord. We set $\epsilon = 1, \delta = 3, \lambda = 1$. Lower right panel: contourplot of the asymptotic value of the quantum discord as a function the input state parameters ϵ and γ. I set $\delta = 3, \lambda = 1$.

5.3 Non Divisibility vs Information Backflow

The presence of revivals of correlations might be interpreted as a signature of some form of information backflow between the system and the environment, a phenomenon typically associated to non-Markovian effects. It is the purpose of this section to explore the connections between non-divisibility and information backflow, analyzing the evolution of the Fidelity of two input states.

As shown in Chapter 3, stochastic interactions lead to non-Markovian dynamics. Dif-

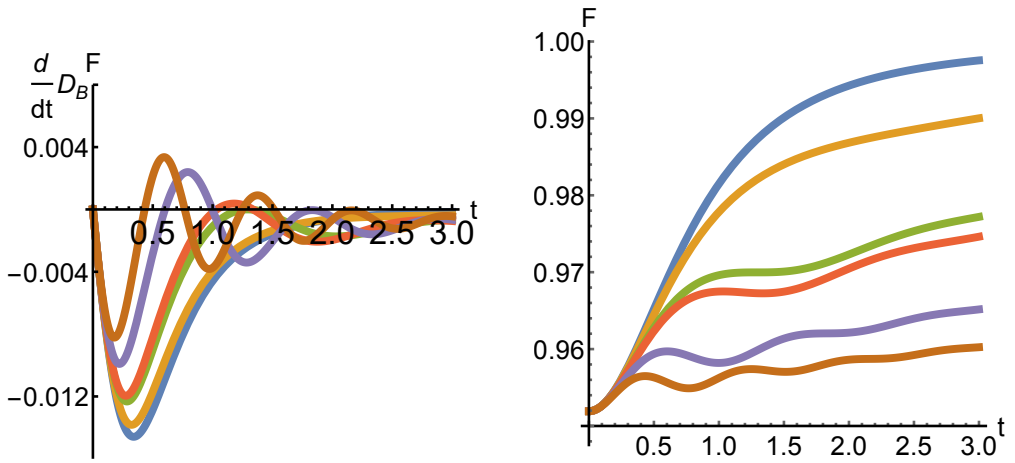

Figure 5.5: Dynamics of Bures distance derivative and Fidelity for different values of rescaled detuning δ in the local noise scenario. Left panel: derivative of Bures distance. Right panel: dynamics of Fidelity. The Fidelity ceases to oscillate when δ is lower than the threshold value δ_0. The distinguishability of the input states diminishes monotonically in time and no backflow of information is detected. The curves with a positive part of derivative of Bures distance have $\delta > \delta_0$ and correspond to the curves where oscillations of Fidelity are shown. In all panels, I set $\epsilon_1 = 2, \epsilon_2 = 1, \gamma_1 = \gamma_2 = 1, \lambda = 1$ and, from top to bottom $\delta = 0$ (blue line), $\delta = 2$ (yellow line), $\delta = \delta_0$ (green line), $\delta = 4$ (red line), $\delta = 6$ (purple line), $\delta = 8$ (brown line).

ferently to what happens in many situations, in the models presented non-Markovianity can be straightforwardly proved, looking for violations of the divisibility property Markovian quantum maps must satisfy. In fact, the composition of maps $\mathcal{E}_{\text{L}}(\Delta t_2)\mathcal{E}_{\text{L}}(\Delta t_1)$ corresponds to a convolution, leading to $\mathcal{E}_{\text{L}}(\Delta t_2)\mathcal{E}_{\text{L}}(\Delta t_1) = \mathcal{E}_{\text{L}}(\Delta t_1 + \Delta t_2)$ if and only if

$$\beta(\Delta t_1 + \Delta t_2) = \beta(\Delta t_1) + \beta(\Delta t_2). \tag{5.29}$$

which is not satisfied for any choice of the parameters δ and λ, thereby implying that the map is always non-Markovian. A similar proof can be obtained for the common noise map $\mathcal{E}_{\text{C}}(\Delta t)$.

Let's now discuss the connections between revivals of correlations, non-divisibility and information backflow [148–150]. As already mentioned in Chapter 1, non Markovianity may be revealed by some witnesses, as the BLP measure or the analogue measure based on fidelity for CV systems. Both techniques are based on the contractive property (valid for Markovian dynamics) of the trace distance and the Bures distance, respectively. Therefore, a non-monotonous behaviour of the trace distance or the fidelity is a signature of non-Markovianity. Furthermore, both these witnesses possess physical meaning: the trace distance is directly related to the probability of discriminating two states in time, whereas the Bures distance may be used to evaluate upper and lower bounds of the very same error probability defined by the trace distance. Therefore, a non-monotonous dynamics also implies a partial clawback of distinguishability of two input states, which has been interpreted as a sign of a backflow of information [151]. Fig.5.6 shows the time evolution of the fidelity and the derivative of the Bures distance between a pair of two-mode squeezed vacuum states ($\gamma = 1$) with different energies ($\epsilon_1 \neq \epsilon_2$). The existence of sets of parameters leading to a non-monotonous behaviour of the fidelity and a region of positive derivative of Bures distance is enough to confirm

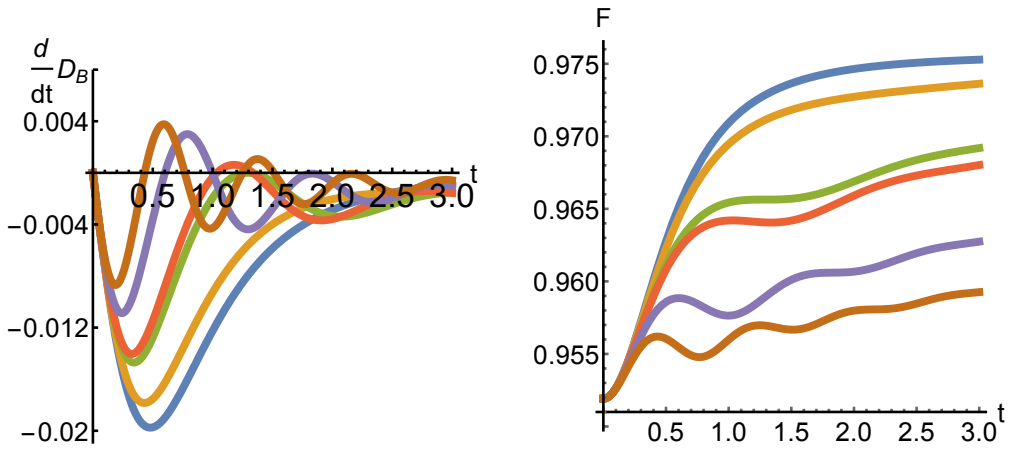

Figure 5.6: Dynamics of Bures distance derivative and Fidelity for different values of rescaled detuning δ in the common noise scenario. Left panel: derivative of Bures distance. Right panel: dynamics of Fidelity. The Fidelity ceases to oscillate when $\delta \leq \delta_0$. The distinguishability of the input states diminishes monotonically in time and no backflow of information is detected. The curves with a partially positive derivative of Bures distance have $\delta > \delta_0$ and correspond to the curves where oscillations of Fidelity are shown. In all panels, I set $\epsilon_1 = 2, \epsilon_2 = 1, \gamma_1 = \gamma_2 = 1, \lambda = 1$ and, from top to bottom $\delta = 0$ (blue line), $\delta = 2$ (yellow line), $\delta = \delta_0$ (green line), $\delta = 4$ (red line), $\delta = 6$ (purple line), $\delta = 8$ (brown line).

the already proven non-Markovianity of both maps. However, non-Markovianity is not detected when $\delta \leq \delta_0$, where δ_0 is the very same threshold obtained in chapter 2, i.e. the threshold to observe revivals of correlations. The same behaviour is observed for any choice of the involved parameters, confirming that non-divisibility itself is not a resource to preserve quantum correlations in this system, i.e. it is not sufficient to observe recoherence phenomena. Rather, it represents a necessary prerequisite to obtain backflow of information, which is the true ingredient to obtain revivals of quantumness and, in turn, the physically relevant resource.

5.4 Summary

- I have investigated the evolution of entanglement and quantum discord for two harmonic oscillators interacting with classical stochastic fields. I analyzed two different regimes: in the first one, the two modes interact with two separate environments describing local noise, whereas in the second case the two oscillators are exposed to a common source of noise.
- The interaction with a classical environment always induces a loss of entanglement, while the quantum discord shows a vanishing behaviour in the local scenario but may exhibit a non zero asymptotic value in the common scenario, independently on the the initial value of the discord.
- The interaction with a common environment is, in general, less detrimental than the interaction with separate ones.
- I have proved the non-divisibility of the maps and found some structural boundaries on the existence of revivals of correlations in terms of a threshold value of the

detuning between the natural frequency of the system and the central frequency of the noise. The same threshold determines the presence of backflow of information, associated to oscillations of the fidelity between a pair of initial states.

- Overall, non-divisibility in itself is not a resource to preserve quantum correlations but is a necessary condition to obtain backflow of information, which is the true ingredient to obtain revivals of quantumness.

CHAPTER 6

Environment discrimination

In general, environment-induced decoherence is detrimental for the quantum features of a localized system: loss of nonclassicality [152, 153] or disentanglement may arise asymptotically or after a finite interaction time [154–157]. On the other hand, extended systems experience more complex decoherence phenomena: the subparts of a system may interact with indepenent environments or, more interestingly, with a common one, corresponding to collective decoherence or dissipation, which may result in preservation of quantum coherence as well as preservation and creation of entanglement [158–163] or superradiance [164–171].

Decoherence and dissipation into a common bath may arise spontaneously in some structured environments, but it may also be engineered [14, 15] to achieve specific goals. In both cases, the common decoherence mechanism may mingle or even being overthrown by local processes, leading to undesidered loss of quantum features. The discrimination between the presence of local or common environments is thus a relevant tool to fight decoherence and preserve quantum coherence.

In this framework, the main goal of this section is to design a successful strategy to discriminate which kind of interaction, either local or common, occurs when an extended quantum probe interacts with a classical fluctuating environment. This is a channel discrimination problem, addressed upon considering a quantum probe interacting with either a local or a common bath, and then solving the corresponding state discrimination problem. In particular, in order to assess the role of entanglement with nearly analytic results, I consider a bipartite system made of two non interacting harmonic oscillators. The local noise scenario is described by the interaction of each oscillator with independent CSFs whereas common noise is described as the coupling between the two oscillators with the same CSF.

In this Chapter, I analyze in details discrimination strategies based on homodyne detection, which has already proven to be useful in discrimination of quantum states [172] or binary communication schemes [173]. Also, we analyze in details the performances of Gaussian states used as probe preparation, including many lab-friendly input signals.

6.1 Discrimination protocol for classical environments

6.1.1 Input states

Before introducing the necessary tools for quantum state discrimination, I briefly discuss what kind of input states I am about to consider. In general, the optimization of a channel discrimination protocol involves the optimization over the possible input states. Considered that the stochastic diffusion preserves the gaussianity of input states, I limit the analysis to gaussian input states.

Among Gaussian states, I focus attention on three relevant classes, squeezed thermal states (STSs), states obtained as a linear mixing of a single-mode Gaussian state with the vacuum (SVs) and standard form SVs, i.e. SV states recast in standard form by local operations. These classes of states may be generated by current quantum optical technology and thus represent good candidates for the experimental implementations of discrimination protocols. STSs and SVs are described by the covariance matrices $\boldsymbol{\sigma}_{\text{STS}}$ and $\boldsymbol{\sigma}_{\text{SV}}$, respectively

$$\boldsymbol{\sigma}_{\text{STS}} = \frac{1}{2}\begin{pmatrix} a & 0 & c & 0 \\ 0 & a & 0 & -c \\ c & 0 & b & 0 \\ 0 & -c & 0 & b \end{pmatrix} \quad \boldsymbol{\sigma}_{\text{SV}} = \frac{1}{4}\begin{pmatrix} m & 0 & s_1 & 0 \\ 0 & n & 0 & s_2 \\ s_1 & 0 & m & 0 \\ 0 & s_2 & 0 & n \end{pmatrix}. \tag{6.1}$$

In particular, I consider symmetrical thermal states $\tilde{n}_1 = \tilde{n}_2 = \tilde{n}$, that can be re-parametrized setting $\epsilon = 2(\bar{n} + n_s + 2\bar{n}\, n_s)$, with $n_s = \sinh^2 r$, and a normalized squeezing parameter $\gamma \in [0, 1]$, such that

$$n_s = \gamma\epsilon \qquad \bar{n} = \frac{(1-\gamma)\epsilon}{1+2\gamma\epsilon}.$$

The covariance matrix $\boldsymbol{\sigma}_{\text{SV}}$ corresponds to a density operator of the form

$$\rho_{\text{SV}} = R\left(\frac{\pi}{4}\right)\Big(S(r)\nu S^{\dagger}(r) \otimes |0\rangle\langle 0|\Big)R^{\dagger}\left(\frac{\pi}{4}\right) \tag{6.2}$$

where $S(r) = \exp\{r(a_1^{\dagger} - a_1^{\dagger})\}$ is the single-mode squeezing operator and the rotation operator$R(\theta) = \exp\{\theta(a_1 a_2^{\dagger} + a_1^{\dagger} a_2\}$ corresponds to a beam-splitter mixing. The physical state depends on two real parameters: the squeezing parameter r and the number $\bar{n}$, which are related to the parameters m, n, s_1, s_2 of eq. (6.1) by the relations

$$\begin{aligned} m &= 1 + (1+2n)e^{2r}, \\ n &= 1 + (1+2n)e^{-2r}, \\ s_1 &= (1+2n)e^{2r} - 1, \\ s_2 &= (1+2n)e^{-2r} - 1. \end{aligned} \tag{6.3}$$

Notice that only STSs already possess a covariance matrix in standard form. However, simply applying local squeezing to both modes the standard form of $\boldsymbol{\sigma}_{\text{SV}}$ can be found. Of course, locally squeezing the modes dramatically changes the energy of the Gaussian state but leaves quantities such purity and entanglement unmodified. These states are referred to as standard form single-vacuum states as SSVs.

6.1.2 Quantum State Discrimination

In this section, I briefly summarize the basic concepts of quantum state discrimination and introduce the tools required to implement a discrimination strategy. The purpose of state discrimination is to distinguish, by looking at the outcome of a measurement performed on the system, between two possible hypothesis on the preparation of the system itself.

In the present case, the bipartite system is prepared in a given Gaussian state and the state discrimination aims to distinguish which kind of noise, local or common, affects

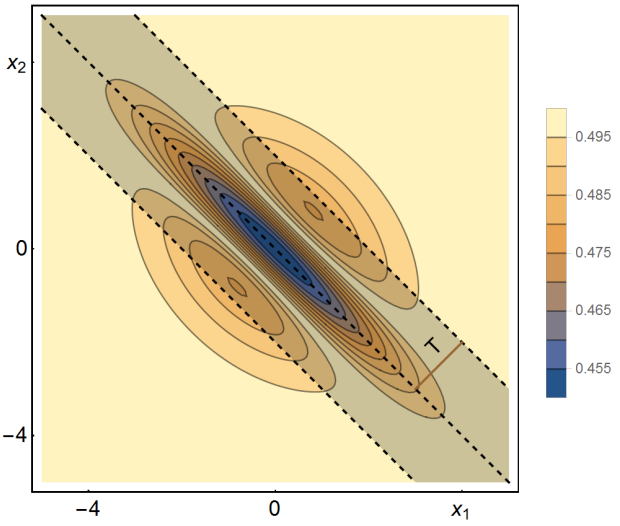

Figure 6.1: (Color Online) Contourplot of $P_{\mathrm{Q}}(x_1, x_2)$ for a STS. The dark region between the two dashed parallel lines represents a choice of $\mathcal{D}_c$, the region of outputs associated to the inference of common noise. States and channel parameters are set as follows: $\epsilon = 1, \gamma = 0.7, \lambda_1 = \lambda_2 = \lambda = 1, t = 1$.

the system. This is done by a discrimination scheme applied to the output states of the Gaussian maps (5.12) and (5.21). Since the two outputs are not orthogonal for any given input, perfect discrimination is impossible and a probability of error appears. Optimal discrimination schemes are those minimizing the probability of error upon a suitable choice of both the input state and the output measurement. The minimum achievable probability is known as the Helstrom Bound, which is based on the Trace Distance.

Unfortunately, for continuous variable systems, evaluating the Helstrom Bound is a challenging task and one usually resorts to alternative upper bounds, such as the fidelity (1.87) and quantum Chernoff (1.89) bounds. However, even when evaluating the Helstrom Bound is possible, it usually corresponds to a POVM which is difficult to implement. In the following, I devote attention to feasible measurements and evaluate their performances in the discrimination of local and common noise, comparing the error probability with the bounds discussed previously, looking for a suitable POVM.

6.1.3 Double Homodyne Measurement

In section 5.1, I have analyzed the dynamics in the presence of either local or common noise. The two dynamical maps are different and, in particular, correlations between the two oscillators appear exclusively in the common noise scenario, as it is apparent from the presence of off-diagonal terms in the common noise matrix. As a matter of fact, the correlation terms in the noise matrix corresponds the variances $var(X_1, X_2)$ and $var(P_1, P_2)$, where $X_j = \frac{1}{\sqrt{2}}(a_j + a_j^\dagger), P_j = \frac{1}{i\sqrt{2}}(a_j - a_j^\dagger)$ are the quadrature operators of the two oscillatos. This argument suggests that joint homodyne detection of the quadratures of the two modes may be a suitable building block to discriminate the two possible environmental scenarios. In the following, I am about to consider the measurement of all possible combinations of quadratures, (X_1, X_2), (P_1, P_2), (X_1, P_2) and (P_1, X_2) and denote the corresponding POVMs as $\Pi(q_1, q_2) = |q_1, q_2\rangle\rangle\langle\langle q_1, q_2| \equiv |q_1\rangle\langle q_1| \otimes |q_2\rangle\langle q_2|$

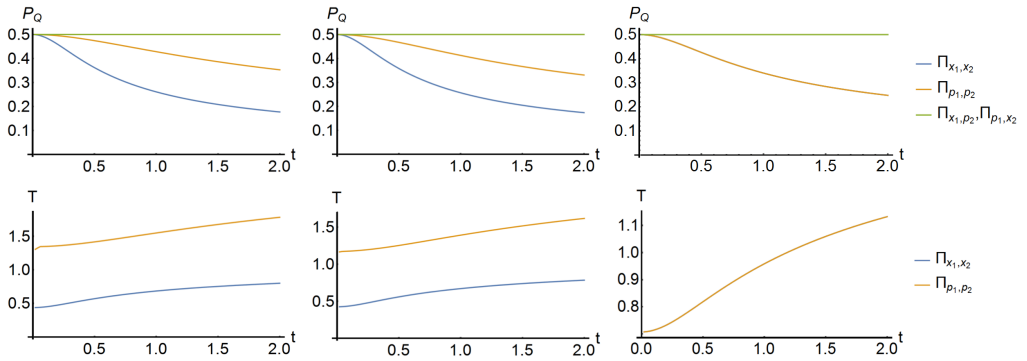

Figure 6.2: (Color Online) Upper panels: Error probability $P_{\rm Q}$ for different POVMs for (left) STS ($\epsilon = 1, \gamma = 0.7$), (center) SV ($n = 1, r = 0.7$) and (right) standard SV ($n = 1, r = 0.7$). The POVM $\Pi(x_1, x_2)$(blue lower line) is always the most efficient. The POVMs $\Pi(x_1, p_2)$ and $\Pi(p_1, x_2)$ (upper red and green) yield the same error probability $P_{\rm Q} = \frac{1}{2}$ independently on the input state and are useless for discrimination purposes. Lower panels: Optimal half-width T as a function of time for POVMs $\Pi(x_1, x_2)$ and $\Pi(p_1, p_2)$. I set $\lambda_1 = \lambda_2 = \lambda = 1$.

with $q_j \in \{x_j, p_j\}$, $j = 1, 2$ and $|q_j\rangle$ being quadrature eigenstates. In order to implement a discrimination strategy, it is necessary to define an inference rule connecting each possible outcome of the measurement to one of the two hypothesis: $H_{\rm L}$, the noise is due to local interaction or $H_{\rm C}$, the noise is due to common interaction with the environment. Denoting by $\mathcal{D}_c \subset \mathbb{R}^2$ the region of outcomes leading to $H_{\rm C}$, i.e. to infer a common noise, then the two-value POVM describing the overall discrimination strategy is given by $E_{\rm C} + E_{\rm L} = \mathbb{I}$, where

$$E_{\rm C} = \iint_{\mathcal{D}_c} dq_1 dq_2 \, \Pi(q_1, q_2) \qquad E_{\rm L} = \mathbb{I} - E_{\rm C} \, . \tag{6.4}$$

The success probabilities, i.e. those of inferring the correct kind of noise, are given by $P_j = \mathrm{Tr}[\rho_j \, E_j]$, $j = L, C$ respectively, whereas the error probability, i.e. the probability of chosing the wrong hypothesis is given by

$$\begin{aligned} P_{\rm Q} &= \frac{1}{2}\big(\mathrm{Tr}[\rho_{\rm L} \, E_{\rm C}] + \mathrm{Tr}[\rho_{\rm C} \, E_{\rm L}]\big) \\ &= \frac{1}{2}\left(1 - \iint_{\mathcal{D}_c} dq_1 dq_2 \, \mathrm{Tr}\left[\Pi(q_1, q_2)\,(\rho_{\rm C} - \rho_{\rm L})\right]\right). \end{aligned} \tag{6.5}$$

The smaller is $P_{\rm Q}$, the more effective is the discrimination strategy. In order to suitably choose $\mathcal{D}_c$ it is useful to analyze the behavior of the quantity

$$p_{\rm Q}(q_1, q_2) = \mathrm{Tr}\left[\Pi(q_1, q_2)\,(\rho_{\rm C} - \rho_{\rm L})\right],$$

in the (q_1, q_2) plane. Fig. 6.1 shows a contourplot of $p_{\rm Q}(x_1, x_2)$ for a given input STS. This probability is squeezed along the $x_1 x_2$ direction, since a common environment induces the build-up of correlations between the quadratures. For this reason, it is convenient to choose $\mathcal{D}_c$ as the region between two straight lines at 45° and denote by T its half-width. The same argument holds also for SV and standard SV.

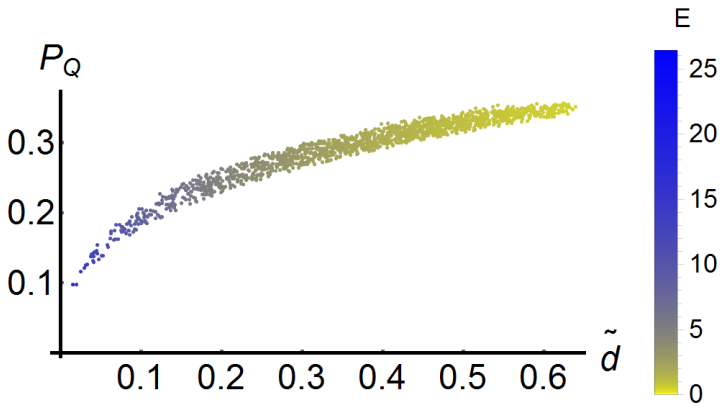

Figure 6.3: (Color Online) Error probability P_Q for random Gaussian input states as a function of the smallest symplectic eigenvalue $\tilde{d}_1$ with POVM $\Pi(x_1, x_2)$. The color scale classifies the initial energy of the state. The error probability scales with the entanglement and the energy of the input state. I set $\lambda_1 = \lambda_2 = \lambda = 1, t = 1$.

In the top panels of Fig. 6.2 I show a comparison between the error probability of the four POVMs described above on some particular STSs (left), standard form SVs (center) and SVs (right). As it is apparent from the plot, the POVMs $\Pi(x_1, p_2)$ and $\Pi(p_1, x_2)$ are useless. In fact, the common environment does not correlate these couples of quadratures. On the other hand, the POVM $\Pi(x_1, x_2)$, represented by the blue lines, always outperforms $\Pi(p_1, p_2)$. The lower panels show the optimal values of the half-width T of the region $\mathcal{D}_c$ as a function of the interaction time for the very same states.

6.2 Random input Gaussian states

In this section, I address the optimization of the discrimination protocol using Gaussian states as input and the optimal homodyne-based POVM $\Pi(x_1, x_2)$. The main purpose is to figure out which Gaussian state leads to the optimal discrimination protocol and understand which lab-friendly states, among the classes of STSs, SVs and SSVs, are the most performant ones. Moreover, I analyze whether the efficiency of the discrimination protocol is affected by some relevant properties of the input states. To this aim I evaluate the error probability P_Q as a function of energy and entanglement, at fixed purity. We recall that the energy E and purity μ of a zero-mean valued two-mode Gaussian state with covariance matrix $\boldsymbol{\sigma}$ are given by

$$\begin{aligned} E(\boldsymbol{\sigma}) &= \mathrm{Tr}\left(\frac{\boldsymbol{\sigma}}{2}\right) - 1 \\ \mu(\boldsymbol{\sigma}) &= \frac{1}{4\sqrt{\det\boldsymbol{\sigma}}}, \end{aligned} \tag{6.6}$$

while the entanglement is quantified by the logarithmic negativity 1.76. In this part of the dissertation, it is convenient to directly use $\tilde{d}_-$ as a quantifier for entanglement: when $\tilde{d}_- < 1/2$, the state is entangled, otherwise it is not.

Fig. 6.3 shows the error probability of randomly generated Gaussian states in standard form with purity $\mu = 0.6$ at fixed time $t = 1$ as a function of the symplectic eigen-

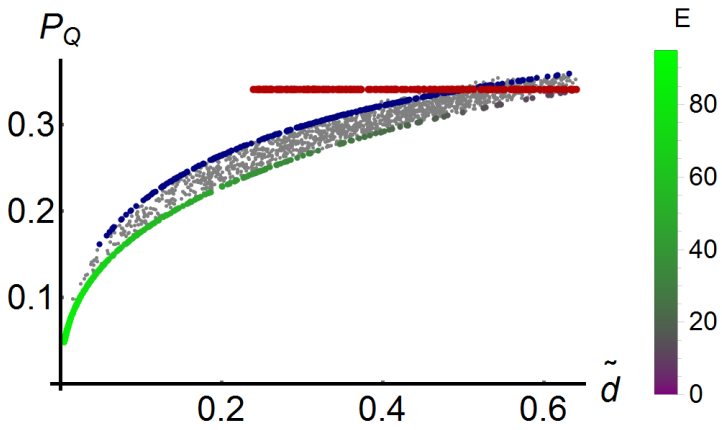

Figure 6.4: (Color Online) Error probability P_Q as a function of the smallest symplectic eigenvalue $\tilde{d}_1$ with POVM $\Pi(x_1, x_2)$ for standard form random Gaussian states (gray dots), STSs (blue upper curve), SVs (red straight line) and SSVs (lower line). The color scale classifies the energies of the SSV states. The error probability of SV states does not depend on the entanglement of the input state. The most performant states are the SSVs. I set $\lambda = 1$.

value $\tilde{d}_1$ of the input state, while the color scale classifies its initial energy. As is apparent from the figures, for non-unitary purity, generating an always more entangled input state does not necessarily imply an improvement in the efficiency of the discrimination protocol. The same happens with energy: the error probability does not scale monotonicly with the energy stored in the input state. Nevertheless, increasing the energy and the entanglement of the input state at the same time, the error probability lowers monotonicly.

Fig. 6.4 shows the efficiency of efficient STSs, SVs and SSVs with respect to all possible Gaussian states with the same purity ($\mu = 0.6$). As a result, the most performant states are the SSVs: these states form a lower bound for every random-generated state, so representing the topmost suitable class state for discrimination protocols. One might make a conjecture that for SSVs entanglement might be the only resource to discrimination: unfortunately, this is true as long as purity is fixed, as the energy of SSVs monotonicly increases with entanglement, but false in general. Concerning SVs and STSs, it is worth noting that STSs are easily outperformed by any other standard form Gaussian state and that the error probability achieved with input SV states is not affected by a change in the initial entanglement (note that SVs' covariance matrix is not in standard form, this explains why the red curve steps over the region of the standard form Gaussian states).

Finally, Fig. 6.5 shows a comparison between the error probability achieved by some lab-friendly states and the bounds introduced in section 1.4. In particular, I choose some highly performant identically entangled STS and SSV. The left panel shows a comparison between the error probability for a STS with the fidelity and the Quantum Chernoff Bound. The double homodyne measurement yields an error probability (green line) that beats the Quantum Chernoff Bound (red line), The right panel shows a similar comparison for a SV state. In this case, even though the SV state yields a lower error probability than a STS does, the QCB can only be saturated in the early dynamics.

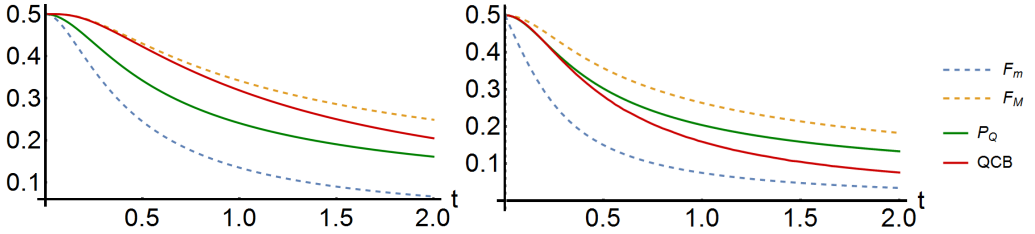

Figure 6.5: (Color Online) Comparison between error probability and fidelity and QCB bounds for STS state (upper panel) and SSV state (lower panel). In both panels, the dashed lines represent the upper bound $\mathcal{F}_M$ (orange line) and lower bound $\mathcal{F}_m$ (blue line), the green line represents the error probability P_Q, the red line represents the QCB. Upper panel: I set $\epsilon = 1.956, \gamma = 0.6593, \lambda = 1.0$. Lower panel: I set $n = 0.3333, r = 1.470, \lambda = 1$.

6.3 Summary

- I have addressed the design of effective strategies to discriminate between the presence of local or common noise effect for a system made of two harmonic quantum oscillators interacting with classical stochastic fields.
- Discrimination protocols based on joint homodyne detection of the position operators yield an error probability that may outperform the Quantum Chernoff Bound, leading to a probability of error close to the Helstrom bound. In particular, I have shown that the QCB can be overtaken by means of Gaussian states feasible with current technology.
- The error probability achieved with joint homodyne measurement strictly depends on the properties of the input state, as it lowers monotonicly with the energy and the entanglement of the input state.

Conclusions

In this dissertation, I presented and discussed the results of the research carried out during the three years of my PhD, mostly devoted to the analysis of the decohence of continuous variable systems subject to classical noise and the investigation of the efficiency of a stochastic approach to describing quantum phenomena.

The interaction between quantum systems and the environment is generally responsible for loss of coherence or quantumness of the system. However, reliable communication protocols, cryptographic schemes or any efficient quantum device, they all benefit from using quantum correlations and require a coherent dynamics of quantum systems. Thus, a deep understanding of decoherence or dissipation mechanisms and a proper characterization of noise affecting the system are the first steps towards efficient quantum technologies. The standard approach to address environment-induced decoherence is to consider the quantum system interacting with a quantum bath. However, in many system of interest, the environment is very complex, with many degrees of freedom, and a full quantum description may be challenging or even unfeasible. In these situation, classical stochastic modeling of the environment represents a valid and reliable alternative.

In this thesis, I have investigated the decoherence induced on continuous variable systems by classical noise, focusing on two different decoherence mechanisms, phase diffusion and dissipation. The aim was twofold: the first was individuating the working regimes where a full quantum description of a system-environment interaction may be substituted by an effective classical (stochastic) one; the second was the analysis of the possible benefits introduced by the noise, either in preserving coherence of harmonic systems or in enhancing their performances in communication and measurement protocols.

In all the models presented, the quantum system under investigation interacts with an external stochastic field having a time-fluctuating (complex) amplitude. The stochastic noise is chosen Gaussian, i.e. fully characterized by its correlations function and by its spectrum. In particular, I focused on a physically-meaningful noise-generating process: the Ornstein-Uhlenbeck, characterized by a Lorentzian spectrum. The effects of noise on the dynamics of the system depend on three main physical parameters: the coupling with the system, its correlation time and the detuning between the frequencies of the quantum system and those characterizing the classical noise.

As a first result, I have shown that the stochastic noise may take over the full quantum description of Markovian dephasing channels: in the regime of small correlation time, a

stochastic phase shift leads the quantum state to the very same dynamics induced by the dephasing Markovian master equation. This result widens to continuous variable systems a previously known result achieved by Joynt and Crow, who proved that dephasing channels for qubit systems could be classically simulated by random unitary evolutions. Conversely, a perfect stochastic model of the time-dependent quantum optical master equation, which rules the dynamics of a quantum harmonic oscillator interacting with a non-zero temperature bath, is not achievable. Actually, a random displacement may mimic quantum dynamics only at small times, when the spontaneous emission is negligible or if the temperature of the bath is sufficiently high. The vary same result holds for the Markovian quantum optical master equation, whose solution at high temperatures can be simulated by means of a low correlated Ornstein-Uhlenbeck process. Moreover, both stochastic models admit as solution for the system dynamics a gaussian channel with variance $\beta(t)$. The function $\beta(t)$ is directly correlated to the Ornstein-Uhlenbeck process and determines the necessary condition for the existence of revivals of any interesting property or correlation of the system. In fact, it is possible to individuate a threshold value $\tilde{\delta}_0$ such that any value of rescaled detuning (in units of the correlation time) larger that $\tilde{\delta}_0$ induces revivals.

As a second result, I have shown that stochastic noise may turn useful to describe physical interactions where the environment exhibits non-trivial features, for instance, a non-zero correlation time of the environment. Furthermore, the stochastic description allows exploring otherwise precluded scenarios, as the off-resonance interactions. While the Markovian quantum optical and the dephasing master equations describe only resonant dynamics, usually inducing decoherence and featuring irreversible loss of correlations, off-resonance stochastic interactions slow the decoherence process down and even introduce revivals of coherence or correlations. In order to display such results, I analyzed the evolution of quantumness of highly nonclassical states in a dissipative environment, the mutual information between two parties in presence of stochastic phase diffusion and the evolution of entanglement and quantum discord of bipartite states.

In the first model, I analyzed the survival times of quantumness according to four different criteria introduced to witness nonclassicality, also relating them to experimentally observable quantities. The results show that a correlated environment strongly influences the decoherence time, increasing the survival time of nonclassicality beyond the Markovian limits and leading to dynamical sudden death and birth of quantumness, as indicated by collapses and revivals of nonclassicality. In particular, sudden death and sudden birth of quantumness may occur only when $\beta(t)$ oscillates, that is, when the rescaled detuning exceeds the threshold value $\tilde{\delta}_0$. In the second model, I addressed the evolution of the performance of a phase-keyed communication channel in presence of stochastic phase diffusion. In particular, I showed that phase-encoding, that is, encoding information onto the phase of an input state, outperforms amplitude-encoding for coherent states in terms of channel capacity. Moreover, the presence of a correlated environment enhances the performance of the communication scheme, while revivals of mutual information appear for values of detuning beyond the threshold $\tilde{\delta}_0$.

As a third result, I have shown that stochastic interactions may be used in order to better explore the relation between non-Markovianity and the evolution of the correlations of quantum systems. In fact, when the non-Markovianity of a quantum map is not provable by its definition, it may be revealed by some sufficient conditions as the BLP and the Fidelity criteria, which are based on the assumption that Markovian dynamics cannot produce any increase of distinguishability between two states in time. For this reason, these markers of non-Markovianity are usually seen as a sign of a backflow

of information from the environment to the system. Within this context, stochastic interactions prove to be a useful example: indeed, the models presented are analytically non-Markovian whatever the parameters of the stochastic noise are, but the markers fail to capture this non-Markovian feature if the system does not exhibit revivals of correlations. Therefore, the models presented stand as a peculiar example, in which non-Markovianity may be proved for any choice of parameters but revealed by the markers only when information flows back to the system in terms of revivals of correlations, that is, when $\beta(t)$ features an oscillating behaviour, suggesting that the information backflow properly is the true resource to produce revivals. Moreover, I have shown that the derivative of $\beta(t)$ coincides with the dynamical damping rate of the time-dependent quantum optical master equation. This implies that whenever $\beta(t)$ oscillates in time, the dynamical damping rate turns negative and the time-dependent master equation becomes non-Markovian. Indeed, I show that the threshold $\tilde{\delta}_0$ for the presence of revivals is not a peculiar feature of the stochastic approach, but exists even in the full quantum model as the minimum value of $\tilde{\delta}_0$ leading to a negative dynamical damping rate at high temperature.

As a fourth result, I designed an experimentally feasible protocol to discriminate whether a composite quantum system suffers decoherence and dissipation on a local or global scale, individuating the optimal measure and the most suitable state to probe the form of the environment, when it is portrayed by a classical field. Indeed, I showed that a discrimination protocol based on standard measurements, as joint homodyne detection of the position operators, yields an error probability that may outperform typical bounds for discrimination problems, such as the Quantum Chernoff Bound. Moreover, I have shown that the QCB may easily be overtaken without resorting to any exotic input quantum state: indeed, good discrimination protocols may be achieved by means of Gaussian states feasible with current technology.

Quantum technologies exploit the properties of quantum systems. However, preservation of coherence or quantum correlations of open systems is a relevant issue which requires a deep understanding of the decoherence mechanisms and a full characterization of noise, in particular when the environment may induce exploitable recoherence phenomena.

In the last years, the role of non-Markovianity in preserving quantum correlations has been thoroughly studied. In many situations, non-Markovianity stands as a resource for quantum information processing, leading to a non-trivial evolution of entanglement or discord [174, 175]. The results presented in this thesis show that non-Markovianity actually sets the natural context for the existence of revivals of correlations, but the true resource is represented by the backflow of information. Stochastic phase diffusion and stochastic dissipation are non-Markovian interactions in terms of non-divisibility, but a non-trivial dynamics of entanglement, discord or non-classicality happens only when backflow of information is detected.

The external noise may then be exploited in order to preserve quantum correlations by suitable reservoir engineering and the complexity of classical noise and its effects on quantum systems may successfully be studied by discrimination schemes, based on standard laboratories techniques.

Appendices

Appendix I

The explicit expression for $\Delta(t)$ valid for all temperatures is given by

$$\begin{aligned}\Delta(t) = \omega_0 \frac{r^2}{1+r^2} \Bigg\{ & \coth(\pi r_0) - \cot(\pi r_c) e^{-\omega_c t}(r\cos(\omega_0 t) - \sin(\omega_0 t)) + \\ & + \frac{1}{\pi r_0}\cos(\omega_0 t)\left[\bar{F}(-r_c,t) + \bar{F}(r_c,t) - \bar{F}(ir_0,t) - \bar{F}(-ir_0,t)\right] \\ & - \frac{1}{\pi}\sin(\omega_0 t)\left[\frac{e^{-\nu_1 t}}{2r_0(1+r_0^2)}\left((r_0-i)\bar{G}(-r_0,t) + (r_0+i)\bar{G}(r_0,t)\right)\right] \\ & + \frac{1}{2r_c}\left(\bar{F}(-r_c,t) - \bar{F}(r_c,t)\right)\Bigg\}\end{aligned}$$

where $r_0 = \omega_0/2\pi k_B T$, $r_c = \omega_c/2\pi k_B T$ and

$$\begin{aligned}\bar{F}(x,t) &= {}_2F_1(x,1,1+x,e^{-\nu_1 t}) \\ \bar{G}(x,t) &= {}_2F_1(2,1+x,2+x,e^{-\nu_1 t})\end{aligned}$$

where ${}_2F_1(a,b,c,z)$ is the hypergeometric function.

Bibliography

[1] M. A. Nielsen and I. L. Chuang, *Quantum Computation and Quantum Information* (Cambridge University Press, Cambridge, Cambridge, 2000).

[2] Artur K. Ekert, Phys. Rev. Lett. **67**, 661

[3] A. Acin, N. Brunner, N. Gisin, S. Massar, S. Pironio, and V. Scarani, Phys. Rev. Lett. 98, 230501 (2007).

[4] V. Giovannetti, S. Lloyd, and L. Maccone, Nat. Photon. 5, 222 (2011).

[5] A. Datta, A., Flammia, S. T. and Caves, C. M. Entanglement and the power of one qubit. Phys. Rev. A **72**, 042316 (2005).

[6] Braunstein, S. L. et al., Phys. Rev. Lett. **83**, 1054–1057 (1999).

[7] B. Dakić, Y. O. Lipp, X. Ma, M. Ringbauer, S. Kropatschek, S. Barz, T. Paterek, V. Vedral, A. Zeilinger, Č. Brukner and P. Walther, Nature Physics **8**, 666–670 (2012)

[8] J. Maziero, L. C. Celeri, R. M. Serra, and V. Vedral, Phys. Rev. A **80**, 044102 (2009).

[9] T. Werlang, S. Souza, F. F. Fanchini, and C. J. Villas Boas, Phys. Rev. A **80**, 024103 (2009).

[10] B.-H. Liu, L. Li, Y.-F. Huang, C.-F. Li, G.-C. Guo, E.-M. Laine, H.-P. Breuer, J. Piilo, Nat. Phys. **7**, 931 (2011).

[11] A. Smirne, D. Brivio, S. Cialdi, B. Vacchini, and M. G. A. Paris, Phys. Rev. A **84**, 032112 (2011).

[12] J. Piilo, S.Maniscalco,K. Harkonen, and K.-A. Suominen, Phys. Rev. Lett. **100**, 180402 (2008).

[13] A. Smirne, S. Cialdi, G. Anelli, M. G. A. Paris, and B. Vacchini, Phys. Rev. A **88**, 012108 (2013).

[14] J. T. Barreiro et al., Nature **470**, 486 (2011).

[15] F. Verstraete, M. M. Wolf, J. I. Cirac, Nature Phys. **5**, 633 (2009).

[16] B. Bylicka, C. D., and M. S., Sci. Rep. 4, 5720 (2014).

[17] S. Lorenzo, F. Plastina, and M. Paternostro, Phys. Rev. A 88, 020102 (2013).

[18] S. Luo, S. Fu, and H. Song, Phys. Rev. A 86, 044101 (2012).

[19] E.-M. Laine, J. Piilo, and H.-P. Breuer, Phys. Rev. A 81, 062115 (2010).

[20] A. Rivas, S. F. Huelga, and M. B. Plenio, Phys. Rev. Lett. 105, 050403 (2010).

[21] X.-M. Lu, X. Wang, and C. P. Sun, Phys. Rev. A 82, 042103 (2010).

[22] M. M.Wolf, J. Eisert, T. S. Cubitt, and J. I. Cirac, Phys. Rev. Lett. 101, 150402 (2008).

[23] S. Maniscalco and F. Petruccione. Phys. Rev. A **73**, 012111 (2006).

[24] X.-T. Liang. Phys. Rev. E **82**, 051918 (2010).

[25] P. Rebentrost and A. Aspuru-Guzik. J. Chem. Phys. **134**, 101103 (2011).

[26] A. Chiuri, C. Greganti, L. Mazzola, M. Paternostro, P. Mataloni, Scient. Rep. **2**, 968 (2012).

[27] B-H. Liu, L. Li, Y-F. Huang, C-F. Li, G-C. Guo, E-M. Laine, H-P. Breuer, J. Piilo, Nat. Phys. **7**, 931 (2011).

[28] A. Smirne, D. Brivio, S. Cialdi, B. Vacchini, M. G. A. Paris, Phys. Rev. A **84**, 032112 (2011).

[29] J. Piilo, S. Maniscalco, K. Harkonen, and K.-A. Suominen, Phys. Rev. Lett. **100**, 180402 (2008).

[30] A. Smirne, S. Cialdi, G. Anelli, M. G. A. Paris, B. Vacchini, Phys. Rev. A **88**, 012108 (2013).

[31] S. Maniscalco, S. Olivares, M. G. A. Paris, Phys. Rev. A **75**, 062119 (2007).

[32] J. Anders, Phys. Rev. A **77**, 062102 (2008).

[33] J. P. Paz, A. J. Roncaglia, Phys. Rev. A **79**, 032102 (2009).

[34] R. Vasile, S. Olivares, M. G. A. Paris, S. Maniscalco, Phys. Rev. A **80**, 062324 (2009).

[35] R. Vasile, S. Olivares, P. Giorda, M. G. A. Paris, S.Maniscalco, Phys. Rev. A **82**, 012313 (2010).

[36] F. Galve, G. L. Giorgi, and R. Zambrini, Phys. Rev. A **81**, 062117 (2010) .

[37] L. A. Correa, A. A. Valido, D. Alonso, Phys. Rev. A **86**, 012110 (2012).

[38] A. Cazzaniga, S. Maniscalco, S. Olivares, M. G. A. Paris, Phys. Rev. A **88**, 032121 (2013).

[39] V. Venkataraman, A. D. K. Plato, T. Tufarelli, M. S. Kim, J. Phys. B. **47**, 015501 (2014).

[40] H.-P. Breuer, E.-M. Laine, and J. Piilo, Phys. Rev. Lett. **103**, 210401 (2009).

[41] A. Rivas, S. Huelga, M. B. Plenio, Phys. Rev. Lett. **105**, 050403 (2010).

[42] X-M. Lu, X. Wang, C. P. Sun, Phys. Rev. A **82**, 042103 (2010).

[43] R. Vasile, S. Maniscalco, M. G. A. Paris, H.-P. Breuer, J. Piilo, Phys. Rev. A **84**, 052118 (2011).

[44] D. Chruściński, S. Maniscalco, Phys. Rev. Lett. **112**, 120404 (2014)

[45] R. Vasile, S. Olivares, M. G. A. Paris, S. Maniscalco, Phys. Rev. A **83**, 042321 (2011).

[46] A. W. Chin, S. F. Huelga, and M. B. Plenio, Phys. Rev. Lett. 109, 233601 (2012).

[47] E.-M. Laine, H.-P. Breuer, and J. Piilo, Sci. Rep. 4, 4620 (2014).

[48] S. F. Huelga, A. Rivas, and M. B. Plenio, Phys. Rev. Lett. 108, 160402 (2012).

[49] M. Thorwart, J. Eckel, J. H. Reina, P. Nalbach, and S.Weiss, Chem. Phys. Lett. 478234 (2009).

[50] K. Stannigel, P. Rabl, and P. Zoller, New Journal of Physics **14**, 063014 (2012).

[51] H. J. Metcalf and P. van Straten, *Laser cooling and trapping Graduate Texts in Contemporary Physics*

[52] M. Wilde, Quantum information theory (Cambridge University Press, Cambridge, 2013).

[53] J. D. Malley and J. Hornstein, Stat. Sci. 8, 433 (1993).

[54] S. Braunstein and C. Caves, Phys. Rev. Lett. 72, 3439 (1994).

[55] M. G. A. Paris, Int. J. Quantum Inf. 7, 125 (2009).

[56] S. M. Barnett and S. Croke, Advances in Optics and Photonics Vol. 1, Issue 2, pp. 238-278 (2009).

[57] J. Helm and W. T. Strunz, Phys. Rev. A **80**, 042108 (2009).

[58] J. Helm, W. T. Strunz, S. Rietzler, and L. E. Würflinger, Phys. Rev. A **83**, 042103 (2011).

[59] W. M. Witzel, K. Young, S. Das Sarma, Phys. Rev. B **90**, 115431 (2014).

[60] W.T. Strunz, L. Diósi, N. Gisin, Phys. Rev. Lett. **82**, 1801, (1999).

[61] J.T. Stockburger, H. Grabert, Phys. Rev. Lett. **88**, 170407 (2002).

[62] D. Crow, R. Joynt, Phys. Rev. A **89**, 042123 (2014).

[63] O. Astafiev, Yu. A. Pashkin, Y. Nakamura, T. Yamamoto and J. S. Tsai, Phys. Rev. Lett. **93**, 267007 (2004).

[64] Y. M. Galperin, B. L. Altshuler, J. Bergli, and D. V. Shantsev, Phys. Rev. Lett. **96**, 097009 (2006).

[65] B. Abel and F. Marquardt, Phys. Rev. B **78**, 201302(R) (2008).

[66] C. Cohen-Tannoudji, F. Laloë, B. Tiu, *Quantum Mechanics*, (1977)

[67] W. Magnus "On the exponential solution of differential equations for a linear operator", Comm. Pure and Appl. Math **7**, 649 (1954).

[68] S. Blanes, F. Casas, J.A. Oteo, and J. Ros, Phys. Rep. **470**, 151 (2008).

[69] K. Kraus, *States, Effects and Operations* (Springer-Verlag, Berlin, 1983).

[70] Á. Rivas, S. F. Huelga, M. B. Plenio, *Quantum Non-Markovianity: Characterization, Quantification and Detection*, (2014).

[71] S. Olivares, Eur. Phys. J. Special Topics **203**, 3-24 (2012).

[72] A. Serafini, F. Illuminati, S. Da Siena, J. Phys. B: At. Mol. Opt. Phys. **37** L21 (2004).

[73] P. Marian, T. A. Marian, Phys. Rev. A **86**, 022340 (2012).

[74] R.F. Werner, Phys. Rev. A **40**, 4277 (1989).

[75] A. Peres, Phys. Rev. Lett. **77**, 1413 (1996)

[76] R. Simon, Phys. Rev. Lett. **84**, 2726 (2000)

[77] G. Vidal, R.F. Werner, Phys. Rev. A **65**, 032314 (2002)

[78] P. Giorda, M. G. A. Paris, Phys. Rev. Lett. **105**, 020503 (2010).

[79] G. Adesso and A. Datta, Phys. Rev. Lett. **105**, 030501 (2010).

[80] R. Blandino, M. G. Genoni, J. Etesse, M. Barbieri, M. G. A. Paris, P. Grangier, R. Tualle-Brouri, Phys. Rev. Lett **109**, 180402 (2012).

[81] C. W. Helstrom, *Quantum Detection and Estimation Theory* (Academic, New York, 1976).

[82] A. Chefles, Contemp. Phys. **41**, 401 (2000).

[83] J. A. Bergou, U. Herzog, and M. Hillery in *Quantum State Estimation*, Lecture Notes in Physics, edited by J. Rehacek and M. G. A. Paris, Vol. 649 (Springer, Berlin, 2004), pp. 417–465.

[84] A. Chefles, in *Quantum State Estimation*, Lecture Notes in Physics, edited by J. Rehacek and M. G. A. Paris, Vol. 649 (Springer, Berlin, 2004), pp. 467–511.

[85] S. Pirandola, Phys. Rev. Lett. **106** , 090504 (2011).

[86] C. Invernizzi, M.G.A. Paris, S. Pirandola, Phys. Rev. A, **84**, 022334 (2011).

[87] A. Rivas, S. F. Huelga, and M. B. Plenio, Phys. Rev. Lett. **105**, 050403 (2010).

[88] G. Torre, W. Roga and F. Illuminati, Phys. Rev. Lett. **115**, 070401 (2015).

[89] L. A. M. Souza, H. S. Dhar, M. N. Bera, P. Liuzzo-Scorpo and G. Adesso, Phys. Rev. A **92**, 052122 (2015).

[90] H.-P. Breuer, E.-M. Laine, and J. Piilo, Phys. Rev. Lett. **103**, 210401 (2009).

[91] E. Parzen, *Stochastic Processes* (Holden-Day Inc., Amsterdam, 1964).

[92] N. G. van Kampen, *Stochastic processes in physics and chemistry* (North-Holland, Amsterdam, 1992).

[93] C. W. Gardiner, *Handbook of Stochastic Methods* (Springer, Berlin, 1983).

[94] R. L. Stratonovich *Topics in the Theory of Random Noise* (1963).

[95] M. G. Genoni, S. Olivares, and M. G. A. Paris, Phys. Rev. Lett. **106**, 153603 (2011).

[96] M. G. Genoni, S. Olivares, D. Brivio, S. Cialdi, D. Cipriani, A. Santamato, S. Vezzoli, and M. G. A. Paris, Phys. Rev. A **85**, 043817 (2012).

[97] S. Maniscalco, J. Piilo, F. Intravaia, F. Petruccione, A. Messina, Phys. Rev. A **70**, 032113 (2004).

[98] H. P. Breuer and F. Petruccione, *The Theory of Open Quantum Systems* (Oxford University Press, Oxford, 2002).

[99] R. J. Glauber, Phys. Rev. **131**, 2766 (1963).

[100] A. S. Holevo, Probl. Peredachi Inf., **9**, 3 (1973).

[101] A. Ferraro, S. Olivares, M.G.A. Paris, *Gaussian states in continuous variable quantum information*, (Bibliopolis, Napoli, 2005).

[102] K. E. Cahill, R. J. Glauber, Phys. Rev. **177**, 1882 (1969).

[103] C. T. Lee, Phys. Rev. A **44**, R2775 (1991).

[104] M. Takeoka, M. Ban, M. Sasaki, J. Opt. B **4** 114 (2002).

[105] N. Lutkenhaus, S. M. Barnett, Phys. Rev. A **51**, 3340 (1995).

[106] A. Kenfack, K. Zyczkowski, J. Opt. B **6**, 396 (2004).

[107] O. Cohen, Phys. Rev. A **56**, 3484 (1997).

[108] K. Banaszek, K. Wodkiewicz, Phys. Rev. A **58**, 4345 (1998).

[109] W. Vogel, Phys. Rev. Lett. **84**, 1849 (2000).

[110] I. Lvovsky, J. H. Shapiro, Phys. Rev. A **65**, 033830 (2002).

[111] D. N. Klyshko, Phys. Lett. A **213**, 7 (1996).

[112] A. R. Rossi, S. Olivares, M. G. A. Paris, Phys. Rev. A **70**, 055801 (2004).

[113] G. Zambra, A. Andreoni, M. Bondani, M. Gramegna, M. Genovese, G. Brida A. Rossi and M. G. A. Paris, Phys. Rev. Lett. **95**, 063602 (2005).

[114] J. Paavola, M. J. Hall, M. G. A. Paris, S. Maniscalco, Phys. Rev. A **84**, 012121 (2011).

[115] L. Diósi, Phys. Rev. Lett. **85**, 2841 (2000).

[116] H. P. Yuen, and M. Ozawa Phys. Rev. Lett. **70**, 363 (1993).

[117] C. M. Caves, and P. D. Drummond, *Rev. Mod. Phys*. **66** (1994) 481.

[118] A. S. Holevo, and R. F. Werner, Phys. Rev. A **63**, 032312 (2001).

[119] V. Giovannetti, S. Guha, S. Lloyd, L. Maccone, J. H. Shapiro, and H. P. Yuen, *Phys. Rev. Lett*. **92** (2004) 027902.

[120] J.H. Shapiro, S. Guha, and B.I. Erkmen, J. Opt. Netw. **4**, 505 (2005).

[121] S. E. Fedorov, and A. N. Mart'yanov, Radio Eng. Electr. Phys. **26**, 36 (1981).

[122] G. M. D'Ariano, C. Macchiavello, N. Sterpi, and H. P. Yuen, Phys. Rev. **54**, 4712 (1996).

[123] M. J. W. Hall, J. Mod. Opt. **40**, 809 (1993)

[124] S. Olivares, S. Cialdi, F. Castelli, and M. G. A. Paris, *Phys. Rev. A*. **87** (2013) 050303(R).

[125] M. G. Genoni, S. Olivares, and M. G. A. Paris, Phys. Rev. Lett. **106**, (2011) 153603.

[126] U. Leonhardt, and J. A. Vaccaro, B. Böhmer, and H. Paul Phys. Rev. A **51**, 84 (1995).

[127] R. Lynch, Phys. Rep. **256**, 367 (1995).

[128] M. G. A. Paris, Nuovo Cim. B **111**, 1151 (1996); Fizika B **6** 63 (1997).

[129] A. Royer, Phys. Rev. A **53** 70 (1996).

[130] M. G. A. Paris, Phys. Rev. A **60** 5136 (1999).

[131] J. W. Noh, A. Fougeres, and L. Mandel, Phys. Rev. Lett. **67**, 1426 (1991); Phys. Rev. A **45**, 424 (1992); Phys. Rev. A **46**, 2840 (1992).

[132] Z. Hradil, Phys. Rev. A **47**, 4532 (1993).

[133] J. W. Noh, A. Fougeres, and L. Mandel, Phys. Rev. A **47**, 4535 (1993).

[134] M. Freiberger, W. Vogel, and W. Schleich, Phys. Lett. A **176**, 41 (1993).

[135] G. M. D'Ariano, and M. G. A. Paris, Phys. Rev. A , **48**, R4039, (1993).

[136] U. Leonhardt, and H. Paul, Phys. Rev. A **48**, 4598 (1993).

[137] G. M. D'Ariano, and M. G. A. Paris, Phys. Rev. A **49**, 3022, (1994).

[138] P. Busch, M. Grabowski, and P. J. Lahti, *Operational quantum physics*, Lect. Not. Phys. **31** (Springer, Berlin, 1995).

[139] H. Wiseman, Phys. Rev. Lett. **75** 4587 (1995).

[140] J.-P. Pellonpää, J. Schultz, and M. G. A. Paris, Phys. Rev. A **83**, 043818 (2011).

[141] M. G. Genoni, S. Olivares, D. Brivio, S. Cialdi, D. Cipriani, A. Santamato, S. Vezzoli, and M. G. A. Paris, Phys. Rev. A **85**, (2012) 043817.

[142] B. Bellomo, R. Lo Franco and G. Compagno, Phys. Rev. Lett. **77**, 032342 (2008).

[143] L. Mazzola, S. Maniscalco, J. Piilo, K.-A. Suominen, and B. M. Garraway, Phys. Rev. A **79**, 042302 (2009).

[144] J. Harrington, J. Preskill, Phys. Rev. A 64, 062301 (2001).

[145] V. Giovannetti, S. Lloyd, L. Maccone, J.H. Shapiro, and B.J. Yen, Phys. Rev. A **70**, 022328 (2004).

[146] M. Brunelli, C. Benedetti, S. Olivares, A. Ferraro, M. G. A. Paris, Phys. Rev. A, Phys. Rev. A **91**, 062315 (2015).

[147] F. Ciccarello, V. Giovannetti, Phys. Rev. A **85**, 010102(R) (2012)

[148] A. Rivas, S.F. Huelga, M.B. Plenio, Rep. Prog. Phys. **77**, 094001 (2014).

[149] P. Haikka, S. Maniscalco, Op. Sys. Inf. Dyn. **21**, 1440005 (2014).

[150] B. Bylicka, D. Chruściński, S. Maniscalco, Sc. Rep. **4**, 5720 (2014).

[151] E.-M. Laine, J. Piilo and H.-P. Breuer, Phys. Rev. A **81**, 062115 (2010).

[152] W. H. Zurek, Phys. Today **44**, 36 (1991).

[153] J. P. Paz, S. Habib, and W. H. Zurek, Phys. Rev. D **47**, 488 (1993).

[154] M. G. A. Paris, A. Serafini, F. Illuminati, S. De Siena, Phys. Rev. A **68**, 012314 (2003).

[155] A. Serafini, S. De Siena, F. Illuminati, and M. G. A. Paris, J. Opt. B. **6**, S591 (2004).

[156] A. Serafini, F. Illuminati, M. G. A. Paris, S. De Siena, Phys. Rev A **69**, 022318 (2004).

[157] T. Yu, J. H. Eberly, Opt. Comm. **283**, 676 (2010).

[158] D. Braun, Phys. Rev. Lett. **89** 277901 (2002).

[159] Y. Zhao, G.H. Chen, Physica A **317**, 13 (2003).

[160] F. Benatti, R. Floreanini, M. Piani, Phys. Rev. Lett. **91**, 070402 (2003).

[161] J. S. Prauzner-Bechcicki, J. Phys. A: Math. Gen. **37**, L173 (2004).

[162] L. D. Contreras-Pulido, R. Aguado, Phys. Rev. B **77**, 155420 (2008).

[163] J. P. Paz, A. J. Roncaglia, Phys. Rev. Lett. **100**, 220401 (2008).

[164] M. Brownnutt, M. Kumph, P. Rabl and R. Blatt, Rev. Mod. Phys. **87**, 1419 (2015).

[165] S. Groeblacher, A. Trubarov, N. Prigge, G. D. Cole, M. As- pelmeyer, J. Eisert, Nature Comm. **6**, 7606 (2015).

[166] G. M. Palma, K.-A. Suominen, A. K. Ekert, Proc. R. Soc. London A **452**, 567 (1996).

[167] A. Rivas, M. Muller, New J. Phys. **17**, 062001 (2015).

[168] P. Zanardi, M. Rasetti, Phys. Rev. Lett. **79**, 3306 (1997).

[169] L.-M. Duan, G.-C. Guo, Phys. Rev. Lett. **79**, 1953 (1997).

[170] P. G. Kwiat, A. J. Berglund, J. B. Altepeter, A. G. White, Science **290**, 498 (2000).

[171] R. H. Dicke, Phys. Rev.**93**, 99 (1954).

[172] C. Wittmann, U. L. Andersen, M. Takeoka, D. Sych, G. Leuchs, Phys. Rev. A **81**, 062338 (2010).

[173] S. Olivares, S. Cialdi, F. Castelli, M.G.A. Paris, Phys. Rev. A **87**, 050303(R), (2013).

[174] C. Benedetti, M.G.A. Paris, S. Maniscalco, Phys. Rev. A, **89** 012114 (2014).

[175] P. Bordone, F. Buscemi, C. Benedetti, Fluct. Noise Lett. **11** 1242003 (2012).